

UAV-assisted Online Machine Learning over Multi-Tiered Networks: A Hierarchical Nested Personalized Federated Learning Approach

Su Wang, *Student Member, IEEE*, Seyyedali Hosseinalipour, *Member, IEEE*, Maria Gorlatova, *Member, IEEE*, Christopher G. Brinton, *Senior Member, IEEE*, and Mung Chiang, *Fellow, IEEE*

Abstract—We consider distributed machine learning (ML) through unmanned aerial vehicles (UAVs) for geo-distributed device clusters. We propose five new technologies/techniques: (i) *stratified UAV swarms* with leader, worker, and coordinator UAVs, (ii) *hierarchical nested personalized federated learning* (HN-PFL): a holistic distributed ML framework for personalized model training across the worker-leader-core network hierarchy, (iii) *cooperative UAV resource pooling* for distributed ML using the UAVs' local computational capabilities, (iv) *aerial data caching and relaying* for efficient data relaying to conduct ML, and (v) *concept/model drift*, capturing online data variations at the devices. We split the UAV-enabled model training problem as two parts. (a) Network-aware HN-PFL, where we optimize a tradeoff between energy consumption and ML model performance by configuring data offloading among devices-UAVs and UAV-UAVs, UAVs' CPU frequencies, and mini-batch sizes subject to communication/computation network heterogeneity. We tackle this optimization problem via the method of posynomial condensation and propose a distributed algorithm with a performance guarantee. (b) Macro-trajectory and learning duration design, which we formulate as a sequential decision making problem, tackled via deep reinforcement learning. Our simulations demonstrate the superiority of our methodology with regards to the distributed ML performance, the optimization of network resources, and the swarm trajectory efficiency.

Index Terms—UAVs, personalized federated learning, distributed model training, network optimization, model drift, concept drift.

1 INTRODUCTION

Unmanned aerial vehicles (UAVs) have been recently incorporated into Internet-of-things (IoT) networks with applications such as surveillance, aerial base station, smart agriculture, and search and rescue [1], [2]. Simultaneously, advancements in machine learning (ML) techniques and their superior performance in a variety of tasks, e.g., keyboard next word prediction, autonomous driving, and object tracking [3], [4], have motivated a new IoT paradigm called *intelligent edge/fog* powered by distributed ML [5], [6], [7].

Current literature has taken some initial steps toward integrating UAVs into distributed ML, e.g., [8], [9], [10], [11], [12], which mostly focused on implementing the classic federated learning architecture using UAVs where either the data is assumed to already be at the UAVs [8], [9], [10], [11] or the UAVs are merely used for parameter aggregation instead of a cellular base station [12]. Specifically, current literature is missing a holistic ML paradigm that develops a UAV-specific learning architecture for UAV-assisted networks, where the UAVs are utilized to train an ML model via data collection from energy-constrained devices. This paradigm should encompass device-UAV-core network collaborations, online data variations at the devices, geographical locations of the devices, existence of recharging stations, and heterogeneity across the UAVs and devices in terms of

computation/communication resources. We are motivated to fill this gap via (i) proposing *hierarchical nested personalized federated learning*, (ii) considering a holistic optimization problem that ties the ML model performance, data offloading, learning parameters, and heterogeneity across the UAVs and the devices together, and (iii) obtaining/optimizing the UAV swarm trajectories and ML model training duration using historic ML model performance under online data variations.

1.1 Motivations and Applications

Motivated by the following scenarios, we propose a system model for UAV-enabled online ML model training, where the UAVs perform both data collection and model training.

Community Service Systems via Amazon Sidewalk: Amazon proposes *Sidewalk* [13] to integrate community networks of IoT devices for household appliance diagnostics (e.g., faulty garage door, pet finding, smart lighting) in the absence of consistent wi-fi connectivity [14], [15] by leveraging device-to-device (D2D) communications. However, efficient training of ML models on IoT devices and sharing them among distant neighborhoods faces four non-trivial challenges: (i) IoT devices may not be idle, plugged into power, or have direct access to a cellular base station, preventing them from performing computationally intensive ML training, (ii) distant neighborhoods may not be reachable through D2D, (iii) neighborhoods' collected data may be time varying, and (iv) the neighborhoods may have extremely heterogeneous data distributions. We address the first two limitations by introducing UAV resource pooling and transferring model training vertically onto UAV swarms (e.g., the Amazon

S. Wang, S. Hosseinalipour, C. Brinton, and M. Chiang are with Purdue University, IN, USA e-mail: {wang2506, hosseina, cgb, chiang}@purdue.edu. M. Gorlatova is with Duke University, Durham, NC, USA e-mail: maria.gorlatova@duke.edu.

Prime Air delivery system [16]). The third is addressed via concept/model drift at different neighborhoods, and the fourth is embedded through model personalization.

Distributed Surveillance in Smart Cities: Our proposed method has natural applications to city surveillance [17]. For instance, multiple UAV swarms can be spread throughout a city, extracting data from sensors and cameras as well as those devices in rural areas without direct access to the closed-circuit cellular network to train an ML model [18], [19], [20]. Additionally, these swarms can travel to diverse neighborhoods (e.g., industrial parks vs. academic campuses) within a city, allowing for model recalibration in the presence of dynamic environments and improving the quality of personalized models through exploiting data commonality.

Machine Learning on Wireless Sensor Networks: ML techniques have been adapted for wireless sensor networks (WSN) with respect to a wide variety of tasks, e.g., object targeting and event detection [21]. Our model can be contextualized, as an example, for integrated-WSN-UAV response systems, wherein wireless sensors collect data, e.g., water level or seismic energy, and offload it to UAVs, which then train ML models [22]. The UAV swarms can travel to distant and disconnected WSNs, e.g., across a beach/coast, to gather heterogeneous and time-varying data, e.g., day vs. night tidal measurements, and train ML models at each WSN cluster, thus integrating the system together.

1.2 Related Work

This paper contributes to both literature in distributed ML over wireless networks and ML for UAV networks. Below, we provide a summary of related works and highlight the main contributions of our methodology.

Distributed ML over wireless networks: Recent literature concerning ML by wireless networks has shifted towards federated learning [23], [24], and is mostly focused on studying the convergence and behavior of federated learning over wireless networks [9], [10], [12], [25], [26], [27], [28], [29], [30], [31], [32], [33]. Conventional federated learning assumes training a single ML model for all the engaged devices. However, upon having extreme data heterogeneity across the devices, training a single model may result in poor model performance for a portion of devices. This has motivated a new trend of research in ML that aims to train user-specific ML models, referred to as multi-task learning [34], [35] or personalized federated learning [36], in the latter of which meta-gradient updates are introduced to enhance the training efficiency. As compared to this literature, we propose and investigate a new distributed ML paradigm over wireless networks called *hierarchical nested personalized federated learning* (HN-PFL) inspired by meta-gradient updates. Furthermore, we develop a new framework for network-aware HN-PFL over UAV-assisted wireless networks that considers model training under heterogeneity of resources in wireless networks. Our resulting optimization formulation balances the tradeoffs between ML model performance and network parameters such as data offloading, training batch sizes, and CPU cycles, and is also part of our contributions.

ML for UAV-assisted networks: Deep neural networks and reinforcement learning (RL) techniques have been utilized to enhance the efficiency of wireless networks [37] in problems such as beamforming [38] and user scheduling [39].

In UAV-assisted networks, especially when the UAVs are deployed as aerial base stations, RL has been utilized to carry out a variety of tasks, such as trajectory and power control for UAVs [40], [41], communication under signal jamming [42], and UAV server quality [43]. A key observation from the aforementioned existing literature is that UAV-assisted networks are difficult to model using traditional closed form methodologies and, as such, benefit from intelligent and autonomous management via RL. As compared to current literature, we introduce a new system model for UAV swarms and develop a RL method that considers UAV trajectory optimization for HN-PFL, aggregation periodicity of HN-PFL, and UAV energy management via recharging stations.

1.3 Outline and Summary of Contributions

Our contributions in this work can be summarized as follows:

- We introduce the framework of UAV-enabled online model training for a set of geo-distributed ground device clusters. We propose *stratified UAV swarms*, which presume different roles for the UAVs: (i) *leader* that micro-manages UAVs within the swarm (e.g., adjusting the CPU cycles and mini-batch sizes), and determines data transfer configurations, (ii) *worker* that conducts ML model training through *resource pooling*, and (iii) *coordinator* that enables data relaying between the devices and the worker UAVs.
- We develop hierarchical nested personalized federated learning (HN-PFL), which exploits the commonality among the data across the device clusters to produce personalized local models. Through the nesting of intra-swarm within inter-swarm aggregations, HN-PFL conducts ML model training across the *worker-leader-core* network hierarchy. We analytically characterize the convergence behavior of HN-PFL, which leads us to new convergence bounds for distributed ML.
- We integrate network-characteristics into ML training/performance by formulating a joint energy and ML performance optimization problem, which aims to configure the data offloading among devices-UAVs and UAVs-UAVs, adjust the CPU cycles of the UAVs, and obtain the mini-batch sizes used at the worker UAVs. This holistic formulation is among the first in literature to consider all these design variables together. We demonstrate that the problem belongs to the category of *complementary geometric programming* problems which are highly non-convex and NP-Hard. We then develop a distributed method, with performance guarantee, based on posynomial condensation to solve the problem for all UAV swarms in parallel.
- We formulate the problem of UAV swarm trajectory design, alongside of which we also optimize the learning duration of HN-PFL. In the formulation, we consider *online model training* under temporal data distribution variations, which is quantified via *concept/model drift*. We demonstrate that the problem solution is intractable and then cast the problem as a sequential decision making problem tackled via a deep reinforcement learning-based method.

2 SYSTEM MODEL

In this section, we introduce the system components, which include IoT device clusters (Sec. 2.1), and UAV swarms, recharging stations, and access points (Sec. 2.2).

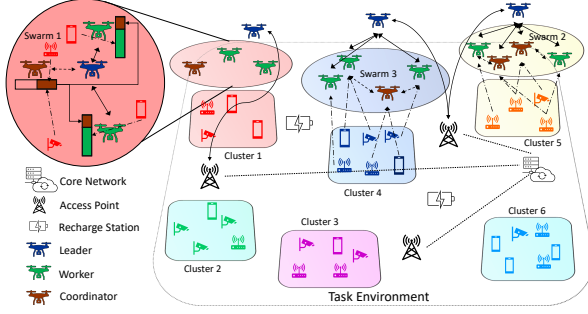


FIGURE 1: Schematic of UAV-enabled HN-PFL. The network consists of multiple IoT device clusters, stratified UAV swarms, access points, and recharging stations. UAV swarm leaders orchestrate swarm-wide ML training by workers, and manage the data collection/transfer process at workers and coordinator UAVs. Periodically, leaders travel to access points connecting to the core network, to perform a global model aggregation.

2.1 Device Clusters and Data Distributions

We consider a collection of geo-distributed IoT devices (e.g., smartphones, wireless sensors) that collect data pertinent to a learning task of interest. The devices are divided into C device clusters, denoted by $\mathcal{C} = \{\mathcal{C}_1, \dots, \mathcal{C}_C\}$, based on geographic proximity. We refer to an arbitrary device cluster via c for brevity. The size of the device cluster can be different and each device belongs to exactly one cluster.

At time instance $t \in \mathcal{T} \triangleq \{1, 2, \dots\}$, we denote $\tilde{\mathcal{D}}_i(t)$ as the set of datapoints device $i \in c$ has collected over time. Each $x \in \tilde{\mathcal{D}}_i(t)$ is a data sample containing model features and (possibly) a target variable. Different from most of the existing literature in distributed learning where the data distributions of the devices/workers are assumed to be static [9], [10], [12], [25], [26], [27], [28], [29], [30], [31], [33], we consider *online* model training and deployment (captured via the notion of *concept/model drift* in Sec. 5), where the goal is to obtain a personalized ML model for each cluster c to use for real-time inference. This is motivated by the real-world applications discussed in Sec. 1, e.g., data gathering via environmental sensors, where the data distributions can be expected to change temporally, and thus the deployed ML model should adapt to these changes.

In our scenarios of interest, the IoT devices are expected to exhibit significant heterogeneity in their computational resources (e.g., newer smartphones may possess higher-grade processors than wireless sensors). Additionally, the devices will have battery constraints and may lack consistent wireless connectivity to a central location [7]. This makes implementation of both centralized ML model training (which requires data transfer to an edge/cloud server) and traditional federated learning (which requires rapid on-device gradient computations of potentially high-dimensional models) challenging due to potential straggler effects. To account for these constraints, we assume that each device $i \in c$ stores its collected data in a buffer $\tilde{\mathcal{B}}_i$ of finite size depending on its storage capability, and that each device is capable of transmitting data over short ranges to UAVs that occasionally visit the device cluster for model training. We consider $\tilde{\mathcal{B}}_i$ as a deque so that, when filled, new datapoints will displace the oldest datapoints within $\tilde{\mathcal{B}}_i$.¹

1. Henceforth, we use calligraphic (e.g., $\tilde{\mathcal{D}}_i(t)$) to denote a set, and non-calligraphic (e.g., $\tilde{D}_i(t)$) to denote its cardinality.

2.2 Swarms, Recharging Stations, and Access Points

To enable ML model training across the computationally-limited IoT devices, we utilize a collection of UAV swarms. Each swarm will travel across device clusters, gather data from the devices, and perform model training through the methodology we will develop in Sec. 3&4. During ML model training, a set of geo-distributed gateway access points, connected through the core network, will coordinate and synchronize the model training process across the swarms. To cope with evolving data distributions at device clusters, the UAV swarms need to consistently (re-)visit the clusters and update their associated ML models (Sec. 5). During this process, UAVs may deplete their batteries and then must be rerouted to one of the geo-distributed recharging stations.

In the following, we formalize each of these network elements (for a high level visualization, see Fig. 1):

2.2.1 UAV Swarms and Stratification

We consider a set of U UAV swarms $\mathcal{U} = \{\mathcal{U}_1, \dots, \mathcal{U}_U\}$, and assume that $U < C$. We denote an arbitrary UAV swarm as u for brevity. We assume that each UAV swarm u is composed of UAVs with heterogeneous capabilities, e.g., from micro-drones weighing under 200grams that have data storage capabilities [44] to medium-sized fixed/rotatory wing UAVs that have more advanced computational capabilities [45]. Subsequently, to maximize the performance of each swarm, we propose a new *swarm stratification* model, which compared to current literature on UAV trajectory design [40], [46] is tailored specifically for ML training tasks. In our swarm stratification, there are three types of UAVs: (i) a leader ℓ_u of each swarm u , with the set of leaders across swarms denoted by $\mathcal{L} = \cup_{u \in \mathcal{U}} \ell_u$, (ii) a set of workers \mathcal{W}_u in swarm u , with the set across swarms denoted by $\mathcal{W} = \cup_{u \in \mathcal{U}} \mathcal{W}_u$, and (iii) a set of coordinators $\widehat{\mathcal{W}}_u$ in u , gathered via the set $\widehat{\mathcal{W}} = \cup_{u \in \mathcal{U}} \widehat{\mathcal{W}}_u$. For convenience, we refer to the workers and coordinators together as $\hat{u} = \mathcal{W}_u \cup \widehat{\mathcal{W}}_u = u \setminus \{\ell_u\}$. UAVs in \hat{u} collect data from nearby IoT devices, with the workers \mathcal{W}_u conducting model training based on their gathered data, and the coordinators $\widehat{\mathcal{W}}_u$ relaying data to other UAVs in \hat{u} and building a data profile of the device cluster under visit.

When swarm u arrives at some device cluster c , the leader ℓ_u scatters the UAVs \hat{u} throughout predetermined locations in c (e.g., using Voronoi diagrams [47]). All UAVs in \hat{u} gather data from devices $i \in c$ through a “wake up and sleep” paradigm, where the UAV notifies nearby IoT devices and prompts them to upload data. We denote $\mathcal{D}_j(t)$ as the dataset UAV $j \in \hat{u}$, with buffer size $B_j^D(t)$, obtains at time t . Workers \mathcal{W}_u form a pool of computation resource above the device cluster and use their gathered data for cooperative ML training, in which they engage in periodic communication with the leader ℓ_u regarding their training results. On the other hand, coordinators $\widehat{\mathcal{W}}_u$ act as *aerial data caches* to relay data to other UAVs in \hat{u} . This arrangement allows data from IoT devices with transmit power limitations to be passed to worker UAVs \mathcal{W}_u for ML training via multi-hop relaying at the coordinators if necessary. We formalize $\mathcal{D}_j(t)$, $\forall j$, through our optimization in Sec. 4.1.

2.2.2 Recharging Stations

We consider a set of geo-distributed recharging stations \mathcal{R} in the network [48], [49]. We assume that when any UAV $j \in u$

TABLE 1: Summary of Key Notations for Devices, UAVs, Network Optimization, Machine Learning, and Swarm Trajectory Design

Device Cluster, UAV Swarm, and Network			Data Processing/Offloading Optimization and Network Energy Consumption		
\mathcal{C}	Set of all device clusters	$\rho_{i,j}(t)$	Data transfer ratio from device i to UAV j	$\rho_{i,j}(t)$	Data transfer ratio from UAV i to j
\mathcal{R}	Set of recharging stations	$g_j(t)$	Adjustable CPU cycle frequency at UAV j	$\zeta_j^S(k)$	Time used by UAV j to gather data
\mathcal{A}	Set of access points	$\zeta_j^P(k)$	Time used by UAV j to process data	$E_j^{\text{Ba}}(s)$	Starting battery of UAV j at the s -th sequence
$U(s)$	Number of active swarms at s -th sequence	M	Number of bits per datapoint	\bar{M}	Number of bits used for model parameters
$\mathcal{U}(s)$	Set of active swarms at s -th sequence	Machine Learning Notation			
ℓ_u	Leader UAV of u -th swarm	F_j	Meta loss function at UAV j	f_j	ML loss over all data in \mathcal{D}_j
\mathcal{W}_u	Worker UAVs in the u -th swarm	\hat{f}_j	ML loss over a datapoint in \mathcal{D}_j	$\mathbf{w}_j(t)$	Model parameters at UAV j
\hat{u}	Non-leader UAVs in u -th swarm	$\alpha_{j,1}(t)$	Inner mini-batch ratio for UAV j	$\alpha_{j,2}(t)$	Outer mini-batch ratio for UAV j
$\hat{\mathcal{W}}_u$	Coordinator UAVs in the u -th swarm	$\alpha_{j,3}(t)$	Hessian mini-batch ratio for UAV j	t_s	Starting time for the s -th sequence
$\mathcal{D}_i(t)$	Dataset of i -th device	τ_s^L	Local aggregation period for s -th sequence	τ_s^G	Global aggregation period for s -th sequence
$\mathcal{D}_j(t)$	Dataset of j -th UAV	k	Local aggregation index	k'	Global aggregation index
$\mathcal{D}_c(t)$	Union of datasets at cluster c	Swarm Trajectory Optimization			
$B_j^P(t)$	Max dataset size for UAV j	$\mathcal{X}(s)$	Swarm positions at s -th sequence	$G_c(s)$	Online gradient as a result of model drift
T_s	Duration of the s -th sequence	$\mathcal{Z}(s)$	Network state encoding at s -th sequence	$\mathcal{H}(s)$	DRL agent action at the end of the s -th sequence
Λ_c	Model drift of cluster c	$V(s)$	Reward of the s -th sequence	Q_θ	Q-network for trajectory design

reaches a minimum battery threshold, the entire swarm u must travel to one of the recharging stations, e.g., $r \in \mathcal{R}$.

2.2.3 Access Points (AP)

We consider a set of gateway APs \mathcal{A} , which can be interpreted for example as cellular base stations. All APs $a \in \mathcal{A}$ are connected through the core network. The APs are used by the leader UAVs \mathcal{L} to communicate with the core network, which determines swarm trajectories and synchronizes ML training among the swarms.

2.3 Metrics of Interest

The evaluation of our methodology requires several primary metrics: classification loss at the UAVs (Thm. 1), the mismatch between the model performance at the UAVs vs. at the device clusters (Prop. 1), and energy consumption (Sec. 4). We will further demonstrate that our learning method provides substantial improvements compared to baselines in terms of convergence rate (Sec. 6.1), network resource savings (Sec. 6.2), and trajectory design efficiency (Sec. 6.3).

3 HIERARCHICAL NESTED PERSONALIZED FEDERATED LEARNING (HN-PFL)

In this section, we develop our UAV-enabled methodology for personalized federated learning (PFL). We begin with the rationale (Sec. 3.1), and then present the HN-PFL algorithm (Sec. 3.2). Finally, we theoretically analyze the convergence of our distributed ML method (Sec. 3.3).

3.1 Overview and Rationale

Conventional federated learning (FL) trains a single ML model suitable for all devices [50], so each device trains a local ML model periodically aggregated by the main server. As devices may exhibit heterogeneity in their data distributions, and may even have different learning objectives, training a global model used for all the devices may lead to poor overall performance. This has motivated PFL [36], which trains device-specific models by leveraging the commonality across the devices' data distributions. Additionally, PFL uses *meta-functions* to obtain faster local model convergence relative to classic gradient descent methods used in FL, and performs unweighted aggregations for device fairness and model agnostic ML. Conventional FL and PFL both assume a "star" learning topology, where a set of workers/devices are connected to a main server [7], which requires direct communication between the devices and the server.

In our setting, the UAVs perform the local model training and thus can be construed as the workers. The star topology assumed in FL/PFL applies poorly, however, as the IoT

device clusters are geographically distributed, and each UAV may not have direct uploading capability to a cellular BS or an AP due to insufficient resources (e.g., limited battery). On the other hand, UAV-to-UAV communications within a swarm is comparatively low in resource consumption, which motivates *local aggregations* inside the swarms that can be facilitated by the leader UAV. The leaders can then occasionally visit their nearest AP for global aggregation of their associated swarm model parameters. By *nesting* intra-swarm (local) aggregations within inter-swarm (global) aggregations, we develop a methodology to generalize the star topology in conventional FL/PFL to that of a *hierarchical* tree, where the ML model training is segmented into two layers: (i) swarm-level between leaders and their constituent workers, and (ii) global-level between access points/core-network and swarm leaders.

Furthermore, data distributions are unique with respect to IoT device cluster, which motivates the need for personalization of ML models. We thus exploit the meta-function approach introduced in [36] that converges rapidly compared to classic gradient descent methods, but is more computationally intensive. This is a desirable trade-off in UAV networks, since energy consumption due to levitation/hovering outweighs that of local computations [51], and faster convergence can help reduce total flight time and energy consumption (see Sec. 6.1).

The methodology we develop in this section, Hierarchical-Nested Personalized Federated Learning (HN-PFL), embeds the ML training of each swarm hierarchically within a global ML training cycle. Recently, there have been a few works on hierarchical FL, e.g., [52], which rely on gradient descent and a uniform aggregation rule among all layers. HN-PFL, by contrast, exploits meta-gradient updates to produces a dynamic ML model that considers both UAV heterogeneity and personalized ML models for device clusters.

3.2 HN-PFL Algorithm

HN-PFL breaks down the model training problem into two layers: (i) *workers-leaders*, in which the worker UAVs carry out the ML model training and the leader UAVs perform swarm-wide (local) aggregations; and (ii) *leaders-APs*, in which the leader UAVs engage in global aggregations.

Since our problem requires the swarms \mathcal{U} to travel between IoT device clusters, HN-PFL carries out the model learning through consecutive *training sequences*. Each training sequence starts when all active UAV swarms (i.e., non-recharging swarms) arrive at their designated device clusters, and concludes when the swarms finish the model training

and begin travelling to their next destination. We denote the start of the s -th training sequence, $s = 1, 2, \dots$, by $t_s \in \mathcal{T}$, its scheduled interval as $\mathcal{T}_s = \{t_s, \dots, t_s + T_s - 1\}$, and the active swarms for the s -th sequence as $\mathcal{U}(s) \subseteq \mathcal{U}$. Defining the active swarms $\mathcal{U}(s)$ with respect to the training sequence encompasses the cases where a portion of UAV swarms recharge their batteries and thus are not engaged in ML model training during \mathcal{T}_s .

At each time $t \in \mathcal{T}_s$, each worker UAV $j \in \mathcal{W}_u, u \in \mathcal{U}(s)$ conducts a *local model update*. This consists of computing its next ML model parameter vector $\mathbf{w}_j(t+1)$ using a meta-gradient update [53] defined as:

$$\mathbf{w}_j(t+1) = \mathbf{w}_j(t) - \eta_2 \nabla \tilde{F}_j(\mathbf{w}_j(t)), \quad t+1 \in \mathcal{T}_s, \quad (1)$$

where $\eta_2 > 0$ is the meta-update step-size, and $\nabla \tilde{F}_j(\mathbf{w}_j(t))$ is the mini-batch approximation of the meta-gradient $\nabla F_j(\mathbf{w}_j(t))$. $\nabla F_j(\mathbf{w}_j(t))$ is the gradient of the meta-function F_j , defined as the loss of the gradient descent procedure:

$$F_j(\mathbf{w}_j(t)) = f_j(\mathbf{w}_j(t) - \eta_1 \nabla f_j(\mathbf{w}_j(t))), \quad (2)$$

where $\eta_1 > 0$ is the step size for gradient descent and f_j is the local loss function over the local dataset $\mathcal{D}_j(t)$ at UAV j :

$$f_j(\mathbf{w}_j(t)) = \frac{\sum_{x \in \mathcal{D}_j(t)} \hat{f}(\mathbf{w}_j(t); x)}{D_j(t)}, \quad (3)$$

and $\hat{f}(\mathbf{w}_j(t); x)$ is the loss per datum x . This meta-gradient procedure effectively updates the parameters on the loss of the update rule. In particular, based on (2), it results in a set of parameters that can adapt fast to changing data distributions with a single additional gradient descent step. We approximate the gradient ∇F_j by mini-batch methods as is common in federated learning [50], [54], obtaining

$$\begin{aligned} \nabla \tilde{F}_j(\mathbf{w}_j(t)) &= \nabla \tilde{f}_j \left(\mathbf{w}_j(t) - \eta_1 \nabla \tilde{f}_j(\mathbf{w}_j(t) | \mathcal{D}_{j,1}(t)) \middle| \mathcal{D}_{j,2}(t) \right) \\ &\quad \cdot \left(\mathbf{I} - \eta_1 \nabla^2 \tilde{f}_j(\mathbf{w}_j(t) | \mathcal{D}_{j,3}(t)) \right), \end{aligned} \quad (4)$$

where ∇^2 is the Hessian operator, and $\mathcal{D}_{j,1}(t), \mathcal{D}_{j,2}(t), \mathcal{D}_{j,3}(t)$ are three independent mini-batches sampled with replacement from $\mathcal{D}_j(t)$.² We denote the mini-batch sampling ratios as $\alpha_{j,1}(t), \alpha_{j,2}(t)$, and $\alpha_{j,3}(t) \in (0, 1)$, i.e., $D_{j,i}(t) = \alpha_{j,i}(t) D_j(t)$, $i = 1, 2, 3$, and the total ratio of data at time t used for processing by worker $j \in \mathcal{W}_u, u \in \mathcal{U}(s)$ is denoted by $\alpha_j(t) = \alpha_{j,1}(t) + \alpha_{j,2}(t) + \alpha_{j,3}(t)$.

HN-PFL performs a series of local and global aggregations during each training sequence \mathcal{T}_s . We conduct local aggregations with period of τ_s^L (i.e., τ_s^L local meta-gradient updates prior to each local aggregation), and global aggregations with period of $\tau_s^L \tau_s^G$, defined such that $T_s \triangleq \tau_s^L K_s^L \equiv \tau_s^L \tau_s^G K_s^G$. τ_s^L is the local aggregation period, τ_s^G is the number of local aggregations performed before each global aggregation, K_s^L is the total number of local aggregations, and K_s^G is the total number of global aggregations conducted in \mathcal{T}_s . Using k for the local aggregation index, $t_s^L(k) = t_s + k\tau_s^L$ is the time of the k -th local aggregation in \mathcal{T}_s . Using k' as the global aggregation index, $t_s^G(k') = t_s + k'\tau_s^L \tau_s^G$ will denote the time of the k' -th global aggregation in \mathcal{T}_s .

At the k -th local aggregation, when $t = t_s^L(k)$, since worker UAVs possess heterogeneous computational capabilities

leading to different number of data points processed, HN-PFL performs a weighted average at each leader $\ell_u, u \in \mathcal{U}(s)$:

$$\bar{\mathbf{w}}_u(t) = \frac{\sum_{j \in \mathcal{W}_u} \mathbf{w}_j(t) \sum_{t'=t_s^L(k-1)+1}^t \alpha_j(t') D_j(t')}{\sum_{j \in \mathcal{W}_u} \sum_{t'=t_s^L(k-1)+1}^t \alpha_j(t') D_j(t')}. \quad (5)$$

To complete the local aggregation, the leader ℓ_u then broadcasts $\bar{\mathbf{w}}_u(t_s^L(k))$ to all worker UAVs \mathcal{W}_u . We term this process as a *swarm-wide aggregation*, and we define the corresponding swarm-wide/local meta-function \bar{F}_u for $t = t_s^L(k)$ as follows:

$$\bar{F}_u(\bar{\mathbf{w}}_u(t)) = \frac{\sum_{j \in \mathcal{W}_u} F_j(\bar{\mathbf{w}}_u(t)) \sum_{t'=t_s^L(k-1)+1}^t \alpha_j(t') D_j(t')}{\sum_{j \in \mathcal{W}_u} \sum_{t'=t_s^L(k-1)+1}^t \alpha_j(t') D_j(t')}. \quad (6)$$

After τ_s^L swarm-wide aggregations at the active swarms, the leaders $\ell_u, u \in \mathcal{U}(s)$, travel to their nearest AP, and transmit their swarm-wide parameters to the core network. At the k' -th global aggregation, when $t = t_s^G(k')$, the core network determines the global model parameters as:

$$\bar{\mathbf{w}}(t) = \frac{1}{U(s)} \sum_{u \in \mathcal{U}(s)} \bar{\mathbf{w}}_u(t). \quad (7)$$

Then, the access points \mathcal{A} broadcast $\bar{\mathbf{w}}(t_s^G(k'))$ to the leaders, which travel back to their swarm and synchronize the model parameters across their associated worker UAVs. We similarly define the global meta-function \bar{F} for $t = t_s^G(k')$ as:

$$\bar{F}(\bar{\mathbf{w}}(t)) = \frac{1}{U(s)} \sum_{u \in \mathcal{U}(s)} \bar{F}_u(\bar{\mathbf{w}}(t)). \quad (8)$$

Note that we use an *unweighted* aggregation rule in (7) and (8) across the UAV swarms, and therefore place equal importance on each swarm, unlike the weighted averages in the local aggregations. This is done to obtain a global model that is not biased towards any particular cluster of IoT devices, since different clusters are assumed to possess different data distributions and meta-functions.

At the final global aggregation of training sequence s , i.e., when $t = t_s + T_s - 1$, active swarms both from s and $s+1$ initialize the next sequence. For each $u \in \mathcal{U}(s) \cup \mathcal{U}(s+1)$, the leader ℓ_u will receive both (i) the global aggregation result $\bar{\mathbf{w}}(t_{s+1} - 1)$ and (ii) instructions on their next destinations from the APs. To conduct model personalization, those swarms which were in $\mathcal{U}(s)$ will perform a *single* stochastic gradient update followed by a swarm-wide aggregation as in (5) before transmitting their swarm-wide model $\bar{\mathbf{w}}_u(t_{s+1} - 1)$ to the IoT devices they were serving. Then, swarms in either $\mathcal{U}(s)$ or $\mathcal{U}(s+1)$ will move to their new destinations (for $u \in \mathcal{U}(s) \setminus \mathcal{U}(s+1)$, this would be a recharging station). Upon arriving at their destinations, those swarms in $\mathcal{U}(s+1)$ will begin training sequence $s+1$ by the leaders initializing their workers with $\bar{\mathbf{w}}(t_{s+1} - 1)$.

The HN-PFL algorithm developed in this section is summarized visually in Fig. 2. While we assume that during each training sequence the data distributions at the IoT device clusters are stationary, between training sequences, these distributions may change. Such changes would be particularly pronounced when a cluster has experienced a prolonged UAV swarm visit hiatus. Thus, the swarms need to return to previously visited device clusters to recalibrate their models as well. We capture the time-varying data distributions at IoT devices via introducing *model drift* (see Sec. 5.1), which is heterogeneous across device clusters.

2. The second argument in $\tilde{f}(\cdot)$ denotes the dataset used to compute the respective function.

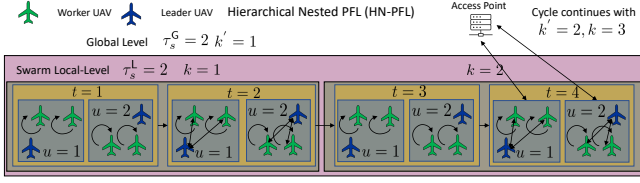


FIGURE 2: Behavior of workers, leaders, and APs in HN-PFL. Workers perform local meta-updates, and leaders aggregate their workers' model parameters with period τ_s^L . After τ_s^G local aggregations, the core network performs a global aggregation, wherein leaders' parameters are re-synchronized.

Our network-aware swarm trajectory design methodology in Sec. 5 will explicitly consider this model drift at different device clusters, in addition to the model training performance obtained via network optimized HN-PFL obtained in Sec. 4, and energy requirements of the UAVs, in determining the optimal trajectories of the UAV swarms and the frequency of local and global updates (i.e., τ_s^L and τ_s^G). We first turn to deriving a convergence bound on HN-PFL, which will be employed in the optimization formulation in Sec. 4.

Remark 1. The computational burden of the Hessian-based gradient descent in (4) can be alleviated by substituting it with approximate methods such as first order or hessian free model agnostic training [36], [53], which have been shown to attain a similar performance to that of exact Hessian computation.

3.3 Convergence Analysis of HN-PFL

In the following, we derive the performance bound of HN-PFL for non-convex loss functions. To this end, in addition to the meta functions defined in (6) and (8), we define the swarm-average loss function $\bar{f}_u(\mathbf{w})$ at $t \in \mathcal{T}_s$ as:

$$\bar{f}_u(\mathbf{w}(t)) = \sum_{j \in \mathcal{W}_u} \frac{\Delta_j(k)}{\bar{\Delta}_u(k)} f_j(\mathbf{w}(t)), \quad (9)$$

where f_j is defined as in (3), k is the most recent local aggregation index, $\Delta_j(k) = \sum_{t'=t_s^L(k-1)+1}^t \alpha_j(t') D_j(t')$, and $\bar{\Delta}_u(k) = \sum_{j \in \mathcal{W}_u} \Delta_j(k)$. Also, we define the global average loss function $\bar{f}(\mathbf{w})$ at time $t \in \mathcal{T}_s$ as:

$$\bar{f}(\mathbf{w}(t)) = \frac{1}{U} \sum_{u \in \mathcal{U}} \bar{f}_u(\mathbf{w}(t)). \quad (10)$$

While (5),(6),(9) are only realized by HN-PFL when $t = t_s^L(k)$, i.e., at a local aggregation, and while (7),(8),(10) are only realized when $t = t_s^G(k')$, i.e., at a global aggregation, defining them for each $t \in \mathcal{T}_s$ will be useful in our theoretical analysis as we model their evolution over time.

Our convergence analysis employs some standard assumptions [55], [56] on non-convex loss functions:

Assumption 1 (Loss function characteristics). We make the following assumptions on f_j at worker $j \in \mathcal{W}_u, \forall u \in \mathcal{U}$:

- 1) f_j is bounded below: $f_j(\mathbf{w}) > -\infty, \forall \mathbf{w}$.
- 2) f_j is twice continuously differentiable and its gradient is μ_j^G -Lipschitz and bounded by B_j : (i) $\|\nabla f_j(\mathbf{w}) - \nabla f_j(\mathbf{w}')\| \leq \mu_j^G \|\mathbf{w} - \mathbf{w}'\|, \forall \mathbf{w}, \mathbf{w}'$, (ii) $\|\nabla f_j(\mathbf{w})\| \leq B_j$.
- 3) The Hessian of f_j is μ_j^H -Lipschitz continuous: $\|\nabla^2 f_j(\mathbf{w}) - \nabla^2 f_j(\mathbf{w}')\| \leq \mu_j^H \|\mathbf{w} - \mathbf{w}'\|, \forall \mathbf{w}, \mathbf{w}'$.
- 4) Bounded local data variability: $\mathbb{E}[\|\nabla \hat{f}(x, \mathbf{w}) - \nabla f_j(\mathbf{w})\|^2] \leq \sigma_j^G$ and $\mathbb{E}[\|\nabla^2 \hat{f}(x, \mathbf{w}) - \nabla^2 f_j(\mathbf{w})\|^2] \leq \sigma_j^H, \forall \mathbf{w}, x$.

- 5) The variance of the gradient and Hessian of $f_j(\mathbf{w})$ are bounded: $\sum_{j \in \mathcal{W}_u} \frac{\Delta_{j,s}(k)}{\bar{\Delta}_{u,s}(k)} \|\nabla f_j(\mathbf{w}) - \nabla \bar{f}_u(\mathbf{w})\|^2 \leq \gamma_u^G$, $\sum_{j \in \mathcal{W}_u} \frac{\Delta_{j,s}(k)}{\bar{\Delta}_{u,s}(k)} \|\nabla^2 f_j(\mathbf{w}) - \nabla^2 \bar{f}_u(\mathbf{w})\|^2 \leq \gamma_u^H, \forall \mathbf{w}, k$.
- 6) The variance of the gradient and Hessian of $\bar{f}_u(\mathbf{w})$ are bounded: $\frac{1}{U} \sum_{u \in \mathcal{U}} \|\nabla \bar{f}_u(\mathbf{w}) - \nabla \bar{f}(\mathbf{w})\|^2 \leq \gamma^G$, $\frac{1}{U} \sum_{u \in \mathcal{U}} \|\nabla^2 \bar{f}_u(\mathbf{w}) - \nabla^2 \bar{f}(\mathbf{w})\|^2 \leq \gamma^H, \forall \mathbf{w}$.

We also require an assumption to characterize the loss function behavior at the device clusters:

Assumption 2 (Device cluster loss function characteristics). For device cluster c and a model parameter \mathbf{w} , let $f_c^D(\mathbf{w}) = \sum_{x \in \tilde{\mathcal{D}}_c(t)} \hat{f}(\mathbf{w}; x) / \tilde{D}_c(t)$, where $\tilde{\mathcal{D}}_c(t) \triangleq \cup_{i \in c} \tilde{D}_i(t)$, denote the local loss at time t . We assume that (i) the gradient of the loss function is μ_c^G -Lipschitz continuous, (ii) the Hessian is μ_c^H -Lipschitz continuous, (iii) $\mathbb{E}[\|\nabla \hat{f}(x, \mathbf{w}) - \nabla f_c^D(\mathbf{w})\|^2] \leq \sigma_c^G$, and (iv) $\mathbb{E}[\|\nabla^2 \hat{f}(x, \mathbf{w}) - \nabla^2 f_c^D(\mathbf{w})\|^2] \leq \sigma_c^H$.

The loss functions of many common ML models (e.g., neural networks with continuous activation functions [28]) will satisfy these assumptions. In the following analysis, we let $B = \max_j \{B_j\}$, $\mu^G = \max_j \{\mu_j^G\}$, and $\mu^H = \max_j \{\mu_j^H\}$.

Our main result in this section will be the convergence behavior of the global meta-function \bar{F} in HN-PFL (Theorem 1). To obtain this, we first derive bounds on the expected error in the meta-gradient approximations at worker UAVs (Lemma 1), and on the meta-gradient variability between workers, leaders, and the core network (Lemma 2).

Lemma 1 (Mini-batch versus full batch meta-gradients). During each training interval \mathcal{T}_s , the expected error of the mini-batch approximation $F_j(\mathbf{w}(t))$ of the true meta-gradient $F_j(\mathbf{w}(t))$ at each worker UAV $j \in \mathcal{W}_u, \forall u \in \mathcal{U}(s)$ satisfies:

$$\mathbb{E}[\|\nabla \tilde{F}_j(\mathbf{w}(t)) - \nabla F_j(\mathbf{w}(t))\|^2] \leq \sigma_j^F(t), \quad (11)$$

where

$$\sigma_j^F(t) = \underbrace{\frac{3\eta_1^2 \sigma_j^H}{\alpha_{j,3}(t) D_j(t)}}_{(a)} \underbrace{\left[B^2 + \frac{\sigma_j^G (\alpha_{j,1}(t) + (\mu^G \eta_1)^2 \alpha_{j,2}(t))}{\alpha_{j,1}(t) \alpha_{j,2}(t) D_j(t)} \right]}_{(b)} + \underbrace{\frac{12\sigma_j^G (\alpha_{j,1}(t) + (\mu^G \eta_1)^2 \alpha_{j,2}(t))}{\alpha_{j,1}(t) \alpha_{j,2}(t) D_j(t)}}_{(c)}. \quad (12)$$

Sketch of Proof: The proof uses similar techniques to those found in Lemma 4.3 in [36]. We use a different definition for the batch sizes based on our introduced data processing ratios (α -s) within the data variability in Assumption 1, and then use Cauchy-Schwarz inequality to obtain the result. ■

We make a few observations from Lemma 1 regarding the mini-batch ratios $\alpha_{j,1}(t)$, $\alpha_{j,2}(t)$, and $\alpha_{j,3}(t)$. Intuitively, if any of these are 0, then the upper bound in (11) should diverge, which is what we observe in (12). Next, the groups (a), (b), and (c) in (12) show that each mini-batch ratio has a unique impact on the bound. In particular, $\alpha_{j,3}(t)$ weighs the Hessian data variability σ_j^H in (a), while $\alpha_{j,1}(t)$ and $\alpha_{j,2}(t)$ scale the gradient data variability σ_j^G in (b) and (c). Due to the multiplicative effect of the Hessian and gradient in the meta-gradient computation (see (4)), the effects of the mini-batch ratios are coupled between (a) and (b), through which $\alpha_{j,3}(t)$ also weights the impact of σ_j^G . Hence, when we are faced with a limited budget for data

processing in a UAV swarm, the mini-batch ratios must be allocated carefully, which we will address through our optimization problem in Sec. 4.1. Additionally, by using Assumption 1, for stochastic gradient/hessian estimates we obtain $\mathbb{E}[\|\nabla \tilde{f}_j(\mathbf{w}(t); \mathcal{D}_{j,i}(t)) - \nabla f_j(\mathbf{w}(t))\|^2] \leq \frac{\sigma_j^G}{D_{j,i}(t)}$ $i \in \{1, 2\}$ and $\mathbb{E}[\|\nabla^2 \tilde{f}_j(\mathbf{w}(t); \mathcal{D}_{j,3}(t)) - \nabla^2 f_j(\mathbf{w}(t))\|^2] \leq \frac{\sigma_j^H}{D_{j,3}(t)}$, and as a result, when the full-batch counterparts are deployed, i.e., $\alpha_{j,1} = \alpha_{j,2} = \alpha_{j,3} = 1$, the local data variability can be replaced with 0 in our bound (i.e., $\sigma_j^G = \sigma_j^H = 0$) so that the bound in Lemma 1 becomes 0 as expected.

Lemma 2 (Intra- and inter-swarm meta-gradient variability). *During each training interval \mathcal{T}_s , the intra-swarm meta-gradient variability at each UAV swarm $u \in \mathcal{U}(s)$ obeys the following upper bound at local aggregation k :*

$$\sum_{j \in \mathcal{W}_u} \frac{\Delta_j(k)}{\Delta_u(k)} \|\nabla F_j(\mathbf{w}) - \nabla \bar{F}_u(\mathbf{w})\|^2 \leq \gamma_u^F, \quad (13)$$

where $\gamma_u^F = 3B^2\eta_1^2\gamma_u^H + 192\gamma_u^G$. Also, the variability of inter-swarm meta-gradients is upper bounded as follows:

$$\frac{1}{U(s)} \sum_{u \in \mathcal{U}(s)} \|\nabla \bar{F}_u(\mathbf{w}) - \nabla F(\mathbf{w})\|^2 \leq \gamma^F, \quad (14)$$

where $\gamma^F = 3B^2\eta_1^2\gamma^H + 192\gamma^G$.

Sketch of Proof: The proof uses similar techniques to those found in Lemma 4.4 in [36]. The difference is that we use weighted aggregation definition for the meta function (6) and then use Assumption 1 and Jensen's inequality. ■

Using Lemmas 1 and 2, we can bound the variance of model parameters across worker UAVs in the network achieved by HN-PFL after a given global aggregation, which is one of our key theoretical results. For brevity, all proofs are given as sketches, with the key steps emphasized. The full versions of the proofs with detailed explanations are provided in the appendices of the supplementary materials.

Proposition 1 (Parameter variability across UAVs). *During interval \mathcal{T}_s , the variance in model parameters across the active worker UAVs in the network at the k' -th global aggregation, i.e., $t = t_s^G(k')$, satisfies the following upper bound:*

$$\mathbb{E}\left[\left\|\frac{1}{U(s)} \sum_{u \in \mathcal{U}(s)} \sum_{j \in \mathcal{W}_u} \frac{\Delta_j(k'\tau_s^G)}{\Delta_u(k'\tau_s^G)} (\mathbf{w}_j(t) - \bar{\mathbf{w}}(t))\right\|^2\right] \leq \Upsilon(t) \quad (15)$$

where $\Upsilon(t)$ is defined in (16) with $\mu^F \triangleq 4\mu^G + \eta_1\mu^HB$, and $\sigma_u^F(t) = \sum_{j \in \mathcal{W}_u} \frac{\Delta_j(k'\tau_s^G)}{\Delta_u(k'\tau_s^G)} \sigma_j^F(t)$.

Sketch of Proof: The complete proof is contained in Appendix A, where we split the expression in (15) into local and global aggregation relationships and then bound each separately using different techniques. The local relationships $\mathbb{E}[\|\sum_{j \in \mathcal{W}_u} \frac{\Delta_j(k'\tau_s^G)}{\Delta_u(k'\tau_s^G)} \mathbf{w}_j(t) - \bar{\mathbf{w}}_u(t)\|^2]$ are expanded via (1), after which approximated gradients $\nabla \tilde{F}_j$ are introduced and the result simplified using Jensen's inequality. Next, applying Assumption 1 for σ_j^F and using recursive techniques over τ_s^L yields an upper bound for the local aggregation relationships. The global term $\mathbb{E}[\|\frac{1}{U(s)} \sum_{u \in \mathcal{U}(s)} \sum_{j \in \mathcal{W}_u} \frac{\Delta_j(k'\tau_s^G)}{\Delta_u(k'\tau_s^G)} \bar{\mathbf{w}}_u(t) - \bar{\mathbf{w}}(t)\|^2]$ requires separate techniques, particularly introducing approximated aggregated gradients $\nabla \tilde{F}_u$ and performing recursion over τ_s^G . ■

Considering the two terms in (16), term (a) captures the impact of the local aggregation frequency τ_s^L while term (b) captures the "nested" impact of the local-global aggregation frequency $\tau_s^L\tau_s^G$. (b) has a dominating effect over (a) as the exponent in (b) (i.e., $\tau_s^L\tau_s^G$) will be significantly larger than that of (a) (i.e., τ_s^L). Therefore, to reduce the variance of ML models \mathbf{w}_j across workers $j \in \mathcal{W}_u \forall u \in \mathcal{U}(s)$, it is preferable to reduce the global aggregation period $\tau_s^L\tau_s^G$, i.e., to conduct global aggregations more frequently; Proposition 1 suggests that the improvement is exponential. However, global aggregations consume more network resources than local aggregations in HN-PFL; it requires bidirectional communication between worker and leader UAVs, and between leaders and APs during which time non-leader UAVs continue to consume energy by remaining idle in the air. We balance this trade-off in the optimization formulation in Sec. 4.1 and learning duration design in Sec. 5.

Finally, we apply Proposition 1 to obtain our main result, which characterizes the decreasing magnitude of the gradient of (8), i.e., the global meta-function in HN-PFL, over training sequences. Since we consider non-convex ML models, the main metric of interest for learning performance is the norm squared of the meta-gradient.

Theorem 1. [Global meta-gradient over training sequences] *For training sequence \mathcal{T}_s , if $\eta_2 < \frac{1}{6\mu^F}$, we have the following upper bound on the expected cumulative average magnitude of the global meta-gradient across the active UAV swarms:*

$$\frac{1}{T_s} \sum_{t=t_s-1}^{t_s-1} \mathbb{E}[\|\nabla \bar{F}(\mathbf{w}(t))\|^2] \leq \Xi(s), \quad (17)$$

where $\Xi(s)$ is given in (18).

Sketch of Proof: It can be verified that the gradient of meta-functions is μ^F -Lipschitz continuous. Using this property for the global meta-function \bar{F} , and decomposing \bar{F} into its weighted average of constituent F_j using (6) and (8), allows us to segment the bound into two terms: (i) $\frac{1}{U(s)} \sum_{u \in \mathcal{U}(s)} \sum_{j \in \mathcal{W}_u} \frac{\Delta_j(k'\tau_s^G)}{\Delta_u(k'\tau_s^G)} [\nabla \tilde{F}_j(\mathbf{w}_j(\tau_s^L\tau_s^Gk' - 1)) - \nabla F_j(\mathbf{w}_j(\tau_s^L\tau_s^Gk' - 1))]$, which is then bounded by successively applying Jensen's inequality and Lemma 1, and (ii) $\frac{1}{U(s)} \sum_{u \in \mathcal{U}(s)} \sum_{j \in \mathcal{W}_u} \frac{\Delta_j(k'\tau_s^G)}{\Delta_u(k'\tau_s^G)} [\nabla F_j(\mathbf{w}_j(\tau_s^L\tau_s^Gk' - 1)) - \nabla F_j(\bar{\mathbf{w}}(\tau_s^L\tau_s^Gk' - 1))]$, which is bounded by Proposition 1, Lemma 1, and Lemma 2. The results are then recursively expanded to get (17). The expressions are lengthy and thus omitted. The full proof is provided in Appendix B. ■

Main takeaways. Theorem 1 yields a general bound on the average gradient for HN-PFL with time-varying mini-batch sizes. Smaller values of the bound are desired, as it indicates closeness to a stationary point. This bound quantifies how several parameters (some controllable and others a factor of the environment) affect training performance. Specifically, the bound in (18) is dependent on the mini-batch ratios and processed data sizes at the UAVs (embedded in Δ_j , and Δ_u), the initial performance of the ML model for the s -th training sequence (embedded in $F^U(\mathbf{w}(t_{s-1}))$), the data variability (embedded in σ_j^F , σ_u^F , and Υ), the gradient/Hessian characteristics (embedded in μ^F , γ_u^F , and γ^F), the local/global aggregation periods (through the nested sums), and the inner and outer step-sizes (η_1 , η_2).

$$\begin{aligned} \Upsilon(t) = & \underbrace{\left(\frac{16\eta_2^2}{U(s)} \sum_{u \in \mathcal{U}(s)} \sum_{j \in \mathcal{W}_u} \frac{\Delta_j(k' \tau_s^G)}{\Delta_u(k' \tau_s^G)} \sum_{y=1}^{\tau_s^L} \sigma_j^F(t-y) + \frac{24\eta_2^2}{U(s)} \sum_{u \in \mathcal{U}(s)} \gamma_u^F \right) \frac{1 - (8 + 48(\eta_2 \mu^F)^2)^{\tau_s^L}}{1 - (8 + 48(\eta_2 \mu^F)^2)}}_{(a)} \\ & + \underbrace{\left(\frac{16\eta_2^2}{U(s)} \sum_{u \in \mathcal{U}(s)} \sum_{y=1}^{\tau_s^L \tau_s^G} \sigma_u^F(t-y) + 24\eta_2^2 \gamma^F \right) \frac{1 - (8 + 48(\eta_2 \mu^F)^2)^{\tau_s^L \tau_s^G}}{1 - (8 + 48(\eta_2 \mu^F)^2)}}_{(b)} \end{aligned} \quad (16)$$

$$\begin{aligned} \Xi(s) \triangleq & \frac{1}{\frac{\eta_2}{2} - 6\eta_2^2 \frac{\mu^F}{2}} \left[\frac{F^U(\mathbf{w}(t_{s-1})) - (F^U)^*}{T_s} + \frac{1}{T_s} \sum_{k'=1}^{K_s^G} \sum_{k=(k'-1)\tau_s^G+1}^{\tau_s^G k'} \sum_{t=(k-1)\tau_s^L}^{\tau_s^L k-1} \left[\left(3\eta_2^2 \frac{\mu^F}{2} + \eta_2 \right) \right. \right. \\ & \left. \left. \times \left(\frac{1}{U(s)} \sum_{u \in \mathcal{U}(s)} \sum_{j \in \mathcal{W}_u} \frac{\Delta_j(k' \tau_s^G)}{\Delta_u(k' \tau_s^G)} \sigma_j^F(t) + (\mu^F)^2 \Upsilon(t_s^G(k')) \right) + 3\eta_2^2 \mu^F \frac{1}{U(s)} \sum_{u \in \mathcal{U}(s)} \gamma_u^F \right] \right] \end{aligned} \quad (18)$$

Since HN-PFL conducts ML model training at the UAVs, the bound in Theorem 1 is based on the meta-functions defined at the UAVs. To connect the performance of the ML models at UAV swarms to the performance of ML models at the device clusters, we bound their mismatch. Henceforth, since the data at UAVs is assumed to be constant within a local aggregation period k , we refer to $D_j(t) \forall j$ as $D_j(k)$.

Lemma 3 (Mismatch of meta-gradient between devices and the swarms). *Let F_c^D denote the meta-function defined based on f_c^D in Assumption 2, $\mathcal{C}(s)$ denote the set of actively trained device clusters for training sequence s , and $\bar{F}^D(\mathbf{w}(t)) = \frac{1}{|\mathcal{C}(s)|} \sum_{c \in \mathcal{C}(s)} F_c^D(\mathbf{w}(t))$, $t \in \mathcal{T}_s$, be the average meta-function for all actively trained device clusters for sequence s for a unique given parameter $\mathbf{w}(t)$ at time t . The difference between the meta-gradient computed at the UAVs vs. those of their respective device clusters for local aggregation k is bounded by:*

$$\mathbb{E} \left[\left\| \nabla \bar{F}(\mathbf{w}(t)) - \nabla \bar{F}^D(\mathbf{w}(t)) \right\|^2 \right] \leq \hat{\Xi}(k), \quad t = \tau_s^L(k), \quad (19)$$

where $\hat{\Xi}(k)$ is given by:

$$\begin{aligned} \hat{\Xi}(k) \triangleq & \frac{1}{U(s)} \sum_{u \in \mathcal{U}(s)} \sum_{j \in \mathcal{W}_u} \frac{\Delta_j(k)}{\Delta_u(k)} \left[\frac{3\eta_1^2 \sigma_{C(u,s)}^H}{D_j(k)} \left[B^2 \right. \right. \\ & \left. \left. + \frac{\sigma_{C(u,s)}^G (1 + \mu^2 \eta_1^2)}{D_j(k)} \right] + \frac{12\sigma_{C(u,s)}^G (1 + \mu^2 \eta_1^2)}{D_j(k)} \right], \end{aligned} \quad (20)$$

where $C(u, s)$ denotes the cluster under which UAV swarm u trains during sequence s .

Proof. Expanding the left hand side of (19) using the definitions of $\nabla \bar{F}$ and $\nabla \bar{F}^D$, and upper bounding it using the Jensen's inequality yields $\frac{1}{U(s)} \sum_{u \in \mathcal{U}(s)} \mathbb{E} [\| \nabla \bar{F}_u(\mathbf{w}(t)) - \nabla F_{C(u,s)}^D(\mathbf{w}(t)) \|^2]$, where we substitute $C(u, s)$ for c as the coupling of active UAV swarm to actively trained device cluster allows us to apply (6) onto $\nabla \bar{F}_u$ and yields: $\frac{1}{U(s)} \sum_{u \in \mathcal{U}(s)} \sum_{j \in \mathcal{W}_u} \frac{\Delta_j(k)}{\Delta_u(k)} \mathbb{E} [\| \nabla F_j(\mathbf{w}(t)) - \nabla F_{C(u,s)}^D(\mathbf{w}(t)) \|^2]$, following application of Jensen's inequality. Similar techniques used in Lemma 1 yield the result. ■

The bound in Lemma 3 takes the value of zero when each worker UAV both has and processes all of data at the device cluster (i.e., $D_j = \sum_{q \in \mathcal{C}(u,s)} \hat{D}_q$), which implies $\sigma_{C(u,s)}^G = 0$ and $\sigma_{C(u,s)}^H = 0$. We will employ this in our network-aware optimization formulation in the next section to ensure the mismatch between the model trained at the UAV swarm and its corresponding device cluster is small.

4 DATA PROCESSING OPTIMIZATION FOR HN-PFL

The HN-PFL algorithm in Sec. 3.2 has several design components that are introduced to optimize the ML model training. We break these down into two main components: (i) learning sequence duration and UAV swarm trajectory/movement patterns in-between training sequences, and (ii) data transfer and processing configurations at UAVs during the training sequences. These two parts are intertwined, i.e., the model training performance at different device clusters affects the UAV trajectory design, and vice versa.

Below, we address the second component, using the result of which we tackle the first part in Sec. 5. We first formulate the UAV data transfer/processing optimization problem, which trades off model performance and energy consumption in configuring data processing (Sec. 4.1). Then, we show that the resulting optimization can be characterized as a complementary geometric program, and develop an iterative distributed approach for solving it (Sec. 4.2).

4.1 Data Processing/Offloading Configuration

4.1.1 Offloading and processing models

At each training sequence s , each active UAV swarm $u \in \mathcal{U}(s)$ is located above a device cluster denoted by $\mathcal{C}(u, s) \in \mathcal{C}$. Let $A(u, s) \in \mathcal{A}$ denote the nearest AP to UAV swarm u , which leader ℓ_u will periodically visit during the model training to conduct global model aggregation. Also, let ψ_j^F denote the energy consumed per unit time by worker/coordinator UAV $j \in \mathcal{W}_u$ for flying/hovering, and $\hat{\psi}_u^F$ that of leader UAV ℓ_u . We denote the geographical distance between leader ℓ_u and its nearest AP as $d(\ell_u, A)$, and denote the movement energy consumption of the leader UAV per unit distance as $\psi_{\ell_u}^M$.

Device-UAV and UAV-UAV data transfers are carried out at the beginning of local aggregation rounds, i.e., when $t = t_s^L(k)$. The data received by the worker UAVs is used throughout the local aggregation period. Upon engaging in data transmission, each device $i \in \mathcal{C}(u, s)$ samples data points uniformly at random from its local buffer and transmits them to the UAVs. We let $\rho_{i,j}(k) \in [0, 1]$ denote the fraction of datapoints in the local dataset $\hat{D}_i(k)$ of the device that is transmitted to worker/coordinator UAV $j \in \hat{u}$. Coordinator UAVs act as data caches that facilitate multi-hop data relaying between the devices to worker UAVs used for ML model training. We let $\varrho_{h,j}(k) \in [0, 1]$ denote the fraction of the datapoints in the local dataset of the coordinator UAV $h \in \hat{\mathcal{W}}_u$ that is forwarded to another UAV $j \in \mathcal{W}_u$. Each

worker UAV $j \in \mathcal{W}_u$ is assumed to process data with CPU cycle frequency $g_j(k) \in [g_j^{\min}, g_j^{\max}]$.

For sequence s , we denote the transmit powers of device i , UAV j , and leader ℓ_u by $P_i(s)$, $P_j(s)$, and $P_{\ell_u}(s)$, respectively. Through transmissions, either data or model parameters are transferred. We denote the number of bits used to represent one data point as \tilde{M} , and the number of bits used to represent the one model parameter vector as M .

UAV-to-UAV data transmissions are carried out through air-to-air (A2A) channels, which are considered to be line-of-sight (LoS). Device-to-UAV and leader UAV-to-AP data transmissions are performed through ground-to-air (G2A) and air-to-ground (A2G) channels, respectively, which are a mixture of LoS and non-line-of-sight (NLoS) links. Denoting $d(a, b)$ as the geographical distance between two nodes a and b ($a, b \in \mathcal{U} \cup \mathcal{C}$), the path-loss model for the LoS link between two nodes a and b is then given by [57]:

$$L_{a,b}^{\text{A2A}} = \eta^{\text{LoS}} (\mu^{\text{Tx}} d(a, b))^{\alpha^{\text{PL}}}, \quad (21)$$

where $\eta^{\text{LoS}} > 1$ denotes the excessive path loss factor for the LoS link, α^{PL} is the path-loss exponent, and $\mu^{\text{Tx}} = 4\pi f^{\text{Tx}}/c^{\text{light}}$ with c^{light} denoting the speed of light and f^{Tx} denoting the carrier frequency. For the G2A/A2G channel, the probability of having an LoS link between two nodes a and b is given by [57], [58]: $P_{a,b}^{\text{LoS}} = (1 + \psi^{\text{Tx}} \exp(-\beta^{\text{Tx}}[\theta_{ab} - \psi^{\text{Tx}}]))^{-1}$, where ψ^{Tx} and β^{Tx} are constants depending on the carrier frequency and the conditions of the environment, and $\theta_{a,b}$ is the elevation angle between the respective nodes defined as: $\theta_{a,b} = \frac{180}{\pi} \times \sin^{-1} \left(\frac{\Delta h_{a,b}}{d(a,b)} \right)$, with $\Delta h_{a,b}$ denoting the difference in altitude between nodes a and b . The probability of NLoS link is given by $P_{a,b}^{\text{NLoS}} = 1 - P_{a,b}^{\text{LoS}}$. With this, the path-loss of an A2G/G2A link from node a to node b can be obtained as:

$$L_{a,b}^{\text{A2G}} = (\mu^{\text{Tx}} d(a, b))^{\alpha^{\text{PL}}} [P_{a,b}^{\text{LoS}} \times \eta^{\text{LoS}} + P_{a,b}^{\text{NLoS}} \times \eta^{\text{NLoS}}], \quad (22)$$

where $\eta^{\text{NLoS}} > \eta^{\text{LoS}}$ denotes the excessive path loss factor for the NLoS link. Finally, the data-rate between two nodes a and b is given by:

$$R_{a,b} = \bar{B}_{a,b} \log_2 \left(1 + \frac{P_a/L_{a,b}}{\sigma^2} \right), \quad a, b \in \mathcal{U} \cup \mathcal{C}, \quad (23)$$

where $\bar{B}_{a,b}$ denotes the bandwidth, $\sigma^2 = N_0 \bar{B}_{a,b}$ denotes the noise power with N_0 as the noise spectral density, P_a is the transmit power of node a , and $L_{a,b}$ is the path-loss obtained through either (21) or (22). In our later formulation, we use the notation $R_{a,b}(s)$ to denote the data rate between two nodes a and b , given their transmit powers and locations during training sequence s . We ignore interference caused by simultaneous data transmissions to the UAVs as they are stationary and can use orthogonal frequency bands [59].

We denote the time used for data gathering at UAV j as $\zeta_j^{\text{G}}(k)$, and the time used for data processing as $\zeta_j^{\text{P}}(k)$. We also define ζ^{Local} as the maximum allowable time for data gathering and local computation before each UAV transmits its parameters to the leader UAV for aggregation.

4.1.2 Joint energy and performance optimization

With the aforementioned models in hand, we formulate the following optimization problem for determining data offloading/processing configuration at training sequence s :

$$(\mathcal{P}) : \min_{\rho, \varrho, \alpha, g} \underbrace{(1 - \theta) \left(\theta_1 \Xi(s) + \theta_2 \sum_{k=1}^{K_s} \hat{\Xi}(k) \right)}_{(a)} \quad (24)$$

$$+ \theta \underbrace{\sum_{k=1}^{K_s} \sum_{u \in \mathcal{U}(s)} \left[\sum_{j \in \widehat{\mathcal{W}}_u} E_j^{\text{Tx}, \text{U}}(k) + \sum_{j \in \mathcal{W}_u} E_j^{\text{P}}(k) + \sum_{i \in \mathcal{C}(u, s)} E_i^{\text{Tx}, \text{C}}(k) \right]}_{(b)} \quad (24)$$

s.t.

$$E_j^{\text{P}}(k) = \tau_s^{\text{L}} \frac{a_j c_j}{2} (\alpha_j(k)) D_j(k) g_j^2(k), \quad j \in \mathcal{W}_u, \forall u \quad (25)$$

$$E_i^{\text{Tx}, \text{C}}(k) = \sum_{j \in \widehat{\mathcal{U}}} \frac{\rho_{i,j}(k) \tilde{D}_i(k) \tilde{M}}{R_{i,j}(s)} P_i(s), \quad i \in \mathcal{C}(u, s), \forall u \quad (26)$$

$$E_j^{\text{Tx}, \text{U}}(k) = \sum_{h \in \mathcal{W}_u} \frac{\varrho_{j,h}(k) D_j(k) \tilde{M}}{R_{j,h}(s)} P_j(s), \quad j \in \widehat{\mathcal{W}}_u, \forall u \quad (27)$$

$$E_j^{\text{Tx}, \text{W}} = K_s^{\text{L}} P_j(s) M / R_{j, \ell_u}(s), \quad j \in \mathcal{W}_u, \forall u \quad (28)$$

$$E_{\ell_u}^{\text{Tx}, \text{L}} = K_s^{\text{L}} P_{\ell_u}(s) \max_{j \in \mathcal{W}_u} \{M / R_{\ell_u, j}(s)\}, \quad \forall u \quad (29)$$

$$E_j^{\text{F}, \text{U}} = T_s \psi_j^{\text{F}}, \quad j \in \widehat{\mathcal{U}}, \forall \widehat{u} \quad (30)$$

$$E_{\ell_u}^{\text{F}, \text{L}} = T_s \psi_{\ell_u}^{\text{F}} + 2K_s^{\text{G}} \psi_u^{\text{M}}(d(\ell_u, A)), \quad \forall u \quad (31)$$

$$\sum_{k=1}^{K_s} E_j^{\text{P}}(k) + E_j^{\text{Tx}, \text{W}} + E_j^{\text{F}, \text{U}} \leq E_j^{\text{Ba}}(s) - E_j^{\text{Th}}, \quad j \in \mathcal{W}_u, \forall u \quad (32)$$

$$\sum_{k=1}^{K_s} E_j^{\text{Tx}, \text{U}}(k) + E_j^{\text{F}, \text{U}} \leq E_j^{\text{Ba}}(s) - E_j^{\text{Th}}, \quad j \in \widehat{\mathcal{W}}_u, \forall u \quad (33)$$

$$E_{\ell_u}^{\text{Tx}, \text{L}} + E_{\ell_u}^{\text{F}, \text{L}} \leq E_{\ell_u}^{\text{Ba}}(s) - E_{\ell_u}^{\text{Th}}, \quad \forall u \quad (34)$$

$$\sum_{j \in \widehat{\mathcal{U}}} \rho_{i,j}(k) \leq 1, \quad i \in \mathcal{C}(u, s), \forall u \quad (35)$$

$$\sum_{h \in \mathcal{W}_u} \varrho_{j,h}(k) \leq 1, \quad j \in \widehat{\mathcal{W}}_u, \forall u \quad (36)$$

$$D_j(k) = \sum_{i \in \mathcal{C}(u, s)} \rho_{i,j}(k) \tilde{D}_i(k) + \sum_{h \in \widehat{\mathcal{W}}_u} \varrho_{h,j}(k) D_h(k) \leq B_j^{\text{D}}(k), \quad j \in \mathcal{W}_u, \forall u \quad (37)$$

$$D_j(k) = \sum_{i \in \mathcal{C}(u, s)} \rho_{i,j}(k) \tilde{D}_i(k) \leq B_j^{\text{D}}(k), \quad j \in \widehat{\mathcal{W}}_u, \forall u \quad (38)$$

$$\zeta_j^{\text{G}}(k) + \zeta_j^{\text{P}}(k) \leq \zeta^{\text{Local}}, \quad j \in \mathcal{U}, \forall u \quad (39)$$

$$\zeta_j^{\text{G}}(k) = \sum_{i \in \mathcal{C}(u, s)} \rho_{i,j}(k) \tilde{D}_i(k) \tilde{M} / R_{i,j}(s) + \sum_{h \in \widehat{\mathcal{W}}_u} \varrho_{h,j}(k) D_h(k) \tilde{M} / R_{h,j}(s), \quad j \in \widehat{\mathcal{U}}, \forall \widehat{u} \quad (40)$$

$$\zeta_j^{\text{P}}(k) = \tau_s^{\text{L}} c_j \alpha_j(k) D_j(k) / g_j(k), \quad j \in \mathcal{W}_u, \forall u \quad (41)$$

$$g_j^{\min} \leq g_j(k) \leq g_j^{\max}, \quad j \in \mathcal{W}_u, \forall u \quad (42)$$

$$0 \leq \rho_{i,j}(k) \leq 1, \quad i \in \mathcal{C}(u, s), j \in \widehat{\mathcal{U}}, \forall u \quad (43)$$

$$0 \leq \varrho_{h,j}(k) \leq 1, \quad h \in \widehat{\mathcal{W}}_u, j \in \mathcal{W}_u \quad (44)$$

$$\alpha_j(k) = \alpha_{j,1}(k) + \alpha_{j,2}(k) + \alpha_{j,3}(k), \quad j \in \mathcal{W}_u, \forall u \quad (45)$$

$$0 < \alpha_{j,1}(k), \alpha_{j,2}(k), \alpha_{j,3}(k) \leq 1, \quad j \in \mathcal{W}_u, \forall u \quad (46)$$

Objective and variables. The objective function in (24) captures the tradeoff between the expected ML model performance (term (a)) and the energy consumption during

the training sequence (term (b)). Term (a) encompasses both the ML performance at the active UAV swarms (through Ξ) and the mismatch to the ML performance at the device cluster (through $\hat{\Xi}$), which we quantified in Theorem 1 and Lemma 3. We weigh the importance of the two terms in (a) with normalized positive coefficients θ_1 and θ_2 . The coefficient $\theta \in [0, 1]$ weighs the importance of the terms in the objective function. The variables in the problem are the device-to-UAV data transfer configurations $\rho = \{\rho_{i,j}\}_{i \in \mathcal{C}(u,s), j \in \hat{u}, u \in \mathcal{U}(s)}$, the UAV-to-UAV data transfer configurations $\varrho = \{\varrho_{h,j}\}_{h \in \hat{\mathcal{W}}_u, j \in \mathcal{W}_u, u \in \mathcal{U}(s)}$, the mini-batch ratios $\alpha = \{\alpha_{j,1}, \alpha_{j,2}, \alpha_{j,3}\}_{j \in \mathcal{W}_u, u \in \mathcal{U}(s)}$, and the UAV CPU frequency cycles $\mathbf{g} = \{g_j\}_{j \in \mathcal{W}_u, u \in \mathcal{U}(s)}$.

For the energy objective terms, $E_j^P(k)$ in (25) denotes the energy consumption used for processing data during each meta-gradient update at worker UAV $j \in \mathcal{W}_u$, where a_j is the effective capacitance coefficient of UAV j 's chipset [25], and c_j is the number of CPU cycles to process each datapoint. In (26), $E_i^{\text{Tx},C}(k)$ is the energy used for data transmission (Tx) from device i in cluster $\mathcal{C}(u, s)$ to the UAVs. In (27), we define $E_j^{\text{Tx},U}(k)$ as the energy used for data transmissions from coordinator UAV $j \in \hat{\mathcal{W}}_u$ to other UAVs. In (28), $E_j^{\text{Tx},W}$ denotes the total energy consumed for ML model parameter transmission from worker UAV $j \in \mathcal{W}_u$ to its associated leader, which occurs K_s^L times during the training sequence. In (29), $E_{\ell_u}^{\text{Tx},L}$ captures the energy consumption used for parameter transmission through broadcasting from leader ℓ_u to worker UAVs $j \in \mathcal{W}_u$. In (30), $E_j^{\text{F},U}$ represents the total energy used for flying/hovering by UAV $j \in \hat{u}$ for the s -th training sequence, which can be obtained using the result of [60] for fixed-wing UAVs, and the result of [61] for rotatory wing UAVs. In (31), $E_{\ell_u}^{\text{F},L}$ captures the energy consumption for flying by leaders ℓ_u , accounting for levitation and round-trips to the nearest APs at the global aggregation instances, both of which can be obtained as in [60], [61].

Constraints. Constraint (32) ensures that the total energy consumed by each worker UAV j for data processing, parameter transmission and flying is less than $E_j^{\text{Ba}}(s) - E_j^{\text{Th}}$, where $E_j^{\text{Ba}}(s)$ represents the battery energy at j at the start of the s -th training sequence and E_j^{Th} encompasses both (i) surplus idle energy needed for extra hovering time caused by potential asynchronicity due to the heterogeneity of leader UAV to AP travel times, and (ii) the minimum energy threshold for j to reach the nearest recharging station after the conclusion of the training sequence. Constraint (33) imposed on the coordinator UAVs is similar to (32), except that coordinator UAVs only conduct data transmission while flying. Constraint (34) imposed on the leader UAVs guarantees that there is enough energy remaining after parameter broadcasting and flying to reach the nearest recharging station. Constraints (35) and (36) ensure that the total amount of data offloaded from each device $i \in \mathcal{C}(u, s)$ and each coordinator UAV $h \in \hat{\mathcal{W}}_u$ is less than the size of the available data set. As a result of this offloading, (37) and (38) capture the total number of datapoints at the UAVs. Constraint (39) ensures that the accumulated time used for data gathering $\zeta_j^G(k)$ and local data processing $\zeta_j^P(k)$ at each worker UAV j during one local aggregation is lower than the maximum allowable time for parameter transfer to the corresponding leader UAV ζ^{Local} . These two quantities are

in turn defined in (40) and (41). Finally, constraints (42)-(46) ensure the feasibility of the optimization variables.

Complementary geometric program. \mathcal{P} is a non-convex problem, since products of the optimization variables are present in the objective. For instance, in the definition $E_j^P(n)$ in (25), there are multiplications between all four variable types: α , g , ρ , and ϱ (the last two are encompassed in term D_j according to (37)). In fact, this problem can be categorized as a *complementary geometric program* [62], a particular class of non-convex and NP-hard optimization problems. Based on this classification, we will develop a distributed iterative approach to solve \mathcal{P} where at each iteration an approximation of the problem in the format of a geometric program (GP) is considered.

4.2 Distributed Algorithm for Data Processing/Offloading Optimization

To solve \mathcal{P} , we first make two key observations:

Observation 1: Complementary Geometric Programming. GP is a method for converting a non-convex optimization problem into convex form when the objective and constraints are composed of *monomials* and *posynomials*. We provide an overview of this for the interested reader in Appendix C. Although the objective in \mathcal{P} is composed of multiplications between the variables, it does not follow the format of GP: the expressions of Ξ and $\hat{\Xi}$ consist of terms that are in the format of ratio of two posynomials, which are not posynomials (e.g., $\frac{\Delta_u}{\Delta_u}$, Υ , and σ_j^F , each of which contain arithmetic relationships of ρ and ϱ in the denominators). Rather, \mathcal{P} is a complementary GP, which cannot readily be translated to convex form [62]. We exploit a method based on *posynomial condensation* to approximate the ratios of two posynomials appearing in the expressions of Ξ and $\hat{\Xi}$ (via approximating Δ_u and D_j where needed) as the ratio between a posynomial and a monomial. Since the ratio of a posynomial and a monomial is a posynomial, we then can convert the approximations into geometric programs.

Observation 2: Potential of Distributed Implementation. In \mathcal{P} , all of the constraints are separable with respect to the UAV swarm index u , and the objective function (including the terms Ξ and $\hat{\Xi}$) can be written as a sum of separable functions with respect to the UAV swarm index. In practice, however, γ^F (defined in Lemma 2) and μ^F (defined in Proposition 1) cannot be locally and independently computed by UAV swarms $u \in \mathcal{U}(s)$, as it depends on the maximum over all worker UAVs in the network. We can approximate γ^F and μ^F by estimating it at the core network at the instance of global aggregations, and subsequently broadcast it to the leader UAVs through the APs. With the knowledge of γ^F and μ^F at the swarm leaders, the problem can then be decomposed among the local aggregation instances $k \in \{1, \dots, K_s^L\}$ and solved distributively by each swarm $u \in \mathcal{U}(s)$ at its leader.

Developing the solver: First, we must convert the ratio of posynomials in the objective of \mathcal{P} into that of a posynomial and a monomial. To do so, we iteratively approximate the posynomial denominators, which are Δ_u and D_j in our case, using the arithmetic-geometric mean inequality (see Lemma 5 in Appendix C). The resulting approximations for iteration $m+1$ are given in (48) and (51), where m is the iteration index. Here, the solution to the

$$\bar{\Delta}_u(k) \triangleq \sum_{j \in \mathcal{W}_u} \left(\alpha_{j,1}(k) + \alpha_{j,2}(k) + \alpha_{j,3}(k) \right) \left(\sum_{i \in \mathcal{C}(u,s)} \rho_{i,j}(k) \tilde{D}_i(k) + \sum_{h \in \tilde{\mathcal{W}}_u} \sum_{i \in \mathcal{C}(u,s)} \varrho_{h,j}(k) \rho_{i,h}(k) \tilde{D}_i(k) \right) \quad (47)$$

$$\begin{aligned} \bar{\Delta}_u(k) \geq \hat{\Delta}_u(k) \triangleq & \prod_{j \in \mathcal{W}_u} \left[\prod_{i \in \mathcal{C}(u,s)} \left[\left(\frac{\tilde{\delta}_{i,j,1}(k) [\bar{\Delta}_u(k;m)]}{\tilde{\delta}_{i,j,1}(k;m)} \right)^{\frac{\tilde{\delta}_{i,j,1}(k;m)}{\bar{\Delta}_u(k;m)}} \left(\frac{\tilde{\delta}_{i,j,2}(k) [\bar{\Delta}_u(k;m)]}{\tilde{\delta}_{i,j,2}(k;m)} \right)^{\frac{\tilde{\delta}_{i,j,2}(k;m)}{\bar{\Delta}_u(k;m)}} \left(\frac{\tilde{\delta}_{i,j,3}(k) [\bar{\Delta}_u(k;m)]}{\tilde{\delta}_{i,j,3}(k;m)} \right)^{\frac{\tilde{\delta}_{i,j,3}(k;m)}{\bar{\Delta}_u(k;m)}} \right] \right. \\ & \left. \prod_{h \in \tilde{\mathcal{W}}_u} \prod_{i \in \mathcal{C}(u,s)} \left[\left(\frac{\delta_{j,h,i,1}(k) [\bar{\Delta}_u(k;m)]}{\delta_{j,h,i,1}(k;m)} \right)^{\frac{\delta_{j,h,i,1}(k;m)}{\bar{\Delta}_u(k;m)}} \left(\frac{\delta_{j,h,i,2}(k) [\bar{\Delta}_u(k;m)]}{\delta_{j,h,i,2}(k;m)} \right)^{\frac{\delta_{j,h,i,2}(k;m)}{\bar{\Delta}_u(k;m)}} \left(\frac{\delta_{j,h,i,3}(k) [\bar{\Delta}_u(k;m)]}{\delta_{j,h,i,3}(k;m)} \right)^{\frac{\delta_{j,h,i,3}(k;m)}{\bar{\Delta}_u(k;m)}} \right] \right], \end{aligned} \quad (48)$$

where

$$\tilde{\delta}_{j,i,n}(k) \triangleq \alpha_{j,i}(k) \rho_{i,j}(k) \tilde{D}_i(k), \quad \delta_{j,h,i,n}(k) \triangleq \alpha_{j,i}(k) \varrho_{h,j}(k) \rho_{i,h}(k) \tilde{D}_i(k), \quad n \in \{1, 2, 3\}. \quad (49)$$

$$D_j(k) \triangleq \sum_{i \in \mathcal{C}(u,s)} \rho_{i,j}(k) \tilde{D}_i(k) + \sum_{h \in \tilde{\mathcal{W}}_u} \sum_{i \in \mathcal{C}(u,s)} \varrho_{h,j}(k) \rho_{i,h}(k) \tilde{D}_i(k), \quad (50)$$

$$D_j(k) \geq \hat{D}_j(k) \triangleq \prod_{i \in \mathcal{C}(u,s)} \left(\frac{\tilde{\lambda}_{i,j}(k) D_j(k;m)}{\tilde{\lambda}_{i,j}(k;m)} \right)^{\frac{\tilde{\lambda}_{i,j}(k;m)}{D_j(k;m)}} \prod_{h \in \tilde{\mathcal{W}}_u} \prod_{i \in \mathcal{C}(u,s)} \left(\frac{\lambda_{h,i,j}(k) D_j(k;m)}{\lambda_{h,i,j}(k;m)} \right)^{\frac{\lambda_{h,i,j}(k;m)}{D_j(k;m)}}, \quad (51)$$

where

$$\lambda_{i,j}(k) \triangleq \rho_{i,j}(k) \tilde{D}_i(k), \quad \tilde{\lambda}_{h,i,j}(k) \triangleq \varrho_{h,j}(k) \rho_{i,h}(k) \tilde{D}_i(k). \quad (52)$$

Algorithm 1: Distributed network-aware optimization of HN-PFL under partial global knowledge

input : Convergence criterion between two consecutive iterations. Estimated Lipschitz continuity factors (i.e., μ^G , μ^H , and μ^F), estimated data variability (i.e., σ^H and σ^G), and estimated data quantities (i.e., $D_j(k)$) at devices, all of which are obtained based on historical data observations.

```

1 // Procedure at the UAV swarms
2 for  $k' \in \{1, \dots, K_s^G\}$  do
3   // Procedure at the core network
4   for  $\ell_u \in \mathcal{L}(s)$  do
5     // Procedure conducted across the UAV swarms in parallel
6     // using their leader
7     for  $k \in \{(k' - 1)\tau_s^G + 1, \dots, k'\tau_s^G\}$  do
8       Initialize the iteration count  $m = 0$ .
9       Choose an initial feasible point
10       $\mathbf{x}[0] = [\rho[0], \varrho[0], \alpha[0], \mathbf{g}[0]]$  for  $\tilde{\mathcal{P}}_0$  at  $k$ .
11      while convergence criterion is not met OR  $m = 0$  do
12        Obtain the scalar values for  $\bar{\Delta}_u(k, m)$ ,
13         $\tilde{\delta}_{j,i,n}(k; m)$ ,  $\delta_{j,h,i,n}(k; m)$ ,  $D_j(k, m)$ , and
14         $\lambda_{i,j}(k; m)$ ,  $\tilde{\lambda}_{h,i,j}(k; m)$  by substituting  $\mathbf{x}[m]$ 
15        in (47), (49), (50), and (52).
16        Use the above scalars to obtain the monomial
17        approximations given in (48) and (51), and
18        replace them in  $\tilde{\mathcal{P}}_m$ .
19        Apply the logarithmic change of variables and
20        take the log from the constraints of  $\tilde{\mathcal{P}}_m$  and
21        convert it to a convex optimization problem
22        (as in (93) in Appendix C).
23        Solve the resulting convex optimization
24        problem to obtain  $\mathbf{x}[m+1]$  (e.g., using
25        CVX [63]), and set  $m = m + 1$ .
26      Choose the obtained point as
27       $\mathbf{x}^* = \mathbf{x}[m] = [\rho^*, \varrho^*, \alpha^*, \mathbf{g}^*]$ .
28    The leader broadcasts the solution  $\mathbf{x}^*$  among its
29    constituent workers/coordinators/devices to start
30    their respective data transfer procedures, and
31    specifically for workers to tune their CPU cycles and
32    mini-batch sizes.
```

problem in the m -th approximation iteration is denoted $\mathbf{x}[m] = \{\varrho[m], \rho[m], \alpha[m], \mathbf{g}[m]\}$. $\bar{\Delta}_u(k; m)$, $\delta_{j,h,i,n}(k; m)$, and $\tilde{\delta}_{j,i,n}(k; m)$, $n \in \{1, 2, 3\}$ in (48) and $D_j(k; m)$, $\lambda_{h,i,j}(k; m)$, and $\tilde{\lambda}_{i,j}(k; m)$ in (51) are scalar values obtained by substituting the solution at iteration m (i.e., $\mathbf{x}[m]$) in

the corresponding expressions in (47), (49), (50), and (52), respectively. It can be verified that the approximations in (48) and (51) are in fact the best local monomial approximations to their respective posynomials near the fixed point $\mathbf{x}[m]$ in the sense of the first-order Taylor approximation.

We solve \mathcal{P} in a distributed manner at each UAV swarm through sequentially applying the above approximations to obtain problem $\tilde{\mathcal{P}}_m$ at iteration m . In $\tilde{\mathcal{P}}_m$, each constraint is an inequality on posynomials, and the objective function is a sum of posynomials, admitting the GP format:

$$(\tilde{\mathcal{P}}_m) : \min_{\rho, \varrho, \alpha, \mathbf{g}} (1 - \theta)(\tilde{a})_m + \theta(b) \quad \text{s.t.} \quad (25) - (46),$$

where term $(\tilde{a})_m$ is obtained from term (a) in problem \mathcal{P} by: (i) decomposing (a) into a sum of separable functions with respect to UAV swarm indexes; and then (ii) using the expressions in (48) and (51) for iteration m in (a) . Note that term (b) defined in (24) is indexed by UAV swarm u , and the constraints of $\tilde{\mathcal{P}}$ are with respect to UAV swarm.

The pseudocode of our resulting sequential approximation method is given in Algorithm 1. The problem is solved at the beginning of each global aggregation interval k' by the leader UAVs in each active swarm. The following proposition shows that the algorithm has the most desirable convergence properties for a non-convex solver:

Proposition 2. *Algorithm 1 generates a sequence of improved feasible solutions for problem \mathcal{P}_m that converge to a point \mathbf{x}^* satisfying the Karush-Kuhn-Tucker (KKT) conditions of \mathcal{P} .*

Sketch of Proof: The proof uses the fact that the algorithm iteratively solves an *inner approximation* for problem \mathcal{P} , where sufficient conditions for convergence to KKT solutions expressed in [64] are satisfied. Details are in Appendix D. ■

5 SWARM TRAJECTORY AND ML DESIGN

Given the solution of the network-aware model training using HN-PFL at some training sequence s developed in the Sec. 3 and Sec. 4, the next step in our framework is to determine the macro trajectories³ of the UAV swarms

3. Micro-trajectories of the UAVs, i.e., how individual UAVs are spread throughout a device cluster and their 3D positions are not the focus of this work and can be computed apriori at the core network [61], [65].

with respect to global ML performance, i.e., the order with which the UAV swarms visit device clusters, and the duration of model training composed of local and global aggregation periods captured via parameters T_s , τ_s^L , and τ_s^G , $\forall s$. Designing these parameters is intertwined with (i) the learning performance obtained in Sec. 4, (ii) the online data variations at the device clusters, and (iii) UAV movement energy consumption used for traveling among the clusters.

5.1 Online Model Training under Model/Concept Drift

Since we consider *online model training*, where the data distributions at the devices is time varying, the performance of the local model changes over time. To capture this effect, we introduce the notion of *model/concept drift*.

Definition 1 (Model/Concept Drift). *For device cluster c with local meta-loss function F_c , we denote the online model drift at time t by $\Lambda_c(t) \in \mathbb{R}^+$, which captures the maximum variation of the gradient for any given model parameter across two consecutive time instances; mathematically:*

$$\left\| \nabla F_c(\mathbf{w} | \tilde{\mathcal{D}}(t)) - \nabla F_c(\mathbf{w} | \tilde{\mathcal{D}}(t-1)) \right\|^2 \leq \Lambda_c(t), \forall \mathbf{w} \quad (53)$$

It can be construed that device clusters with higher values of model drift will require more frequent recalibration of their local models (achieved via UAV swarms re-visits), as their current local models become obsolete faster. In contrast, device clusters with small fluctuations in local gradient, i.e., smaller values of model drift, may not be worth revisiting, due to marginal rewards (in terms of model performance gains) per energy consumed. Also, in scenarios with highly dynamic data, i.e., majority of device clusters experience large and consistent model/concept drift, the learning duration T_s should be smaller as the network will require swarms to recalibrate local models more frequently. The model drift can be estimated every time a UAV swarm returns to a previously visited cluster by measuring the change in meta-gradient calculated beforehand vs. the current meta-gradient computed by the UAVs upon arrival.

Next, we demonstrate how the model drift can be utilized to estimate the performance of the local model given the current data distribution at the device clusters:

Lemma 4 (Estimating online gradient via model drift). *Let t_c^V denote a time instance when device cluster c got visited by a UAV swarm, $\mathbf{w}_c(t_c^V)$ denote the corresponding local model, and $\nabla F_c(\mathbf{w}_c(t_c^V) | \tilde{\mathcal{D}}_c(t_c^V))$ denote the local gradient. Consider time instance $t \geq t_c^V + 1$, where during the time interval $[t_c^V + 1, t]$ cluster c remains unvisited by UAV swarms. Given the updated data at device cluster c , i.e., $\tilde{\mathcal{D}}_c(t)$, the local meta gradient at the device cluster for the outdated local model is upper bounded as:*

$$\begin{aligned} \left\| \nabla F_c(\mathbf{w}_c(t_c^V) | \tilde{\mathcal{D}}_c(t)) \right\|^2 &\leq \underbrace{(t - t_c^V + 1) \left\| \nabla F_c(\mathbf{w}_c(t_c^V) | \tilde{\mathcal{D}}_c(t_c^V)) \right\|^2}_{(a)} \\ &\quad + \underbrace{(t - t_c^V + 1) \sum_{t'=t_c^V+1}^t \Lambda_c(t')}_{(b)}, \end{aligned} \quad (54)$$

where $\Lambda_c(\cdot)$ is defined in (53). Subsequently, assuming an upper bound on the model drift at the device cluster $\Lambda_c(t') \leq \Lambda_c$, $t' \in [t_c^V + 1, t]$, we have: $\left\| \nabla F_c(\mathbf{w}_c(t_c^V) | \tilde{\mathcal{D}}_c(t)) \right\|^2 \leq (t - t_c^V + 1) \left\| \nabla F_c(\mathbf{w}_c(t_c^V) | \tilde{\mathcal{D}}_c(t_c^V)) \right\|^2 + (t - t_c^V + 1)(t - t_c^V)\Lambda_c$.

Sketch of Proof: The proof is carried out using the definition of model drift in (53) and applying the Cauchy-Schwarz inequality. Refer to Appendix E for the complete proof. ■

The bound in (54) demonstrates that the real-time performance of the outdated model, measured through the value of the meta gradient, becomes obsolete linearly with time (term (a)) and cumulative value of the model drift at the device cluster (term (b)). We will incorporate this result in the design of UAV swarm trajectories.

5.2 Problem Formulation and DRL Characteristics

5.2.1 Preface and Background

In the following, we first formulate the problem of UAV swarm trajectory design and learning sequence duration. We then cast the problem as a sequential decision making problem. Subsequently, we develop a deep reinforcement learning (DRL) methodology by encoding the real-time characteristics of our network into *states* for the DRL, defining a calculation methodology for the *actions* available for the DRL, and linking the actions to DRL *reward* calculations by embedding the optimization methodology from Section 4.

For training sequence s , let $X_u(s)$ denote the location of UAV swarm u , $\Lambda_c(s)$ denote the latest estimation of the model drift of device cluster c , $E_u(s)$ denote the minimum remaining battery among the UAVs belong to swarm u , and $G_c(s)$ denote the latest value of the gradient at device cluster c . Since the duration of ML model training T_s , $\forall s$, is usually far smaller than the delay between consecutive visits to the same device cluster, we assume that the effect of model drift during model training is negligible, as we do so in Section 3, and instead integrate the effects of model drift in our DRL design caused by delay between consecutive visits of the device cluster. For device cluster c , if it has been visited during sequence s , i.e., $c \in \mathcal{C}(s)$, $G_c(s)$ captures its recent gradient: $G_c(s) = \left\| \nabla F_c(\mathbf{w}_c(t_s + T_s) | \tilde{\mathcal{D}}_c(t_s + T_s)) \right\|^2$ measured at the end of the training sequence; however, if it is not visited, i.e., $c \in \bar{\mathcal{C}}(s)$, then $G_c(s) = \left\| \nabla F_c(\mathbf{w}_c(t_c^V) | \tilde{\mathcal{D}}_c(t)) \right\|^2$, which is computed via the bound in (54). Also, we let $E^M(s)$ denote the sum of energy of movement of the UAV swarms to travel to their current location in training sequence s from their previous locations in sequence $s-1$, and let $O(s)$ denote the value of the final objective function of \mathcal{P} solved in Section 4 encompassing both the energy used for model training and the gradient of those devices under model training.

5.2.2 Problem Formulation

Given a total of S ML model training sequences, we propose the following formulation to determine the optimal trajectory design and temporal ML characteristics:

$$(\hat{\mathcal{P}}) : \min_{\substack{\{\mathcal{X}(s)\}_{s=1}^S \\ \{\mathcal{T}(s)\}_{s=1}^S}} \frac{1}{S} \sum_{s=1}^S \left[c_1 E^M(s) + c_2 O(s) + c_3 \sum_{c \in \bar{\mathcal{C}}(s)} G_c(s) \right] \quad (55)$$

s.t.

$$E_u(s) \geq E^T, u \in \mathcal{U}(s), s \in \{1, \dots, S\} \quad (56)$$

$$\mathcal{T}(s) \in \mathcal{T}^F, s \in \{1, \dots, S\}, \quad (57)$$

where $\mathcal{X}(s) \triangleq \{X_1(s), \dots, X_U(s)\}$, and $\mathcal{T}(s) \triangleq \{T_s \cup \tau_s^L \cup \tau_s^G\}$. The objective function in (55) consists of three parts, the energy required for swarms to move to their next destination ($E^M(s)$), the data offloading/processing objective function

result ($O(s)$ derived from \mathcal{P}), and the estimated online gradient as a result of model drift at clusters without UAV training ($G_c(s), c \in \mathcal{C}(s)$). Constraint (56) ensures that swarms have sufficient energy E^T , at all times, to travel to a recharging station before they can no longer sustain their flight, and constraint (57) guarantees that the temporal ML characteristics $\mathcal{T}(s) \triangleq \{T_s \cup \tau_s^L \cup \tau_s^G\}$, $\forall s$, are always within some feasible set \mathcal{T}^F . Finally, c_1 , c_2 , and c_3 in (55) are non-negative normalized coefficients weighting the objectives.

Solving $\hat{\mathcal{P}}$ faces the following challenges: (i) the effects of training at a previous device cluster carries over to all future training sequences, at any device cluster, (ii) $\hat{\mathcal{P}}$ is a combinatorial problem, which suffers from *curse of dimensionality*, since at each sequence the core network must assign the swarms to either device clusters or recharging stations, and (iii) $\hat{\mathcal{P}}$ is defined over an unknown environment, i.e., neither the data distributions at the device clusters nor the model/concept drift are known apriori. These facts motivate us to cast the problem as a *sequential decision making problem*, which is solved at the core network for each training sequence by encoding the network aspects as reinforcement learning objectives. Classical reinforcement learning methods rely on a pre-built Q-table to determine future actions and associated network states [66], but, due to the aforementioned challenges of our problem, in particular the curse of dimensionality, building a Q-table is infeasible. We thus develop a methodology based on deep Q-networks, in which the Q-table is modelled via a neural network.

5.2.3 State of the DRL

We encode the locations of the UAV swarms, the model drift and gradients at device clusters, and the temporal ML characteristics (i.e., total time, local-global aggregation periods) as the state of the DRL. Formally, we define the state of the DRL at the end of training sequence s , $\mathcal{Z}(s)$, as:

$$\mathcal{Z}(s) = \mathcal{U}(s) \cup \mathcal{X}(s) \cup \Lambda(s) \cup \mathcal{E}(s) \cup \mathcal{G}(s) \cup \mathcal{T}(s), \quad (58)$$

where $\mathcal{U}(s)$ denotes the set of active UAV swarms, $\mathcal{X}(s)$ denotes the locations of all the swarms, $\Lambda(s) = \{\Lambda_1(s), \dots, \Lambda_C(s)\}$ are the latest model drift estimates observed at the device clusters, $\mathcal{E}(s) = \{E_1(s), \dots, E_U(s)\}$, $\mathcal{G}(s) = \{G_1(s), \dots, G_C(s)\}$, and $\mathcal{T}(s) = \{T_s \cup \tau_s^L \cup \tau_s^G\}$.

5.2.4 Action of the DRL

The core network, as the DRL agent, determines the active UAV swarms $\mathcal{U}(s+1)$, their locations $\mathcal{X}(s+1)$, and the temporal behavior $\mathcal{T}(s+1)$ of the next training sequence. In particular, we define the action, $\mathcal{H}(s)$, of the DRL agent as:

$$\mathcal{H}(s) = \mathcal{X}(s+1) \cup \mathcal{U}(s+1) \cup \mathcal{T}(s+1). \quad (59)$$

5.2.5 Reward of the DRL

The DRL agent aims to maximize the reward of each action $\mathcal{H}(s)$ with respect to the current state $\mathcal{Z}(s)$ via the objective value of $\hat{\mathcal{P}}$. Formally, we define the reward of the agent as:

$$V(s) = C \left(\underbrace{c_1 O(s) + c_2 \sum_{c \in \mathcal{C}(s)} G_c(s) + c_3 E^M(s)}_{(a)} \right)^{-1} - \underbrace{P \sum_{u \in \mathcal{U}} \mathbb{1}_{\{E_u \leq E^T\}}}_{(b)} \quad (60)$$

where (a) captures the (inverse) value of the objective function of $\hat{\mathcal{P}}$ for a particular training sequence s , and (b) is a penalty function with $P \gg 1$, capturing the case where UAVs' battery level drops below E^T , upon which the indicator $\mathbb{1}_{\{E_u \leq E^T\}}$ takes the value of one for UAV swarm u .

Main Takeaways. The proposed reward function in (60) captures multiple possibly competing objectives: (i) it always motivates visiting those device cluster that benefit from network aware ML model training, i.e., those that require less energy consumption to achieve a better model training, (ii) it avoids leaving those clusters with higher model drift unvisited for longer period of time and simultaneously promotes less frequent visit of those clusters with small value of model drift where their last captured value of gradient is very small, (iii) it promotes a sequence of visits of the device clusters that leads to the least movement energy consumption, and (iv) it avoids the situations where the battery level of the UAV swarms drops below a threshold.

5.2.6 DRL Learning Architecture

We exploit a deep neural network to approximate the optimal action-value function based on the Bellman equation [66]:

$$Q^*(\mathcal{Z}(s), \mathcal{H}(s)) = \mathbb{E} \left[V(s) + \gamma \max_{\mathcal{H}(s+1)} Q^*(\mathcal{Z}(s+1), \mathcal{H}(s+1)) \mid \mathcal{Z}(s), \mathcal{H}(s) \right], \quad (61)$$

where γ is the future reward discount. We use one deep neural network (DNN) to approximate Q^* called the *train Q-network* $Q_\theta(\mathcal{Z}(s), \mathcal{H}(s))$, which we train by adjusting its parameters θ to reduce the mean-squared error (MSE). Classical deep Q-network techniques determine the MSE of the train Q-network with respect to a target reward $y(s)$ that also depends on the train Q-network's model parameters θ . This self-coupling produces over-estimation, so we use an additional DNN called *target Q-network* $\hat{Q}_{\hat{\theta}}$ with parameters $\hat{\theta}$ to produce accurate loss measurements and periodically synchronize the target Q-network to the train Q-network [66]. Furthermore, to prevent correlations in the environment observation sequence from influencing the parameters θ in the *train Q-network*, we use *experience replay* to sample a randomized mini-batch of M^Q experience tuples, each of which is of the form $(\mathcal{Z}(s), \mathcal{H}(s), V(s), \mathcal{Z}(s+1))$, to calculate MSE. In particular, we compute the mean-squared error as:

$$L(\theta) = \frac{1}{|M^Q|} \sum_{s \in M^Q} (Q_\theta(\mathcal{Z}(s), \mathcal{H}(s)) - y(s))^2, \quad (62)$$

where $y(s) = V(s) + \gamma \max_{\mathcal{H}(s+1)} \hat{Q}_{\hat{\theta}}(\mathcal{Z}(s+1), \mathcal{H}(s+1))$ is the target reward. Using the MSE, we then perform SGD to adjust the parameters θ . Since this procedure requires at least M^Q previous experience tuples (saved in a deque-style buffer of size B^Q), and each training sequence s only generates a single tuple, the DNN training requires at least M^Q training sequences before it begins. In order to generate representative experience tuples from the environment before the DNN is properly trained, we utilize an ϵ -greedy policy [67] wherein with probability ϵ the agent will select an action randomly and with probability $(1 - \epsilon)$ the agent will determine the action based on the train Q-network Q_θ . As the train Q-network improves over time, ϵ decreases with limit $\epsilon^{\min} \leq \epsilon$.

5.3 System Integration: A Holistic Solution for UAV-enabled Online ML Over Heterogeneous Networks

To produce a self-sufficient system methodology that integrates dynamic (i.e., online data distributions) and distributed ML at large-scales, we develop a holistic framework of network-aware UAV-enabled online model training,

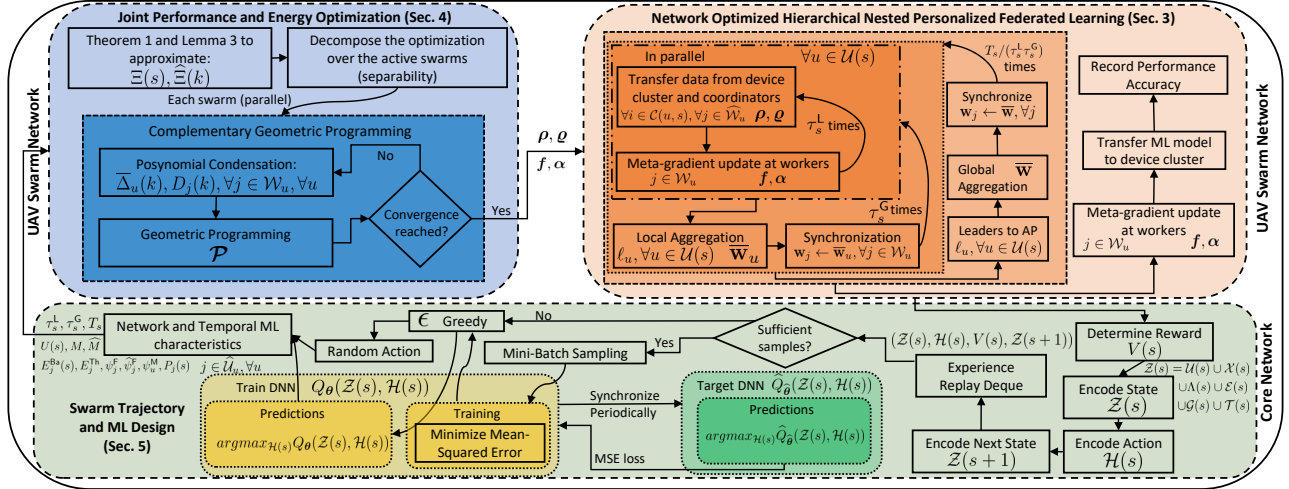


FIGURE 3: Overall flow of our methodology, connecting HN-PFL (Sec. 3), the data processing optimization (Sec. 4), and the swarm trajectory and ML design (Sec. 5).

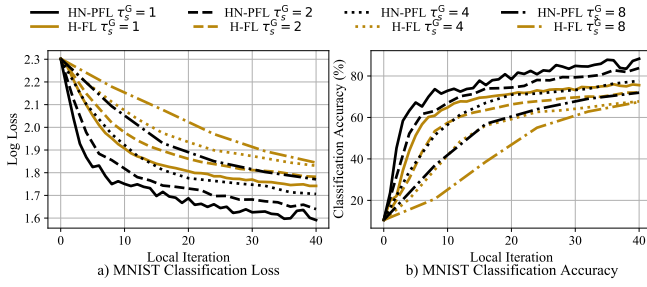


FIGURE 4: ML architecture comparisons for MNIST with fixed $\tau_s^L = 1$. HN-PFL demonstrates faster convergence and better final classification accuracy than H-FL for various τ_s^G .

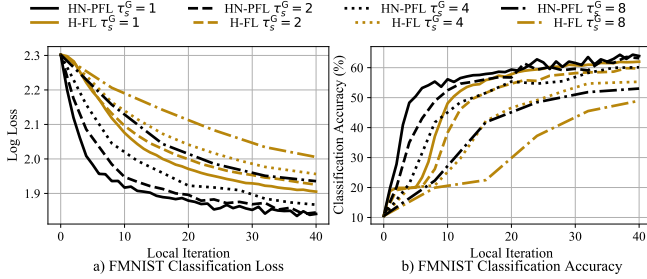


FIGURE 5: ML architecture comparisons for FMNIST with fixed $\tau_s^L = 1$. HN-PFL demonstrates faster convergence than H-FL for various τ_s^G in this more challenging task.

which combines HN-PFL from Sec. 3, the data processing/offloading optimization from Sec. 4, and the swarm trajectory and ML design from Sec. 5. We present our holistic system architecture diagrammatically in Fig. 3, and explain how system components interact with one another below.

Life-long ML Cycle: At a high level, our holistic framework is composed of three individual blocks. The HN-PFL methodology, in the orange block in Fig. 3, is implemented by the UAV swarms, and operates based on the reception of transfer/processing parameters (i.e., $\rho, \varrho, \alpha, \mathbf{f}$) from the data processing optimization at the swarm leaders obtained from the blue block in Fig. 3. The ML training results (captured as the state $\mathcal{Z}(s)$ which includes the meta-gradient output $\mathcal{G}(s)$) of the orange block (i.e., HN-PFL) are saved as experience tuples by the DRL agent and form the basis for our DRL methodology for swarm trajectory and ML design optimization in the green block in Fig. 3. Once the reinforcement

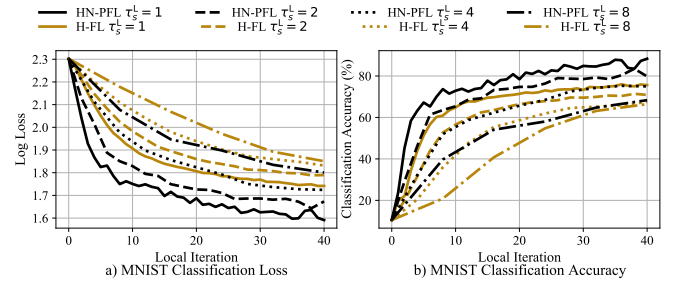


FIGURE 6: Using the same network for MNIST as Fig. 4, this experiment fixes $\tau_s^G = 1$ to vary τ_s^L instead. Our methodology HN-PFL continues to outperform H-FL consistently.

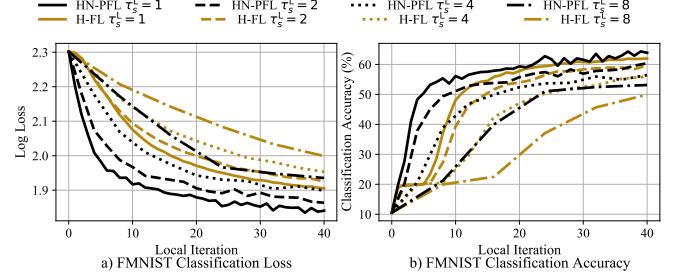


FIGURE 7: Using the same network for FMNIST as Fig. 5, this experiment fixes $\tau_s^G = 1$ to vary τ_s^L instead. Our methodology HN-PFL converges more rapidly than H-FL for all test cases.

learning agent at the core network determines trajectory (i.e., $\mathcal{X}(s)$) and ML design decisions (i.e., $\mathcal{T}(s), \tau_s^L, \tau_s^G$), the core network will send it to the swarm leaders to optimize HN-PFL procedures (i.e., the blue block). In this manner, our framework cycles through (i) data offloading/processing parameter determination, (ii) distributed ML model training for the devices, and (iii) trajectory design for UAV swarms.

6 NUMERICAL EVALUATION AND DISCUSSION

In this section, we conduct numerical evaluation of our proposed methodology. When literature contains existing techniques, such as hierarchical federated learning (H-FL) [52], we compare our methodology against it; otherwise, we develop heuristic algorithms as baselines.

Network Characteristics and Parameters. To calculate data rates among pairs of networked devices/UAVs, i.e., (21), (22), we use the following set of values [58]:

TABLE 2: Energy Consumption for MNIST to Reach 65% Classification Accuracy

Ratio		MNIST (kJ)			Ratio			MNIST (kJ)		
τ_s^L	τ_s^G	HFL	HN-PFL	Savings		τ_s^L	τ_s^G	HFL	HN-PFL	Savings
1	1	4.64	2.32	50.0%	1	1	4.64	2.32	50.0%	
1	2	8.13	4.06	50.1%	2	1	9.29	4.64	50.1%	
1	4	14.51	8.13	44.0%	4	1	15.10	8.13	46.2%	
1	8	19.73	17.99	8.8 %	8	1	18.57	14.51	21.9%	

$N_0 = -174\text{dBm/Hz}$, $\alpha^{\text{PL}} = 2$, $\eta^{\text{LoS}} = 3\text{dB}$, $\eta^{\text{NLoS}} = 23\text{dB}$, $f = 2\text{GHz}$, $\psi = 11.95$, $\beta = 0.14$, $\bar{B} = 2\text{MHz}$. We set the transmit power of the devices in the range $[23, 25]\text{dBm}$ and the transmit power of UAVs to 20dBm . The UAVs' altitude are also selected from $[25, 30]\text{m}$.

Datasets. We consider the MNIST (<http://yann.lecun.com/exdb/mnist/>) and Fashion-MNIST (FMNIST) datasets (<https://github.com/zalandoresearch/fashion-mnist>). Each dataset contains 70K images (60K for training, 10K for testing), where each image belongs to one of 10 labels of handwritten digits and fashion products, respectively. FMNIST can be considered as a harder classification task as compared to MNIST due to its more complex images.

6.1 HN-PFL Proof-of-Concept

We start by investigating the HN-PFL procedure from Sec. 3, by comparing its performance (measured via classification accuracy, loss, and energy consumption) to that of hierarchical federated learning (H-FL) proposed in [52]. For this simulation, we consider a network composed of 4 UAV swarms with 2-3 workers, where each swarm has data from only 3 labels (thus, non-i.i.d. data distributions) and data quantity determined randomly from a Gaussian distribution: $\mathcal{N}(2500, 250)$ for MNIST and $\mathcal{N}(3500, 350)$ for FMNIST. As a proof-of-concept, we strictly isolate the performance of the distributed ML methodologies to the UAV layers, i.e., we assume the data has already been transferred to the worker UAVs. For a fair comparison between HN-PFL and H-FL, we ensure that both methodologies train over the same amount of data for each of their iterations by defining the batch size for H-FL as α^{HFL} and setting each batch ratio for HN-PFL as $\alpha_{j,i} \triangleq \lfloor \frac{1}{3}\alpha^{\text{HFL}} \rfloor \forall i \in \{1, 2, 3\}$. Finally, we use the following settings for ML model training: $\eta = \eta_1 = 10^{-3}$ and $\eta_2 = 10^{-2}$, where η is the learning rate for gradient descent in H-FL, and to avoid lengthy Hessian computations, we use the Hessian first-order approximation (see Remark 1).

Due to the hierarchical nature of HN-PFL, we investigate the impacts of local and global aggregations on the performance and efficiency of the ML training separately. We first investigate the effects of varying global aggregation period τ_s^G from $[1, 8]$ and fix local aggregation period (i.e., $\tau_s^L = 1$) in Fig. 4 for MNIST. We repeat this experiment with fixed $\tau_s^G = 1$ and vary τ_s^L from $[1, 8]$ in Fig. 6, also for MNIST. The corresponding FMNIST experiments are in Fig. 5 and 7.

For both MNIST and FMNIST, HN-PFL attains better final model accuracy and classification loss over its H-FL counterpart. For example, when $\tau_s^L = \tau_s^G = 1$, HN-PFL outperforms H-FL in classification accuracy by $\sim 10\%$ for MNIST and $\sim 3\%$ for FMNIST. When we increase the aggregation period, the model performances decrease for all test cases because the total iterations are fixed and thus longer aggregation periods result in fewer aggregations within the same timeframe. Fewer aggregations leads to worse performance as a result.

TABLE 3: Energy Consumption for FMNIST to Reach 45% Classification Accuracy

Ratio		FMNIST (kJ)			Ratio			FMNIST (kJ)		
τ_s^L	τ_s^G	HFL	HN-PFL	Savings		τ_s^L	τ_s^G	HFL	HN-PFL	Savings
1	1	5.22	2.32	55.6%	1	1	5.22	2.32	55.6%	
1	2	6.96	3.48	50.0%	2	1	6.96	4.06	41.7%	
1	4	11.03	6.38	42.2%	4	1	11.61	7.55	35.0%	
1	8	17.99	11.61	35.5%	8	1	18.57	11.61	37.5%	

Nonetheless, HN-PFL is able to maintain its advantage as τ_s^G or τ_s^L increases for both MNIST and FMNIST. Furthermore, HN-PFL has notably faster convergence speed than H-FL, e.g., to attain 55% accuracy for MNIST when $\tau_s^L = 1$ and $\tau_s^G = 2$, HN-PFL needs only 5 iterations while H-FL uses 10 iterations. The faster convergence of HN-PFL results in less network energy expenditures in the form of flight, processing, and communication energy among UAVs in order to reach desired accuracy thresholds. We demonstrate the energy savings of HN-PFL in Table 2 for MNIST and Tables 3 for FMNIST. For each table, we selected model accuracies that is reachable for all combinations of τ_s^L and τ_s^G under test. As such, we used 65% for MNIST and 45% for FMNIST. On average, our method saves 38.7% and 42.5%, for MNIST and FMNIST respectively, of the energy used for H-FL.

6.2 Data Offloading/Processing Optimization

We next focus on the optimization (i.e., blue) block from Fig. 3. First, recall that the joint energy and performance optimization from Sec. 4 is separable with respect to each swarm. As a result, we investigate the performance of our optimization solver on a single swarm composed of two workers and two coordinators training for a device cluster composed of ten devices in Figs. 8-9, averaging over 10 experiments. In particular, Fig. 8 varies $1 - \theta$, i.e. scaling the importance of the ML model performance in the objective of \mathcal{P} , and evaluates the resulting optimization parameters: device-to-UAV data offloading (ρ), coordinator-to-worker offloading (ϱ), aggregate data processing (i.e., $D_j \times \alpha_j$, $\alpha_j = \alpha_{j,1} + \alpha_{j,2} + \alpha_{j,3}$), and worker CPU frequency determination (g). As the network operator places greater importance on ML model performance (i.e., increasing $1 - \theta$), our solver increases data offloading, i.e., larger average ρ in Fig. 8(a), and swarm leaders also instruct their workers to increase their CPU frequencies in Fig. 8(c). Fig. 8(b) also demonstrates that the coordinators never retain data for themselves as the average ϱ is 0.5, which implies that all the data is getting offloaded to the 2 workers. The joint effect of larger average ρ and g is more average total data processed, seen in Fig. 8(d).

As no alternative methodology for our optimization problem exists, we develop two methods, called greedy offloading (G.O.) and maximum processed (M.P.), and use them as baselines to compare the effectiveness of our data offloading/processing optimization in Fig. 9. In G.O., the devices always offload their entire datasets to the UAVs, and, in M.P., the UAVs overclock their CPU frequencies (reaching 2.3GHz for all UAVs) and maximize mini-batch ratios. Both G.O. and M.P. are determined in a fashion that adheres to the constraints in (25)-(46), and we use our solver to determine the rest of the optimization variables in each baseline. We show the percentage savings of our method over the two baselines in Fig. 9. When the network operator places greater emphasis on energy efficiency (i.e., small $1 - \theta$), our joint

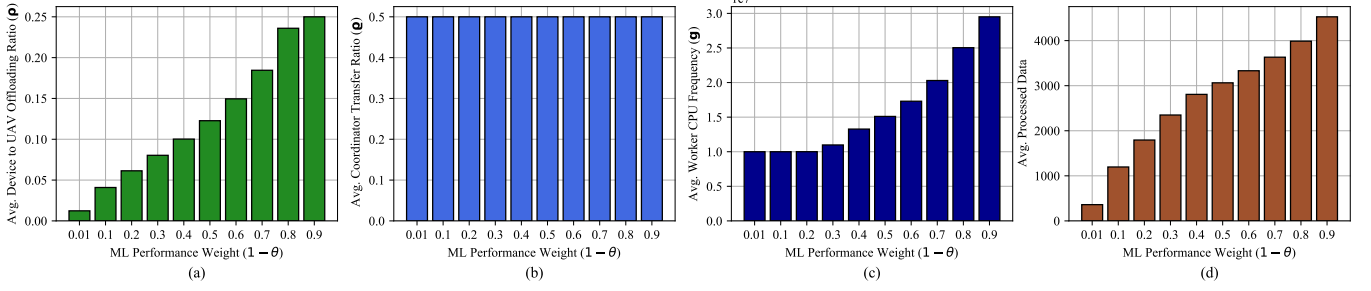


FIGURE 8: The behavior of the optimization variables: ρ, α, g depends on the ML learning importance factor $1 - \theta$ in the optimization formulation. As $1 - \theta$ increases, i.e., the importance of ML model performance increases, the network responds by offloading more data on average, increasing the CPU frequencies of workers, and processing more data on average as a result.

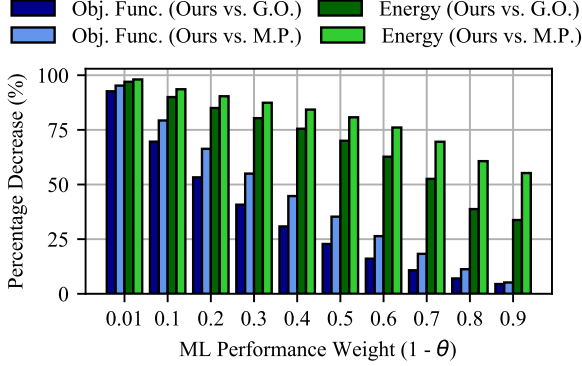


FIGURE 9: Our data offloading/processing optimization minimizes the network objective better than the two baselines, greedy offloading (G.O.) and maximum processed (M.P.). For comparison, we show the percentage decrease of energy consumption and objective function that our optimization achieves when compared to the baselines. For the baselines, M.P. outperforms G.O. as M.P. is able to schedule the data offloading more efficiently, consuming less energy and processing more data.

optimization will decrease data offloading and processing to conserve energy. As a result, our method achieves over 80% decrease in objective function value and energy consumption compared to either baseline when $1 - \theta = 0.01$. Even when $1 - \theta = 0.9$, i.e., the network aims to process more data in order to improve the ML component of the objective function, our method retains a roughly 6% improvement for the objective function and a 25% improvement for the energy consumption against both baselines. Fig. 9 also reveals that, between the baselines, M.P. outperforms G.O. because M.P. always processes more data and can offload data from device-to-UAV more optimally, which leads to both less energy consumption and smaller objective function value.

6.3 Trajectory Optimization with Model/Concept Drift

Next, we turn to the trajectory optimization component of Sec. 5 (green block) in Fig. 3. We consider 2 recharging stations and 8 device clusters separated by distances in $[500, 2000]$ m, where each device cluster has $[8, 10]$ devices. At the UAV level, we consider 3 swarms, each of which has $[3, 5]$ workers and $[1, 2]$ coordinators. Additionally, we will refer to the recharging stations as R:1 and R:2, and the clusters as C:1, \dots , C:8. First, we evaluate the performance of the DRL methodology by calculating the moving average reward from (60), average UAV battery levels, and learning objective (isolated to demonstrate the online ML model performance over epochs, which is sum of the objective function $O(s)$ derived from \mathcal{P} and the estimated online gradient $G_c(s)$ across the unvisited device clusters) for two

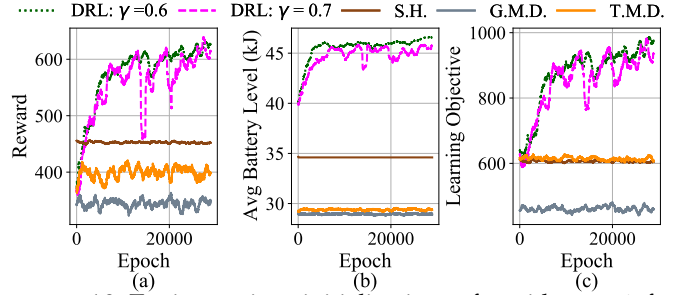


FIGURE 10: Testing various initializations of γ with $\epsilon = 0.7$ for our DRL agent reveals that it learns how to schedule swarm trajectory decisions to maximize network and ML reward, especially when comparing to baseline methods. Each point is a moving average over 1k epochs.

DRL combinations of γ and comparing their performance against three baselines in Fig. 10. Since existing baselines do not exist, we developed three baseline algorithms: (i) sequential heuristic (S.H.), (ii) greedy minimum distance (G.M.D.), and (iii) threshold minimum distance (T.M.D.), and calculated their rewards using the reward function in (60). S.H. cycles through the sites sequentially from C:1 to R:2, in the order presented in the x-axis of Fig. 11. On the other hand, our minimum distance methods determine the next destination for a swarm based on closest proximity, with G.M.D. always selecting the minimum distance and T.M.D. choosing between a random option or the minimum distance based on a probability threshold (set at 20% probability to select the random option). Both minimum distance based methods will reroute swarms to the nearest recharging station when UAV batteries fall within the threshold. As seen in Fig. 10, the DRL agent initially undergoes a training phase to learn the optimal travel patterns to maximize the reward function. It also must learn how to schedule recharging (hence the initial lower battery). The DRL agent learns to schedule cluster training visits and UAV recharging so that the average reward, battery levels, and learning objectives outperform those of baseline algorithms by 28.9% versus S.H. and by 65.7% versus G.M.D. in Fig. 10.

As the other goal for our DRL-based trajectory optimization is adaptability to changing model drifts, we use the same network as that in Fig. 10 with time-varying model drifts for each device cluster, and measure the cluster visit rate per 1k epochs in Fig. 11. Each cluster has a unique affine function to model its model drift growth. Initially, the 8 clusters have scaled model drifts of $[2, 4, 6, 8, 10, 12, 14, 16]$, but end at $[15, 15, 21, 11, 12, 17, 19, 17]$. So, initially, the cluster visit rate favors C:8 and C:7, which have the highest model drifts. However, as the epochs increase, the model drift begins

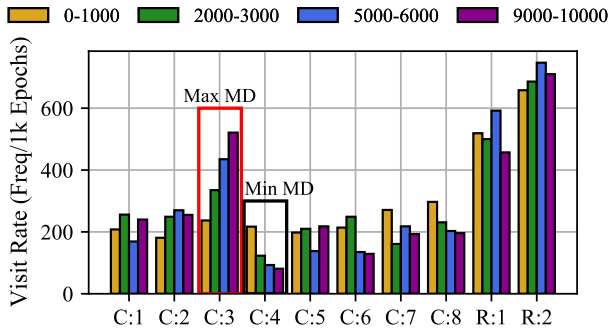


FIGURE 11: Average visit rate of different device clusters and recharging stations for select intervals. The DRL agent learns to adjust its visit frequency to those device clusters with the largest model drift (MD), even when the model drift is time-varying. Initially, cluster C:8 has the most model drift at 16 and C:3 has only 6, but cluster C:3's model drift rapidly grows to 21. The DRL agent consequently adjusts the frequency of visits to favor C:3, increasing its visit rate over time.

skewing towards C:3, and our methodology responds by increasing its visit rate from 237 to 521. Inversely, C:4 has the smallest final model drift and the DRL is able to adjust its visit rate from 217 to 81.

7 CONCLUSION

We developed a holistic framework for integrating UAV swarm networks for online distributed machine learning. This involved a number of unique modelling decisions and analysis. We proposed a swarm stratification architecture tailored for our distributed machine learning framework. Our introduced distributed machine learning architecture, hierarchical nested personalized federated learning $HN-PFL$, nests meta-function based gradient descent into local and global aggregations through the worker-leader-core network hierarchy, for which we characterized the performance bound. Finally, we proposed and developed a holistic framework for network-aware UAV-enabled model training, consisting of two intertwined parts: (i) data offloading and processing optimization, for which we developed a distributed algorithm with performance guarantee, and (ii) learning duration and trajectory design, for which we developed a solution based on deep reinforcement learning.

REFERENCES

- [1] N. H. Motlagh, T. Taleb, and O. Arouk, "Low-altitude unmanned aerial vehicles-based internet of things services: Comprehensive survey and future perspectives," *IEEE Internet Things J.*, vol. 3, no. 6, pp. 899–922, 2016.
- [2] Y. Zeng, R. Zhang, and T. J. Lim, "Wireless communications with unmanned aerial vehicles: Opportunities and challenges," *IEEE Commun. Mag.*, vol. 54, no. 5, pp. 36–42, 2016.
- [3] Ç. Kaymak and A. Uçar, "A brief survey and an application of semantic image segmentation for autonomous driving," in *Handbook Deep Learn. Appl.* Springer, 2019, pp. 161–200.
- [4] A. Hard, K. Rao, R. Mathews, S. Ramaswamy, F. Beaufays, S. Augenstein, H. Eichner, C. Kiddon, and D. Ramage, "Federated learning for mobile keyboard prediction," *arXiv preprint arXiv:1811.03604*, 2018.
- [5] Y. Zhang, X. Ma, J. Zhang, M. S. Hossain, G. Muhammad, and S. U. Amin, "Edge intelligence in the cognitive internet of things: Improving sensitivity and interactivity," *IEEE Netw.*, vol. 33, no. 3, pp. 58–64, 2019.
- [6] Y. Xiao, G. Shi, Y. Li, W. Saad, and H. V. Poor, "Toward self-learning edge intelligence in 6g," *IEEE Commun. Mag.*, vol. 58, no. 12, pp. 34–40, 2020.
- [7] S. Hosseinalipour, C. G. Brinton, V. Aggarwal, H. Dai, and M. Chiang, "From federated to fog learning: Distributed machine learning over heterogeneous wireless networks," *IEEE Commun. Mag.*, vol. 58, no. 12, pp. 41–47, 2020.
- [8] Q. Wu, J. Xu, Y. Zeng, D. W. K. Ng, N. Al-Dhahir, R. Schober, and A. L. Swindlehurst, "5g-and-beyond networks with UAVs: From communications to sensing and intelligence," *arXiv preprint arXiv:2010.09317*, 2020.
- [9] W. Y. B. Lim, J. Huang, Z. Xiong, J. Kang, D. Niyato, X.-S. Hua, C. Leung, and C. Miao, "Towards federated learning in UAV-enabled internet of vehicles: A multi-dimensional contract-matching approach," *arXiv preprint arXiv:2004.03877*, 2020.
- [10] T. Zeng, O. Semiari, M. Mozaffari, M. Chen, W. Saad, and M. Bennis, "Federated learning in the sky: Joint power allocation and scheduling with UAV swarms," *arXiv:2002.08196*, 2020.
- [11] H. Zhang and L. Hanzo, "Federated learning assisted multi-UAV networks," *IEEE Trans. Veh. Technol.*, vol. 69, no. 11, pp. 14 104–14 109, 2020.
- [12] H. Yang, J. Zhao, Z. Xiong, K.-Y. Lam, S. Sun, and L. Xiao, "Privacy-preserving federated learning for UAV-enabled networks: Learning-based joint scheduling and resource management," *arXiv preprint arXiv:2011.14197*, 2020.
- [13] "Amazon details its low bandwidth sidewalk neighborhood network coming to echo and tile devices soon." [Online]. Available: <https://tcrn.ch/2TvixL6>
- [14] "Amazon sidewalk a new way to stay connected." [Online]. Available: <https://blog.aboutamazon.com/devices/amazon-sidewalk-a-new-way-to-stay-connected>
- [15] R. Ciovacco, "Amazon Sidewalk Privacy and Security Whitepaper," Tech. Rep., 09 2020.
- [16] "Amazon prime air." [Online]. Available: <https://www.amazon.com/Amazon-Prime-Air/b?ie=UTF8&node=8037720011>
- [17] S. Hosseinalipour, A. Rahmati, D. Y. Eun, and H. Dai, "Energy-aware stochastic uav-assisted surveillance," *IEEE Trans. Wireless Commun.*, vol. 20, no. 5, pp. 2820–2837, 2021.
- [18] E. L. Piza, B. C. Welsh, D. P. Farrington, and A. L. Thomas, "Cctv surveillance for crime prevention: A 40-year systematic review with meta-analysis," *Criminology & Public Policy*, vol. 18, no. 1, pp. 135–159, 2019.
- [19] "The pentagon has a laser that can identify people from a distance by their heartbeat." [Online]. Available: <https://bit.ly/35EcS6P>
- [20] C. Benedek, B. Gálai, B. Nagy, and Z. Jankó, "Lidar-based gait analysis and activity recognition in a 4d surveillance system," *IEEE Trans. Circuits Syst. Video Technol.*, vol. 28, no. 1, pp. 101–113, 2016.
- [21] M. A. Alsheikh, S. Lin, D. Niyato, and H.-P. Tan, "Machine learning in wireless sensor networks: Algorithms, strategies, and applications," *IEEE Commun. Surveys & Tuts.*, vol. 16, no. 4, pp. 1996–2018, 2014.
- [22] M. Erdelj, E. Natalizio, K. R. Chowdhury, and I. F. Akyildiz, "Help from the sky: Leveraging UAVs for disaster management," *IEEE Pervasive Comput.*, vol. 16, no. 1, pp. 24–32, 2017.
- [23] G. Zhu, D. Liu, Y. Du, C. You, J. Zhang, and K. Huang, "Toward an intelligent edge: Wireless communication meets machine learning," *IEEE Commun. Mag.*, vol. 58, no. 1, pp. 19–25, 2020.
- [24] J. Park, S. Samarakoon, M. Bennis, and M. Debbah, "Wireless network intelligence at the edge," *Proc. IEEE*, vol. 107, no. 11, pp. 2204–2239, 2019.
- [25] C. T. Dinh, N. H. Tran, M. N. H. Nguyen, C. S. Hong, W. Bao, A. Y. Zomaya, and V. Gramoli, "Federated learning over wireless networks: Convergence analysis and resource allocation," *IEEE/ACM Trans. Netw.*, pp. 1–12, 2020.
- [26] M. M. Amiri and D. Gündüz, "Federated learning over wireless fading channels," *IEEE Trans. Wireless Commun.*, vol. 19, no. 5, pp. 3546–3557, 2020.
- [27] M. Chen, Z. Yang, W. Saad, C. Yin, H. V. Poor, and S. Cui, "A joint learning and communications framework for federated learning over wireless networks," *arXiv preprint arXiv:1909.07972*, 2019.
- [28] S. Wang, T. Tuor, T. Salonidis, K. K. Leung, C. Makaya, T. He, and K. Chan, "Adaptive federated learning in resource constrained edge computing systems," *IEEE J. Sel. Areas Commun.*, vol. 37, no. 6, pp. 1205–1221, 2019.
- [29] Z. Yang, M. Chen, W. Saad, C. S. Hong, and M. Shikh-Bahaei, "Energy efficient federated learning over wireless communication networks," *arXiv preprint arXiv:1911.02417*, 2019.
- [30] Y. Tu, Y. Ruan, S. Wagle, C. G. Brinton, and C. Joe-Wong, "Network-aware optimization of distributed learning for fog computing," in *IEEE Conf. Comput. Commun. (INFOCOM)*, 2020, pp. 2509–2518.

- [31] S. Hosseinalipour, S. Azam, C. Brinton, N. Michelusi, V. Aggarwal, D. Love, and H. Dai, "Multi-stage hybrid federated learning over large-scale D2D-enabled fog networks," *arXiv preprint arXiv:2007.09511*, 2020.
- [32] F. P.-C. Lin, S. Hosseinalipour, S. S. Azam, C. G. Brinton, and N. Michelusi, "Two timescale hybrid federated learning with cooperative D2D local model aggregations," 2021.
- [33] K. Yang, T. Jiang, Y. Shi, and Z. Ding, "Federated learning via over-the-air computation," *IEEE Trans. Wireless Commun.*, vol. 19, no. 3, pp. 2022–2035, 2020.
- [34] V. Smith, C.-K. Chiang, M. Sanjabi, and A. S. Talwalkar, "Federated multi-task learning," in *Adv. Neural Inf. Process. Syst.*, 2017, pp. 4424–4434.
- [35] R. Li, F. Ma, W. Jiang, and J. Gao, "Online federated multitask learning," in *IEEE Int. Conf. Big Data (Big Data)*, 2019, pp. 215–220.
- [36] A. Fallah, A. Mokhtari, and A. Ozdaglar, "Personalized federated learning: A meta-learning approach," *arXiv preprint arXiv:2002.07948*, 2020.
- [37] Y. Sun, M. Peng, Y. Zhou, Y. Huang, and S. Mao, "Application of machine learning in wireless networks: Key techniques and open issues," *IEEE Commun. Surveys & Tuts.*, vol. 21, no. 4, pp. 3072–3108, 2019.
- [38] F. B. Mismar, B. L. Evans, and A. Alkhateeb, "Deep reinforcement learning for 5G networks: Joint beamforming, power control, and interference coordination," *IEEE Trans. Commun.*, vol. 68, no. 3, pp. 1581–1592, 2019.
- [39] Y. Wei, F. R. Yu, M. Song, and Z. Han, "User scheduling and resource allocation in hetnets with hybrid energy supply: An actor-critic reinforcement learning approach," *IEEE Trans. Wireless Commun.*, vol. 17, no. 1, pp. 680–692, 2017.
- [40] X. Liu, Y. Liu, Y. Chen, and L. Hanzo, "Trajectory design and power control for multi-UAV assisted wireless networks: A machine learning approach," *IEEE Trans. Veh. Technol.*, vol. 68, no. 8, pp. 7957–7969, 2019.
- [41] N. Zhao, Z. Liu, and Y. Cheng, "Multi-agent deep reinforcement learning for trajectory design and power allocation in multi-UAV networks," *IEEE Access*, vol. 8, pp. 139 670–139 679, 2020.
- [42] Y. Zhang, Z. Mou, F. Gao, J. Jiang, R. Ding, and Z. Han, "UAV-enabled secure communications by multi-agent deep reinforcement learning," *IEEE Trans. Veh. Technol.*, vol. 69, no. 10, pp. 11 599–11 611, 2020.
- [43] J. Cui, Y. Liu, and A. Nallanathan, "Multi-agent reinforcement learning-based resource allocation for UAV networks," *IEEE Trans. Wireless Commun.*, vol. 19, no. 2, pp. 729–743, 2020.
- [44] "Collaborating with UAVTEK to develop nano 'bug' drone." [Online]. Available: <https://www.baesystems.com/en/collaborating-with-uavtek-to-develop-nano-bug-drone>
- [45] K. Lu, J. Xie, Y. Wan, and S. Fu, "Toward UAV-based airborne computing," *IEEE Wireless Commun.*, vol. 26, no. 6, pp. 172–179, 2019.
- [46] C. H. Liu, Z. Chen, J. Tang, J. Xu, and C. Piao, "Energy-efficient UAV control for effective and fair communication coverage: A deep reinforcement learning approach," *IEEE J. Sel. Areas Commun.*, vol. 36, no. 9, pp. 2059–2070, 2018.
- [47] A. V. Savkin and H. Huang, "Asymptotically optimal deployment of drones for surveillance and monitoring," *Sensors*, vol. 19, no. 9, p. 2068, 2019.
- [48] M. Won, "UBAT: On jointly optimizing UAV trajectories and placement of battery swap stations," 2020.
- [49] C. H. Choi, H. J. Jang, S. G. Lim, H. C. Lim, S. H. Cho, and I. Gaponov, "Automatic wireless drone charging station creating essential environment for continuous drone operation," in *Int. Conf. Control, Autom. Inf. Sci. (ICCAIS)*, 2016, pp. 132–136.
- [50] H. B. McMahan, E. Moore, D. Ramage, S. Hampson, and B. A. y Arcas, "Communication-Efficient Learning of Deep Networks from Decentralized Data," in *Proc. Int. Conf. Artif. Intell. Stat. (AISTATS)*, 2017.
- [51] D. Yang, Q. Wu, Y. Zeng, and R. Zhang, "Energy tradeoff in ground-to-UAV communication via trajectory design," *IEEE Trans. Vehicular Technol.*, vol. 67, no. 7, pp. 6721–6726, 2018.
- [52] L. Liu, J. Zhang, S. Song, and K. B. Letaief, "Client-edge-cloud hierarchical federated learning," in *IEEE Int. Conf. Commun. (ICC)*, IEEE, 2020, pp. 1–6.
- [53] C. Finn, P. Abbeel, and S. Levine, "Model-agnostic meta-learning for fast adaptation of deep networks," *arXiv:1703.03400*, 2017.
- [54] S. Wang, M. Lee, S. Hosseinalipour, R. Morabito, M. Chiang, and C. G. Brinton, "Device sampling for heterogeneous federated learning: Theory, algorithms, and implementation," *arXiv preprint arXiv:2101.00787*, 2021.
- [55] A. Fallah, A. Mokhtari, and A. Ozdaglar, "On the convergence theory of gradient-based model-agnostic meta-learning algorithms," in *Int. Conf. Artificial Intell. Stat.* PMLR, 2020, pp. 1082–1092.
- [56] C. T. Dinh, N. H. Tran, and T. D. Nguyen, "Personalized federated learning with moreau envelopes," *arXiv:2006.08848*, 2020.
- [57] A. Al-Hourani, S. Kandeepan, and A. Jamalipour, "Modeling air-to-ground path loss for low altitude platforms in urban environments," in *Proc. of IEEE Global Commun. Conf. (GLOBECOM)*, pp. 2898–2904, Austin, TX, USA, Dec. 2014.
- [58] M. Mozaffari, W. Saad, M. Bennis, and M. Debbah, "Mobile unmanned aerial vehicles (UAVs) for energy-efficient internet of things communications," *IEEE Trans. Wireless Commun.*, vol. 16, no. 11, pp. 7574–7589, 2017.
- [59] V. Vahidi and E. Saberinia, "Orthogonal frequency division multiplexing and channel models for payload communications of unmanned aerial systems," in *Int. Conf. Unmanned Aircraft Syst. (ICUAS)*, 2016, pp. 1156–1161.
- [60] Y. Zeng and R. Zhang, "Energy-efficient UAV communication with trajectory optimization," *IEEE Trans. Wireless Commun.*, vol. 16, no. 6, pp. 3747–3760, June 2017.
- [61] Y. Zeng, J. Xu, and R. Zhang, "Energy minimization for wireless communication with rotary-wing UAV," *IEEE Trans. Wireless Commun.*, vol. 18, no. 4, pp. 2329–2345, 2019.
- [62] M. Chiang, C. W. Tan, D. P. Palomar, D. O'Neill, and D. Julian, "Power control by geometric programming," *IEEE Trans. Wireless Commun.*, vol. 6, no. 7, pp. 2640–2651, 2007.
- [63] S. Diamond and S. Boyd, "CVXPY: A Python-embedded modeling language for convex optimization," *J. Machine Learn. Research*, vol. 17, no. 83, pp. 1–5, 2016.
- [64] B. R. Marks and G. P. Wright, "A general inner approximation algorithm for nonconvex mathematical programs," *Oper. Res.*, vol. 26, no. 4, pp. 681–683, 1978.
- [65] Y. Zeng and R. Zhang, "Energy-efficient UAV communication with trajectory optimization," *IEEE Trans. Wireless Commun.*, vol. 16, no. 6, pp. 3747–3760, 2017.
- [66] V. Mnih, K. Kavukcuoglu, D. Silver, A. A. Rusu, J. Veness, M. G. Bellemare, A. Graves, M. Riedmiller, A. K. Fidjeland, G. Ostrovski et al., "Human-level control through deep reinforcement learning," *nature*, vol. 518, no. 7540, pp. 529–533, 2015.
- [67] B. C. Stadie, S. Levine, and P. Abbeel, "Incentivizing exploration in reinforcement learning with deep predictive models," *arXiv preprint arXiv:1507.00814*, 2015.
- [68] S. Boyd, S.-J. Kim, L. Vandenbergh, and A. Hassibi, "A tutorial on geometric programming," *Opt. Eng.*, vol. 8, no. 1, p. 67, 2007.

APPENDIX A

PROOF OF PROPOSITION 1

Proof. To bound

$$\mathbb{E} \left[\left\| \frac{1}{U(s)} \sum_{u \in \mathcal{U}(s)} \sum_{j \in \mathcal{W}_u} \frac{\Delta_j(k' \tau_s^G)}{\Delta_u(k' \tau_s^G)} \left(\mathbf{w}_j(t) - \bar{\mathbf{w}}(t) \right) \right\|^2 \right], \quad (63)$$

where $t = t_s^G(k') = t_s + k' \tau_s^L \tau_s^G$, we introduce $\bar{\mathbf{w}}_u(t)$ and omit the t_s aspect of $t_s^G(k')$, i.e., ignoring the starting time of the sequence t_s in all the derivations since it is just a constant, to obtain:

$$\begin{aligned} & \mathbb{E} \left[\left\| \frac{1}{U(s)} \sum_{u \in \mathcal{U}(s)} \sum_{j \in \mathcal{W}_u} \frac{\Delta_j(k' \tau_s^G)}{\Delta_u(k' \tau_s^G)} \left(\mathbf{w}_j(\tau_s^L \tau_s^G k') - \bar{\mathbf{w}}_u(\tau_s^L \tau_s^G k') + \bar{\mathbf{w}}_u(\tau_s^L \tau_s^G k') - \bar{\mathbf{w}}(\tau_s^L \tau_s^G k') \right) \right\|^2 \right] \\ & \leq \underbrace{2 \frac{1}{U(s)} \sum_{u \in \mathcal{U}(s)} \sum_{j \in \mathcal{W}_u} \frac{\Delta_j(k' \tau_s^G)}{\Delta_u(k' \tau_s^G)} \mathbb{E} [\| \mathbf{w}_j(\tau_s^L \tau_s^G k') - \bar{\mathbf{w}}_u(\tau_s^L \tau_s^G k') \|^2]}_{(i)} + \underbrace{2 \frac{1}{U(s)} \sum_{u \in \mathcal{U}(s)} \mathbb{E} [\| \bar{\mathbf{w}}_u(\tau_s^L \tau_s^G k') - \bar{\mathbf{w}}(\tau_s^L \tau_s^G k') \|^2]}_{(ii)}, \end{aligned} \quad (64)$$

where the inequality is due to Jensen's inequality and $\|a + b\|^2 \leq 2(\|a\|^2 + \|b\|^2)$. We first upper bound (64)(i), omitting the summations for simplicity:

$$\begin{aligned} & 2 \mathbb{E} [\| \mathbf{w}_j(\tau_s^L \tau_s^G k') - \bar{\mathbf{w}}_u(\tau_s^L \tau_s^G k') \|^2] \stackrel{(a)}{=} 2 \mathbb{E} \left[\left\| \mathbf{w}_j(\tau_s^L \tau_s^G k') - \sum_{\hat{j} \in \mathcal{W}_u} \frac{\Delta_{\hat{j}}(k' \tau_s^G)}{\Delta_u(k' \tau_s^G)} \mathbf{w}_{\hat{j}}(\tau_s^L \tau_s^G k') \right\|^2 \right] \\ & \stackrel{(b)}{=} 2 \mathbb{E} \left[\left\| \mathbf{w}_j(\tau_s^L \tau_s^G k' - 1) - \eta_2 \nabla \tilde{F}_j(\mathbf{w}_j(\tau_s^L \tau_s^G k' - 1)) - \sum_{\hat{j} \in \mathcal{W}_u} \frac{\Delta_{\hat{j}}(k' \tau_s^G)}{\Delta_u(k' \tau_s^G)} \left(\mathbf{w}_{\hat{j}}(\tau_s^L \tau_s^G k' - 1) - \eta_2 \nabla \tilde{F}_{\hat{j}}(\mathbf{w}_{\hat{j}}(\tau_s^L \tau_s^G k' - 1)) \right) \right\|^2 \right] \\ & \stackrel{(c)}{\leq} \underbrace{8 \mathbb{E} [\| \mathbf{w}_j(\tau_s^L \tau_s^G k' - 1) - \bar{\mathbf{w}}_u(\tau_s^L \tau_s^G k' - 1) \|^2]}_{(i)} + \underbrace{8 \eta_2^2 \mathbb{E} [\| \nabla F_j(\mathbf{w}_j(\tau_s^L \tau_s^G k' - 1)) - \nabla \tilde{F}_j(\mathbf{w}_j(\tau_s^L \tau_s^G k' - 1)) \|^2]}_{(ii)} \\ & + \underbrace{8 \eta_2^2 \mathbb{E} \left[\left\| \sum_{\hat{j} \in \mathcal{W}_u} \frac{\Delta_{\hat{j}}(k' \tau_s^G)}{\Delta_u(k' \tau_s^G)} \left(\nabla \tilde{F}_{\hat{j}}(\mathbf{w}_{\hat{j}}(\tau_s^L \tau_s^G k' - 1)) - \nabla F_{\hat{j}}(\mathbf{w}_{\hat{j}}(\tau_s^L \tau_s^G k' - 1)) \right) \right\|^2 \right]}_{(iii)} \\ & + \underbrace{8 \eta_2^2 \mathbb{E} \left[\left\| \nabla F_j(\mathbf{w}_j(\tau_s^L \tau_s^G k' - 1)) - \sum_{\hat{j} \in \mathcal{W}_u} \frac{\Delta_{\hat{j}}(k' \tau_s^G)}{\Delta_u(k' \tau_s^G)} \nabla F_{\hat{j}}(\mathbf{w}_{\hat{j}}(\tau_s^L \tau_s^G k' - 1)) \right\|^2 \right]}_{(iv)}, \end{aligned} \quad (65)$$

where (a) is the aggregation rule of $\bar{\mathbf{w}}_u$, (b) uses the gradient update from (1), and (c) introduces $\eta_2 \nabla F_j$ and $\eta_2 \nabla \tilde{F}_j$ terms and then applies Cauchy-Schwarz, i.e., $(\sum_i a_i)^2 \leq n(\sum_i a_i^2)$. The bounds for (65)(ii) and (65)(iii) follow immediately from Lemma 1, and we analyze (65)(iv), while recalling the summations from (64) as follows:

$$\begin{aligned} & 8 \eta_2^2 \frac{1}{U(s)} \sum_{u \in \mathcal{U}(s)} \sum_{j \in \mathcal{W}_u} \frac{\Delta_j(k' \tau_s^G)}{\Delta_u(k' \tau_s^G)} \mathbb{E} \left[\left\| \nabla F_j(\mathbf{w}_j(\tau_s^L \tau_s^G k' - 1)) - \sum_{\hat{j} \in \mathcal{W}_u} \frac{\Delta_{\hat{j}}(k' \tau_s^G)}{\Delta_u(k' \tau_s^G)} \nabla F_{\hat{j}}(\mathbf{w}_{\hat{j}}(\tau_s^L \tau_s^G k' - 1)) \right\|^2 \right] \\ & \stackrel{(a)}{=} 8 \eta_2^2 \frac{1}{U(s)} \sum_{u \in \mathcal{U}(s)} \sum_{j \in \mathcal{W}_u} \frac{\Delta_j(k' \tau_s^G)}{\Delta_u(k' \tau_s^G)} \mathbb{E} \left[\left\| \nabla F_j(\mathbf{w}_j(\tau_s^L \tau_s^G k' - 1)) - \nabla F_j(\bar{\mathbf{w}}_u(\tau_s^L \tau_s^G k' - 1)) + \nabla F_j(\bar{\mathbf{w}}_u(\tau_s^L \tau_s^G k' - 1)) \right. \right. \\ & \quad \left. \left. - \sum_{\hat{j} \in \mathcal{W}_u} \frac{\Delta_{\hat{j}}(k' \tau_s^G)}{\Delta_u(k' \tau_s^G)} \left(\nabla F_{\hat{j}}(\mathbf{w}_{\hat{j}}(\tau_s^L \tau_s^G k' - 1)) + \nabla F_{\hat{j}}(\bar{\mathbf{w}}_u(\tau_s^L \tau_s^G k' - 1)) - \nabla F_{\hat{j}}(\bar{\mathbf{w}}_u(\tau_s^L \tau_s^G k' - 1)) \right) \right\|^2 \right] \\ & \stackrel{(b)}{\leq} 24 \eta_2^2 \frac{1}{U(s)} \sum_{u \in \mathcal{U}(s)} \sum_{j \in \mathcal{W}_u} \frac{\Delta_j(k' \tau_s^G)}{\Delta_u(k' \tau_s^G)} \mathbb{E} [\| \nabla F_j(\mathbf{w}_j(\tau_s^L \tau_s^G k' - 1)) - \nabla F_j(\bar{\mathbf{w}}_u(\tau_s^L \tau_s^G k' - 1)) \|^2] \\ & + 24 \eta_2^2 \frac{1}{U(s)} \sum_{u \in \mathcal{U}(s)} \sum_{j \in \mathcal{W}_u} \frac{\Delta_j(k' \tau_s^G)}{\Delta_u(k' \tau_s^G)} \mathbb{E} \left[\left\| \sum_{\hat{j} \in \mathcal{W}_u} \frac{\Delta_{\hat{j}}(k' \tau_s^G)}{\Delta_u(k' \tau_s^G)} \left(\nabla F_{\hat{j}}(\bar{\mathbf{w}}_u(\tau_s^L \tau_s^G k' - 1)) - \nabla F_{\hat{j}}(\mathbf{w}_{\hat{j}}(\tau_s^L \tau_s^G k' - 1)) \right) \right\|^2 \right] \\ & + 24 \eta_2^2 \frac{1}{U(s)} \sum_{u \in \mathcal{U}(s)} \sum_{j \in \mathcal{W}_u} \frac{\Delta_j(k' \tau_s^G)}{\Delta_u(k' \tau_s^G)} \mathbb{E} \left[\left\| \nabla F_j(\bar{\mathbf{w}}_u(\tau_s^L \tau_s^G k' - 1)) - \sum_{\hat{j} \in \mathcal{W}_u} \frac{\Delta_{\hat{j}}(k' \tau_s^G)}{\Delta_u(k' \tau_s^G)} \nabla F_{\hat{j}}(\bar{\mathbf{w}}_u(\tau_s^L \tau_s^G k' - 1)) \right\|^2 \right] \end{aligned} \quad (66)$$

$$\begin{aligned}
&\stackrel{(c)}{\leq} 24\eta_2^2 \frac{1}{U(s)} \sum_{u \in \mathcal{U}(s)} \sum_{j \in \mathcal{W}_u} \frac{\Delta_j(k' \tau_s^G)}{\bar{\Delta}_u(k' \tau_s^G)} \mathbb{E}[\|\nabla F_j(\mathbf{w}_j(\tau_s^L \tau_s^G k' - 1)) - \nabla F_j(\bar{\mathbf{w}}_u(\tau_s^L \tau_s^G k' - 1))\|^2] \\
&+ 24\eta_2^2 \frac{1}{U(s)} \sum_{u \in \mathcal{U}(s)} \sum_{j \in \mathcal{W}_u} \frac{\Delta_j(k' \tau_s^G)}{\bar{\Delta}_u(k' \tau_s^G)} \sum_{\hat{j} \in \mathcal{W}_u} \frac{\Delta_{\hat{j}}(k' \tau_s^G)}{\bar{\Delta}_u(k' \tau_s^G)} \mathbb{E}\left[\left\|\nabla F_{\hat{j}}(\bar{\mathbf{w}}_u(\tau_s^L \tau_s^G k' - 1)) - \nabla F_{\hat{j}}(\mathbf{w}_{\hat{j}}(\tau_s^L \tau_s^G k' - 1))\right\|^2\right] \\
&+ 24\eta_2^2 \frac{1}{U(s)} \sum_{u \in \mathcal{U}(s)} \sum_{j \in \mathcal{W}_u} \frac{\Delta_j(k' \tau_s^G)}{\bar{\Delta}_u(k' \tau_s^G)} \mathbb{E}\left[\left\|\nabla F_j(\bar{\mathbf{w}}_u(\tau_s^L \tau_s^G k' - 1)) - \nabla \bar{F}_u(\bar{\mathbf{w}}_u(\tau_s^L \tau_s^G k' - 1))\right\|^2\right] \\
&\stackrel{(d)}{\leq} 24\eta_2^2 \frac{1}{U(s)} \sum_{u \in \mathcal{U}(s)} \sum_{j \in \mathcal{W}_u} \frac{\Delta_j(k' \tau_s^G)}{\bar{\Delta}_u(k' \tau_s^G)} \mu_F^2 \mathbb{E}[\|\mathbf{w}_j(\tau_s^L \tau_s^G k' - 1) - \bar{\mathbf{w}}_u(\tau_s^L \tau_s^G k' - 1)\|^2] \\
&+ 24\eta_2^2 \frac{1}{U(s)} \sum_{u \in \mathcal{U}(s)} \sum_{\hat{j} \in \mathcal{W}_u} \frac{\Delta_{\hat{j}}(k' \tau_s^G)}{\bar{\Delta}_u(k' \tau_s^G)} \mu_F^2 \mathbb{E}[\|\bar{\mathbf{w}}_u(\tau_s^L \tau_s^G k' - 1) - \mathbf{w}_{\hat{j}}(\tau_s^L \tau_s^G k' - 1)\|^2] \\
&+ 24\eta_2^2 \frac{1}{U(s)} \sum_{u \in \mathcal{U}(s)} \sum_{j \in \mathcal{W}_u} \frac{\Delta_j(k' \tau_s^G)}{\bar{\Delta}_u(k' \tau_s^G)} \mathbb{E}\left[\left\|\nabla F_j(\bar{\mathbf{w}}_u(\tau_s^L \tau_s^G k' - 1)) - \nabla \bar{F}_u(\bar{\mathbf{w}}_u(\tau_s^L \tau_s^G k' - 1))\right\|^2\right] \\
&\stackrel{(e)}{\leq} 48\mu_F^2 \eta_2^2 \frac{1}{U(s)} \sum_{u \in \mathcal{U}(s)} \sum_{j \in \mathcal{W}_u} \frac{\Delta_j(k' \tau_s^G)}{\bar{\Delta}_u(k' \tau_s^G)} \mathbb{E}[\|\mathbf{w}_j(\tau_s^L \tau_s^G k' - 1) - \bar{\mathbf{w}}_u(\tau_s^L \tau_s^G k' - 1)\|^2] + 24\eta_2^2 \frac{1}{U(s)} \sum_{u \in \mathcal{U}(s)} (\gamma_F^u)^2,
\end{aligned}$$

where (a) introduces $\nabla F_j(\bar{\mathbf{w}}_u)$ and $\nabla F_{\hat{j}}(\bar{\mathbf{w}}_u)$, (b) applies Jensen's inequality, (c) recalls the aggregation rule of $\nabla \bar{F}_u$ and applies Jensen's inequality, (d) uses μ_F -smoothness (i.e., $\|\nabla F_j(\mathbf{w}) - \nabla F_j(\mathbf{w}')\| \leq \mu_F \|\mathbf{w} - \mathbf{w}'\| \forall i \in \cup_{u \in \mathcal{U}(s)} \mathcal{W}_u$), and (e) leverages Lemma 2. Combining (65) and (66) yields:

$$\begin{aligned}
&2 \frac{1}{U(s)} \sum_{u \in \mathcal{U}(s)} \sum_{j \in \mathcal{W}_u} \frac{\Delta_j(k' \tau_s^G)}{\bar{\Delta}_u(k' \tau_s^G)} \mathbb{E}[\|\mathbf{w}_j(\tau_s^L \tau_s^G k' - 1) - \bar{\mathbf{w}}_u(\tau_s^L \tau_s^G k' - 1)\|^2] \tag{67} \\
&\stackrel{(a)}{\leq} 8 \frac{1}{U(s)} \sum_{u \in \mathcal{U}(s)} \sum_{j \in \mathcal{W}_u} \frac{\Delta_j(k' \tau_s^G)}{\bar{\Delta}_u(k' \tau_s^G)} \mathbb{E}[\|\mathbf{w}_j(\tau_s^L \tau_s^G k' - 1) - \bar{\mathbf{w}}_u(\tau_s^L \tau_s^G k' - 1)\|^2] \\
&+ 8\eta_2^2 \frac{1}{U(s)} \sum_{u \in \mathcal{U}(s)} \sum_{j \in \mathcal{W}_u} \frac{\Delta_j(k' \tau_s^G)}{\bar{\Delta}_u(k' \tau_s^G)} \mathbb{E}[\|\nabla F_j(\mathbf{w}_j(\tau_s^L \tau_s^G k' - 1)) - \nabla \tilde{F}_j(\mathbf{w}_j(\tau_s^L \tau_s^G k' - 1))\|^2] \\
&+ 8\eta_2^2 \frac{1}{U(s)} \sum_{u \in \mathcal{U}(s)} \sum_{j \in \mathcal{W}_u} \frac{\Delta_j(k' \tau_s^G)}{\bar{\Delta}_u(k' \tau_s^G)} \mathbb{E}\left[\left\|\sum_{\hat{j} \in \mathcal{W}_u} \frac{\Delta_{\hat{j}}(k' \tau_s^G)}{\bar{\Delta}_u(k' \tau_s^G)} \left(\nabla \tilde{F}_{\hat{j}}(\mathbf{w}_{\hat{j}}(\tau_s^L \tau_s^G k' - 1)) - \nabla F_{\hat{j}}(\mathbf{w}_{\hat{j}}(\tau_s^L \tau_s^G k' - 1))\right)\right\|^2\right] \\
&+ 8\eta_2^2 \frac{1}{U(s)} \sum_{u \in \mathcal{U}(s)} \sum_{j \in \mathcal{W}_u} \frac{\Delta_j(k' \tau_s^G)}{\bar{\Delta}_u(k' \tau_s^G)} \mathbb{E}\left[\left\|\nabla F_j(\mathbf{w}_j(\tau_s^L \tau_s^G k' - 1)) - \sum_{\hat{j} \in \mathcal{W}_u} \frac{\Delta_{\hat{j}}(k' \tau_s^G)}{\bar{\Delta}_u(k' \tau_s^G)} \nabla F_{\hat{j}}(\mathbf{w}_{\hat{j}}(\tau_s^L \tau_s^G k' - 1))\right\|^2\right] \\
&\stackrel{(b)}{\leq} 8 \frac{1}{U(s)} \sum_{u \in \mathcal{U}(s)} \sum_{j \in \mathcal{W}_u} \frac{\Delta_j(k' \tau_s^G)}{\bar{\Delta}_u(k' \tau_s^G)} \mathbb{E}[\|\mathbf{w}_j(\tau_s^L \tau_s^G k' - 1) - \bar{\mathbf{w}}_u(\tau_s^L \tau_s^G k' - 1)\|^2] + 16\eta_2^2 \frac{1}{U(s)} \sum_{u \in \mathcal{U}(s)} \sum_{j \in \mathcal{W}_u} \frac{\Delta_j(k' \tau_s^G)}{\bar{\Delta}_u(k' \tau_s^G)} (\sigma_j^F(\tau_s^L \tau_s^G k' - 1))^2 \\
&+ 8\eta_2^2 \frac{1}{U(s)} \sum_{u \in \mathcal{U}(s)} \sum_{j \in \mathcal{W}_u} \frac{\Delta_j(k' \tau_s^G)}{\bar{\Delta}_u(k' \tau_s^G)} \mathbb{E}\left[\left\|\nabla F_j(\mathbf{w}_j(\tau_s^L \tau_s^G k' - 1)) - \sum_{\hat{j} \in \mathcal{W}_u} \frac{\Delta_{\hat{j}}(k' \tau_s^G)}{\bar{\Delta}_u(k' \tau_s^G)} \nabla F_{\hat{j}}(\mathbf{w}_{\hat{j}}(\tau_s^L \tau_s^G k' - 1))\right\|^2\right] \\
&\stackrel{(c)}{\leq} (8 + 48\eta_2^2 \mu_F^2) \frac{1}{U(s)} \sum_{u \in \mathcal{U}(s)} \sum_{j \in \mathcal{W}_u} \frac{\Delta_j(k' \tau_s^G)}{\bar{\Delta}_u(k' \tau_s^G)} \mathbb{E}[\|\mathbf{w}_j(\tau_s^L \tau_s^G k' - 1) - \bar{\mathbf{w}}_u(\tau_s^L \tau_s^G k' - 1)\|^2] \\
&+ 16\eta_2^2 \frac{1}{U(s)} \sum_{u \in \mathcal{U}(s)} \sum_{j \in \mathcal{W}_u} \frac{\Delta_j(k' \tau_s^G)}{\bar{\Delta}_u(k' \tau_s^G)} (\sigma_j^F(\tau_s^L \tau_s^G k' - 1))^2 + 24\eta_2^2 \frac{1}{U(s)} \sum_{u \in \mathcal{U}(s)} (\gamma_F^u)^2,
\end{aligned}$$

where (a) restates (65) with the previously omitted summations, (b) applies Jensen's inequality and Lemma 1, and (c) uses the result in (66). Solving (67) recursively yields:

$$2 \frac{1}{U(s)} \sum_{u \in \mathcal{U}(s)} \sum_{j \in \mathcal{W}_u} \frac{\Delta_j(k' \tau_s^G)}{\bar{\Delta}_u(k' \tau_s^G)} \mathbb{E}[\|\mathbf{w}_j(\tau_s^L \tau_s^G k' - 1) - \bar{\mathbf{w}}_u(\tau_s^L \tau_s^G k' - 1)\|^2] \tag{68}$$

$$\stackrel{(a)}{\leq} 16\eta_2^2 \frac{1}{U(s)} \sum_{u \in \mathcal{U}(s)} \sum_{j \in \mathcal{W}_u} \frac{\Delta_j(k' \tau_s^G)}{\bar{\Delta}_u(k' \tau_s^G)} \left(\sum_{y=0}^{\tau_s^L-1} (\sigma_j^F(\tau_s^L \tau_s^G k' - 1 - y))^2 (8 + 48\eta_2^2 \mu_F^2)^y \right) + 24\eta_2^2 \frac{1}{U(s)} \sum_{u \in \mathcal{U}(s)} (\gamma_F^u)^2 \frac{1 - (8 + 48\eta_2^2 \mu_F^2)^{\tau_s^L}}{1 - (8 + 48\eta_2^2 \mu_F^2)} \tag{69}$$

$$\stackrel{(b)}{\leq} \left(16\eta_2^2 \frac{1}{U(s)} \sum_{u \in \mathcal{U}(s)} \sum_{j \in \mathcal{W}_u} \frac{\Delta_j(k' \tau_s^G)}{\Delta_u(k' \tau_s^G)} \sum_{y=0}^{\tau_s^L-1} (\sigma_j^F(\tau_s^L \tau_s^G k' - 1 - y))^2 + 24\eta_2^2 \frac{1}{U(s)} \sum_{u \in \mathcal{U}(s)} (\gamma_F^u)^2 \right) \frac{1 - (8 + 48\eta_2^2 \mu_F^2)^{\tau_s^L}}{1 - (8 + 48\eta_2^2 \mu_F^2)}, \quad (70)$$

where (a) is the result of recursion and the finite sum of geometric series, and (b) uses $\sum_i a_i b_i \leq \sum_i a_i \sum_i b_i \forall a_i, b_i \geq 0$. Next, we bound (64)(ii) as follows:

$$\begin{aligned} & 2 \frac{1}{U(s)} \sum_{u \in \mathcal{U}(s)} \mathbb{E}[\|\bar{\mathbf{w}}_u(\tau_s^L \tau_s^G k') - \bar{\mathbf{w}}(\tau_s^L \tau_s^G k')\|^2] \stackrel{(a)}{=} 2 \frac{1}{U(s)} \sum_{u \in \mathcal{U}(s)} \mathbb{E} \left[\left\| \bar{\mathbf{w}}_u(\tau_s^L \tau_s^G k') - \frac{1}{U(s)} \sum_{\hat{u} \in \mathcal{U}(s)} \bar{\mathbf{w}}_{\hat{u}}(\tau_s^L \tau_s^G k') \right\|^2 \right] \\ & \stackrel{(b)}{=} 2 \frac{1}{U(s)} \sum_{u \in \mathcal{U}(s)} \mathbb{E} \left[\left\| \bar{\mathbf{w}}_u(\tau_s^L \tau_s^G k' - 1) - \eta_2 \nabla \tilde{F}_u(\bar{\mathbf{w}}_u(\tau_s^L \tau_s^G k' - 1)) - \frac{1}{U(s)} \sum_{\hat{u} \in \mathcal{U}(s)} \left(\bar{\mathbf{w}}_{\hat{u}}(\tau_s^L \tau_s^G k' - 1) - \eta_2 \nabla \tilde{F}_{\hat{u}}(\bar{\mathbf{w}}_{\hat{u}}(\tau_s^L \tau_s^G k' - 1)) \right) \right\|^2 \right] \\ & \stackrel{(c)}{=} 2 \frac{1}{U(s)} \sum_{u \in \mathcal{U}(s)} \mathbb{E} \left[\left\| \bar{\mathbf{w}}_u(\tau_s^L \tau_s^G k' - 1) - \eta_2 \nabla \tilde{F}_u(\bar{\mathbf{w}}_u(\tau_s^L \tau_s^G k' - 1)) + \eta_2 \nabla \bar{F}_u(\bar{\mathbf{w}}_u(\tau_s^L \tau_s^G k' - 1)) - \eta_2 \nabla \bar{F}_u(\bar{\mathbf{w}}_u(\tau_s^L \tau_s^G k' - 1)) \right. \right. \\ & \quad \left. \left. - \frac{1}{U(s)} \sum_{\hat{u} \in \mathcal{U}(s)} \left(\bar{\mathbf{w}}_{\hat{u}}(\tau_s^L \tau_s^G k' - 1) - \eta_2 \nabla \tilde{F}_{\hat{u}}(\bar{\mathbf{w}}_{\hat{u}}(\tau_s^L \tau_s^G k' - 1)) + \eta_2 \nabla \bar{F}_{\hat{u}}(\bar{\mathbf{w}}_{\hat{u}}(\tau_s^L \tau_s^G k' - 1)) - \eta_2 \nabla \bar{F}_{\hat{u}}(\bar{\mathbf{w}}_{\hat{u}}(\tau_s^L \tau_s^G k' - 1)) \right) \right\|^2 \right] \\ & \stackrel{(d)}{\leq} \underbrace{8 \frac{1}{U(s)} \sum_{u \in \mathcal{U}(s)} \mathbb{E} \left[\left\| \bar{\mathbf{w}}_u(\tau_s^L \tau_s^G k' - 1) - \frac{1}{U(s)} \sum_{\hat{u} \in \mathcal{U}(s)} \bar{\mathbf{w}}_{\hat{u}}(\tau_s^L \tau_s^G k' - 1) \right\|^2 \right]}_{(i)} \\ & \quad + \underbrace{8\eta_2^2 \frac{1}{U(s)} \sum_{u \in \mathcal{U}(s)} \mathbb{E}[\|\nabla \bar{F}_u(\bar{\mathbf{w}}_u(\tau_s^L \tau_s^G k' - 1)) - \nabla \tilde{F}_u(\bar{\mathbf{w}}_u(\tau_s^L \tau_s^G k' - 1))\|^2]}_{(ii)} \\ & \quad + \underbrace{8\eta_2^2 \frac{1}{U(s)} \sum_{u \in \mathcal{U}(s)} \mathbb{E} \left[\left\| \frac{1}{U(s)} \sum_{\hat{u} \in \mathcal{U}(s)} \left(\nabla \tilde{F}_{\hat{u}}(\bar{\mathbf{w}}_{\hat{u}}(\tau_s^L \tau_s^G k' - 1)) - \nabla \bar{F}_{\hat{u}}(\bar{\mathbf{w}}_{\hat{u}}(\tau_s^L \tau_s^G k' - 1)) \right) \right\|^2 \right]}_{(iii)} \\ & \quad + \underbrace{8\eta_2^2 \frac{1}{U(s)} \sum_{u \in \mathcal{U}(s)} \mathbb{E} \left[\left\| \frac{1}{U(s)} \sum_{\hat{u} \in \mathcal{U}(s)} \nabla \bar{F}_{\hat{u}}(\bar{\mathbf{w}}_{\hat{u}}(\tau_s^L \tau_s^G k' - 1)) - \nabla \bar{F}_u(\bar{\mathbf{w}}_u(\tau_s^L \tau_s^G k' - 1)) \right\|^2 \right]}_{(iv)}, \end{aligned} \quad (71)$$

where (a) uses the definition of $\bar{\mathbf{w}}$ from (7), (b) is the global parameter update rule with \tilde{F}_u using an approximation \tilde{F} of F in (6) (the same applies for \tilde{F}), (c) introduces $\eta_2 \nabla \bar{F}_u(\bar{\mathbf{w}}_u)$ and $\eta_2 \nabla \bar{F}_{\hat{u}}(\bar{\mathbf{w}}_{\hat{u}})$, and (d) follows from Cauchy-Schwarz inequality. Upper bounds for (71)(ii) and (71)(iii) follow immediately from Lemma 1, and we bound (71)(iv) as follows:

$$\begin{aligned} & 8\eta_2^2 \frac{1}{U(s)} \sum_{u \in \mathcal{U}(s)} \mathbb{E} \left[\left\| \frac{1}{U(s)} \sum_{\hat{u} \in \mathcal{U}(s)} \nabla \bar{F}_{\hat{u}}(\bar{\mathbf{w}}_{\hat{u}}(\tau_s^L \tau_s^G k' - 1)) - \nabla \bar{F}_u(\bar{\mathbf{w}}_u(\tau_s^L \tau_s^G k' - 1)) \right\|^2 \right] \\ & \stackrel{(a)}{=} 8\eta_2^2 \frac{1}{U(s)} \sum_{u \in \mathcal{U}(s)} \mathbb{E} \left[\left\| \frac{1}{U(s)} \sum_{\hat{u} \in \mathcal{U}(s)} \left(\nabla \bar{F}_{\hat{u}}(\bar{\mathbf{w}}_{\hat{u}}(\tau_s^L \tau_s^G k' - 1)) - \nabla \bar{F}_{\hat{u}}(\bar{\mathbf{w}}(\tau_s^L \tau_s^G k' - 1)) + \nabla \bar{F}_{\hat{u}}(\bar{\mathbf{w}}(\tau_s^L \tau_s^G k' - 1)) \right. \right. \right. \\ & \quad \left. \left. - \nabla \bar{F}_u(\bar{\mathbf{w}}_u(\tau_s^L \tau_s^G k' - 1)) + \nabla \bar{F}_u(\bar{\mathbf{w}}(\tau_s^L \tau_s^G k' - 1)) - \nabla \bar{F}_u(\bar{\mathbf{w}}(\tau_s^L \tau_s^G k' - 1)) \right) \right\|^2 \right] \\ & \stackrel{(b)}{\leq} 24\eta_2^2 \frac{1}{U(s)} \sum_{u \in \mathcal{U}(s)} \mathbb{E} \left[\left\| \frac{1}{U(s)} \sum_{\hat{u} \in \mathcal{U}(s)} \sum_{j \in \mathcal{W}_{\hat{u}}} \frac{\Delta_j(k' \tau_s^G)}{\Delta_{\hat{u}}(k' \tau_s^G)} \left(\nabla F_j(\bar{\mathbf{w}}_{\hat{u}}(\tau_s^L \tau_s^G k' - 1)) - \nabla F_j(\bar{\mathbf{w}}(\tau_s^L \tau_s^G k' - 1)) \right) \right\|^2 \right] \\ & \quad + 24\eta_2^2 \frac{1}{U(s)} \sum_{u \in \mathcal{U}(s)} \mathbb{E} \left[\left\| \sum_{j \in \mathcal{W}_{\hat{u}}} \frac{\Delta_j(k' \tau_s^G)}{\Delta_{\hat{u}}(k' \tau_s^G)} \left(\nabla F_j(\bar{\mathbf{w}}(\tau_s^L \tau_s^G k' - 1)) - \nabla F_j(\bar{\mathbf{w}}_u(\tau_s^L \tau_s^G k' - 1)) \right) \right\|^2 \right] \\ & \quad + 24\eta_2^2 \frac{1}{U(s)} \sum_{u \in \mathcal{U}(s)} \mathbb{E}[\|\nabla \bar{F}(\bar{\mathbf{w}}(\tau_s^L \tau_s^G k' - 1)) - \nabla \bar{F}_u(\bar{\mathbf{w}}(\tau_s^L \tau_s^G k' - 1))\|^2] \\ & \stackrel{(c)}{\leq} 24\eta_2^2 \frac{1}{U(s)} \sum_{u \in \mathcal{U}(s)} \frac{1}{U(s)} \sum_{\hat{u} \in \mathcal{U}(s)} \sum_{j \in \mathcal{W}_{\hat{u}}} \frac{\Delta_j(k' \tau_s^G)}{\Delta_{\hat{u}}(k' \tau_s^G)} \mathbb{E} \left[\left\| \nabla F_j(\bar{\mathbf{w}}_{\hat{u}}(\tau_s^L \tau_s^G k' - 1)) - \nabla F_j(\bar{\mathbf{w}}(\tau_s^L \tau_s^G k' - 1)) \right\|^2 \right] \\ & \quad + 24\eta_2^2 \frac{1}{U(s)} \sum_{u \in \mathcal{U}(s)} \sum_{j \in \mathcal{W}_{\hat{u}}} \frac{\Delta_j(k' \tau_s^G)}{\Delta_{\hat{u}}(k' \tau_s^G)} \mathbb{E} \left[\left\| \nabla F_j(\bar{\mathbf{w}}(\tau_s^L \tau_s^G k' - 1)) - \nabla F_j(\bar{\mathbf{w}}_u(\tau_s^L \tau_s^G k' - 1)) \right\|^2 \right] \end{aligned}$$

$$\begin{aligned}
& + 24\eta_2^2 \frac{1}{U(s)} \sum_{u \in \mathcal{U}(s)} \mathbb{E}[\|\nabla \bar{F}(\bar{\mathbf{w}}(\tau_s^L \tau_s^G k' - 1)) - \nabla \bar{F}_u(\bar{\mathbf{w}}(\tau_s^L \tau_s^G k' - 1))\|^2] \\
& \stackrel{(d)}{\leq} 24\eta_2^2 \mu_F^2 \frac{1}{U(s)} \sum_{u \in \mathcal{U}(s)} \frac{1}{U(s)} \sum_{\hat{u} \in \mathcal{U}(s)} \sum_{j \in \mathcal{W}_{\hat{u}}} \frac{\Delta_j(k' \tau_s^G)}{\Delta_{\hat{u}}(k' \tau_s^G)} \mathbb{E}[\|\bar{\mathbf{w}}_{\hat{u}}(\tau_s^L \tau_s^G k' - 1) - \bar{\mathbf{w}}(\tau_s^L \tau_s^G k' - 1)\|^2] \\
& + 24\eta_2^2 \mu_F^2 \frac{1}{U(s)} \sum_{u \in \mathcal{U}(s)} \sum_{j \in \mathcal{W}_{\hat{u}}} \frac{\Delta_j(k' \tau_s^G)}{\Delta_{\hat{u}}(k' \tau_s^G)} \mathbb{E}[\|\bar{\mathbf{w}}(\tau_s^L \tau_s^G k' - 1) - \bar{\mathbf{w}}_u(\tau_s^L \tau_s^G k' - 1)\|^2] \\
& + 24\eta_2^2 \frac{1}{U(s)} \sum_{u \in \mathcal{U}(s)} \mathbb{E}[\|\nabla \bar{F}(\bar{\mathbf{w}}(\tau_s^L \tau_s^G k' - 1)) - \nabla \bar{F}_u(\bar{\mathbf{w}}(\tau_s^L \tau_s^G k' - 1))\|^2] \\
& \stackrel{(e)}{\leq} 48\eta_2^2 \mu_F^2 \frac{1}{U(s)} \sum_{u \in \mathcal{U}(s)} \mathbb{E}[\|\bar{\mathbf{w}}_{\hat{u}}(\tau_s^L \tau_s^G k' - 1) - \bar{\mathbf{w}}(\tau_s^L \tau_s^G k' - 1)\|^2] + 24\eta_2^2 \gamma_F^2, \tag{72}
\end{aligned}$$

where (a) introduces $\nabla \bar{F}_{\hat{u}}(\mathbf{w})$ and $\nabla \bar{F}_u(\mathbf{w})$ terms, (b) uses the Cauchy-Schwarz followed by the swarm-wide meta-gradient definition from (6), (c) applies Jensen's inequality to the expectations, (d) recalls the μ_F -smoothness property of ∇F_j , and (e) uses the result of Lemma 2. Combining (71) and (72) yields:

$$\begin{aligned}
& 2 \frac{1}{U(s)} \sum_{u \in \mathcal{U}(s)} \mathbb{E}[\|\bar{\mathbf{w}}_u(\tau_s^L \tau_s^G k' - 1) - \bar{\mathbf{w}}(\tau_s^L \tau_s^G k' - 1)\|^2] \\
& \stackrel{(a)}{\leq} 8 \frac{1}{U(s)} \sum_{u \in \mathcal{U}(s)} \mathbb{E} \left[\left\| \bar{\mathbf{w}}_u(\tau_s^L \tau_s^G k' - 1) - \frac{1}{U(s)} \sum_{\hat{u} \in \mathcal{U}(s)} \bar{\mathbf{w}}_{\hat{u}}(\tau_s^L \tau_s^G k' - 1) \right\|^2 \right] \\
& + 8\eta_2^2 \frac{1}{U(s)} \sum_{u \in \mathcal{U}(s)} \mathbb{E}[\|\nabla \bar{F}_u(\bar{\mathbf{w}}_u(\tau_s^L \tau_s^G k' - 1)) - \nabla \tilde{F}_u(\bar{\mathbf{w}}_u(\tau_s^L \tau_s^G k' - 1))\|^2] \\
& + 8\eta_2^2 \frac{1}{U(s)} \sum_{u \in \mathcal{U}(s)} \mathbb{E} \left[\left\| \frac{1}{U(s)} \sum_{\hat{u} \in \mathcal{U}(s)} \left(\nabla \tilde{F}_{\hat{u}}(\bar{\mathbf{w}}_{\hat{u}}(\tau_s^L \tau_s^G k' - 1)) - \nabla \bar{F}_{\hat{u}}(\bar{\mathbf{w}}_{\hat{u}}(\tau_s^L \tau_s^G k' - 1)) \right) \right\|^2 \right] \\
& + 48\eta_2^2 \mu_F^2 \frac{1}{U(s)} \sum_{u \in \mathcal{U}(s)} \mathbb{E}[\|\bar{\mathbf{w}}_{\hat{u}}(\tau_s^L \tau_s^G k' - 1) - \bar{\mathbf{w}}(\tau_s^L \tau_s^G k' - 1)\|^2] + 24\eta_2^2 \gamma_F^2 \\
& \stackrel{(b)}{\leq} (8 + 48\eta_2^2 \mu_F^2) \frac{1}{U(s)} \sum_{u \in \mathcal{U}(s)} \mathbb{E} \left[\left\| \bar{\mathbf{w}}_u(\tau_s^L \tau_s^G k' - 1) - \frac{1}{U(s)} \sum_{\hat{u} \in \mathcal{U}(s)} \bar{\mathbf{w}}_{\hat{u}}(\tau_s^L \tau_s^G k' - 1) \right\|^2 \right] + 24\eta_2^2 \gamma_F^2 \\
& + 8\eta_2^2 \frac{1}{U(s)} \sum_{u \in \mathcal{U}(s)} \mathbb{E} \left[\left\| \sum_{j \in \mathcal{W}_u} \frac{\Delta_j(k' \tau_s^G)}{\Delta_u(k' \tau_s^G)} \left(\nabla F_j(\bar{\mathbf{w}}_u(\tau_s^L \tau_s^G k' - 1)) - \nabla \tilde{F}_j(\bar{\mathbf{w}}_u(\tau_s^L \tau_s^G k' - 1)) \right) \right\|^2 \right] \\
& + 8\eta_2^2 \frac{1}{U(s)} \sum_{u \in \mathcal{U}(s)} \mathbb{E} \left[\left\| \frac{1}{U(s)} \sum_{\hat{u} \in \mathcal{U}(s)} \sum_{j \in \mathcal{W}_{\hat{u}}} \frac{\Delta_j(k' \tau_s^G)}{\Delta_{\hat{u}}(k' \tau_s^G)} \left(\nabla \tilde{F}_j(\bar{\mathbf{w}}_{\hat{u}}(\tau_s^L \tau_s^G k' - 1)) - \nabla F_j(\bar{\mathbf{w}}_{\hat{u}}(\tau_s^L \tau_s^G k' - 1)) \right) \right\|^2 \right] \\
& \stackrel{(c)}{\leq} (8 + 48\eta_2^2 \mu_F^2) \frac{1}{U(s)} \sum_{u \in \mathcal{U}(s)} \mathbb{E}[\|\bar{\mathbf{w}}_u(\tau_s^L \tau_s^G k' - 1) - \bar{\mathbf{w}}(\tau_s^L \tau_s^G k' - 1)\|^2] + 24\eta_2^2 \gamma_F^2 \\
& + 16\eta_2^2 \frac{1}{U(s)} \sum_{u \in \mathcal{U}(s)} \sum_{j \in \mathcal{W}_u} \frac{\Delta_j(k' \tau_s^G)}{\Delta_u(k' \tau_s^G)} (\sigma_F^j(\tau_s^L \tau_s^G k' - 1))^2, \tag{73}
\end{aligned}$$

where (a) combines (71) and (72), (b) applies definition of $\nabla \bar{F}_u$ from (6), (c) uses Jensen's inequality followed by Lemma 1 and the definition of $\bar{\mathbf{w}}$ from (7). Solving (73) recursively yields:

$$2 \frac{1}{U(s)} \sum_{u \in \mathcal{U}(s)} \mathbb{E}[\|\bar{\mathbf{w}}_u(\tau_s^L \tau_s^G k' - 1) - \bar{\mathbf{w}}(\tau_s^L \tau_s^G k' - 1)\|^2] \tag{74}$$

$$\stackrel{(a)}{\leq} 16\eta_2^2 \frac{1}{U(s)} \sum_{u \in \mathcal{U}(s)} \sum_{j \in \mathcal{W}_u} \frac{\Delta_j(k' \tau_s^G)}{\Delta_u(k' \tau_s^G)} \left(\sum_{y=0}^{\tau_s^L \tau_s^G - 1} (\sigma_F^j(\tau_s^L \tau_s^G k' - 1 - y))^2 (8 + 48\eta_2^2 \mu_F^2)^y \right) + 24\eta_2^2 \gamma_F^2 \frac{1 - (8 + 48\eta_2^2 \mu_F^2)^{\tau_s^L \tau_s^G}}{1 - (8 + 48\eta_2^2 \mu_F^2)} \tag{75}$$

$$\stackrel{(b)}{\leq} \left(16\eta_2^2 \frac{1}{U(s)} \sum_{u \in \mathcal{U}(s)} \sum_{j \in \mathcal{W}_u} \frac{\Delta_j(k' \tau_s^G)}{\Delta_u(k' \tau_s^G)} \sum_{y=0}^{\tau_s^L \tau_s^G - 1} (\sigma_F^j(\tau_s^L \tau_s^G k' - 1 - y))^2 + 24\eta_2^2 \gamma_F^2 \right) \frac{1 - (8 + 48\eta_2^2 \mu_F^2)^{\tau_s^L \tau_s^G}}{1 - (8 + 48\eta_2^2 \mu_F^2)}, \tag{76}$$

where (a) is the result of recursion and the finite sum of geometric series, and (b) uses $\sum_i a_i b_i \leq \sum_i a_i \sum_i b_i \forall a_i, b_i \geq 0$. Combining the results of (68) and (74) in (64) yields:

$$\begin{aligned}
& 2 \frac{1}{U(s)} \sum_{u \in \mathcal{U}(s)} \sum_{j \in \mathcal{W}_u} \frac{\Delta_j(k' \tau_s^G)}{\bar{\Delta}_u(k' \tau_s^G)} \left(\mathbb{E}[\|\mathbf{w}_j(\tau_s^L \tau_s^G k') - \bar{\mathbf{w}}_u(\tau_s^L \tau_s^G k')\|^2] + \mathbb{E}[\|\bar{\mathbf{w}}_u(\tau_s^L \tau_s^G k') - \bar{\mathbf{w}}(\tau_s^L \tau_s^G k')\|^2] \right) \\
& \leq \left(16\eta_2^2 \frac{1}{U(s)} \sum_{u \in \mathcal{U}(s)} \sum_{j \in \mathcal{W}_u} \frac{\Delta_j(k' \tau_s^G)}{\bar{\Delta}_u(k' \tau_s^G)} \sum_{y=1}^{\tau_s^L} (\sigma_j^F(\tau_s^L \tau_s^G k' - y))^2 + 24\eta_2^2 \frac{1}{U(s)} \sum_{u \in \mathcal{U}(s)} (\gamma_F^u)^2 \right) \frac{1 - (8 + 48\eta_2^2 \mu_F^2)^{\tau_s^L}}{1 - (8 + 48\eta_2^2 \mu_F^2)} \\
& + \left(16\eta_2^2 \frac{1}{U(s)} \sum_{u \in \mathcal{U}(s)} \sum_{j \in \mathcal{W}_u} \frac{\Delta_j(k' \tau_s^G)}{\bar{\Delta}_u(k' \tau_s^G)} \sum_{y=1}^{\tau_s^L \tau_s^G} (\sigma_j^F(\tau_s^L \tau_s^G k' - y))^2 + 24\eta_2^2 \gamma_F^2 \right) \frac{1 - (8 + 48\eta_2^2 \mu_F^2)^{\tau_s^L \tau_s^G}}{1 - (8 + 48\eta_2^2 \mu_F^2)},
\end{aligned} \tag{77}$$

with the summation shifted from $y = 0$ to $y = 1$. ■

APPENDIX B

PROOF OF THEOREM 1

Proof. First, from Assumption 1, we see that $F_j(t)$, $F_u(t)$, and $F(t)$ are all μ_F -smooth where $\mu_F = 4\mu^G + \eta_1\mu^H B$ (result follows immediately from [36] upon using triangle inequality). In order to bound the first-order stationary point, $\mathbb{E}[\|\nabla \bar{F}(\bar{\mathbf{w}})\|^2]$, we start with

$$\begin{aligned}
\bar{F}(\bar{\mathbf{w}}(\tau_s^L \tau_s^G k')) &\stackrel{(a)}{\leq} \bar{F}(\bar{\mathbf{w}}(\tau_s^L \tau_s^G k' - 1)) + \nabla \bar{F}(\bar{\mathbf{w}}(\tau_s^L \tau_s^G k' - 1))^T (\bar{\mathbf{w}}(\tau_s^L \tau_s^G k') - \bar{\mathbf{w}}(\tau_s^L \tau_s^G k' - 1)) + \frac{\mu_F}{2} \|\bar{\mathbf{w}}(\tau_s^L \tau_s^G k') - \bar{\mathbf{w}}(\tau_s^L \tau_s^G k' - 1)\|^2 \\
&\stackrel{(b)}{=} \bar{F}(\bar{\mathbf{w}}(\tau_s^L \tau_s^G k' - 1)) - \eta_2 \nabla \bar{F}(\bar{\mathbf{w}}(\tau_s^L \tau_s^G k' - 1))^T \left(\frac{1}{U(s)} \sum_{u \in \mathcal{U}(s)} \sum_{j \in \mathcal{W}_u} \frac{\Delta_j(k' \tau_s^G)}{\bar{\Delta}_u(k' \tau_s^G)} \nabla \tilde{F}_j(\mathbf{w}_j(\tau_s^L \tau_s^G k' - 1)) \right) \\
&\quad + \frac{\mu_F}{2} \left\| -\eta_2 \frac{1}{U(s)} \sum_{u \in \mathcal{U}(s)} \sum_{j \in \mathcal{W}_u} \frac{\Delta_j(k' \tau_s^G)}{\bar{\Delta}_u(k' \tau_s^G)} \nabla \tilde{F}_j(\mathbf{w}_j(\tau_s^L \tau_s^G k' - 1)) \right\|^2 \\
&\stackrel{(c)}{=} \bar{F}(\bar{\mathbf{w}}(\tau_s^L \tau_s^G k' - 1)) - \eta_2 \nabla \bar{F}(\bar{\mathbf{w}}(\tau_s^L \tau_s^G k' - 1))^T \left(\frac{1}{U(s)} \sum_{u \in \mathcal{U}(s)} \sum_{j \in \mathcal{W}_u} \frac{\Delta_j(k' \tau_s^G)}{\bar{\Delta}_u(k' \tau_s^G)} \nabla \tilde{F}_j(\mathbf{w}_j(\tau_s^L \tau_s^G k' - 1)) \right) \\
&\quad + \eta_2^2 \frac{\mu_F}{2} \left\| \frac{1}{U(s)} \sum_{u \in \mathcal{U}(s)} \sum_{j \in \mathcal{W}_u} \frac{\Delta_j(k' \tau_s^G)}{\bar{\Delta}_u(k' \tau_s^G)} \nabla \tilde{F}_j(\mathbf{w}_j(\tau_s^L \tau_s^G k' - 1)) \right\|^2,
\end{aligned} \tag{78}$$

where (a) follows from the μ_F -smoothness property of F , F_u , and F_j , (b) uses the meta-gradient update procedure from (1) and the definition of $\bar{\mathbf{w}}$ from (7), and (c) simplifies the algebra. Taking the expectation of both sides of (78) yields:

$$\begin{aligned}
&\mathbb{E}[\bar{F}(\bar{\mathbf{w}}(\tau_s^L \tau_s^G k'))] - \mathbb{E}[\bar{F}(\bar{\mathbf{w}}(\tau_s^L \tau_s^G k' - 1))] \leq \\
&\quad \underbrace{-\eta_2 \mathbb{E} \left[\nabla \bar{F}(\bar{\mathbf{w}}(\tau_s^L \tau_s^G k' - 1))^T \left(\frac{1}{U(s)} \sum_{u \in \mathcal{U}(s)} \sum_{j \in \mathcal{W}_u} \frac{\Delta_j(k' \tau_s^G)}{\bar{\Delta}_u(k' \tau_s^G)} \nabla \tilde{F}_j(\mathbf{w}_j(\tau_s^L \tau_s^G k' - 1)) \right) \right]}_{(i)} \\
&\quad + \underbrace{\eta_2^2 \frac{\mu_F}{2} \mathbb{E} \left[\left\| \frac{1}{U(s)} \sum_{u \in \mathcal{U}(s)} \sum_{j \in \mathcal{W}_u} \frac{\Delta_j(k' \tau_s^G)}{\bar{\Delta}_u(k' \tau_s^G)} \nabla \tilde{F}_j(\mathbf{w}_j(\tau_s^L \tau_s^G k' - 1)) \right\|^2 \right]}_{(ii)}.
\end{aligned} \tag{79}$$

Before we bound (79)(i) and (79)(ii), we first analyze

$$\begin{aligned}
&\frac{1}{U(s)} \sum_{u \in \mathcal{U}(s)} \sum_{j \in \mathcal{W}_u} \frac{\Delta_j(k' \tau_s^G)}{\bar{\Delta}_u(k' \tau_s^G)} \nabla \tilde{F}_j(\mathbf{w}_j(\tau_s^L \tau_s^G k' - 1)) \\
&= X + Y + \frac{1}{U(s)} \sum_{u \in \mathcal{U}(s)} \sum_{j \in \mathcal{W}_u} \frac{\Delta_j(k' \tau_s^G)}{\bar{\Delta}_u(k' \tau_s^G)} \nabla F_j(\bar{\mathbf{w}}(\tau_s^L \tau_s^G k' - 1)),
\end{aligned} \tag{80}$$

where:

$$\begin{aligned}
X &\triangleq \frac{1}{U(s)} \sum_{u \in \mathcal{U}(s)} \sum_{j \in \mathcal{W}_u} \frac{\Delta_j(k' \tau_s^G)}{\bar{\Delta}_u(k' \tau_s^G)} \left[\nabla \tilde{F}_j(\mathbf{w}_j(\tau_s^L \tau_s^G k' - 1)) - \nabla F_j(\mathbf{w}_j(\tau_s^L \tau_s^G k' - 1)) \right] \\
Y &\triangleq \frac{1}{U(s)} \sum_{u \in \mathcal{U}(s)} \sum_{j \in \mathcal{W}_u} \frac{\Delta_j(k' \tau_s^G)}{\bar{\Delta}_u(k' \tau_s^G)} \left[\nabla F_j(\mathbf{w}_j(\tau_s^L \tau_s^G k' - 1)) - \nabla F_j(\bar{\mathbf{w}}(\tau_s^L \tau_s^G k' - 1)) \right].
\end{aligned} \tag{81}$$

We now bound $\|X\|^2$ as follows:

$$\begin{aligned}
\mathbb{E}[\|X\|^2] &= \mathbb{E} \left[\left\| \frac{1}{U(s)} \sum_{u \in \mathcal{U}(s)} \sum_{j \in \mathcal{W}_u} \frac{\Delta_j(k' \tau_s^G)}{\bar{\Delta}_u(k' \tau_s^G)} \left(\nabla \tilde{F}_j(\mathbf{w}_j(\tau_s^L \tau_s^G k' - 1)) - \nabla F_j(\mathbf{w}_j(\tau_s^L \tau_s^G k' - 1)) \right) \right\|^2 \right] \\
&\stackrel{(a)}{\leq} \frac{1}{U(s)} \sum_{u \in \mathcal{U}(s)} \sum_{j \in \mathcal{W}_u} \frac{\Delta_j(k' \tau_s^G)}{\bar{\Delta}_u(k' \tau_s^G)} \mathbb{E}[\|\nabla \tilde{F}_j(\mathbf{w}_j(\tau_s^L \tau_s^G k' - 1)) - \nabla F_j(\mathbf{w}_j(\tau_s^L \tau_s^G k' - 1))\|^2] \\
&\stackrel{(b)}{\leq} \frac{1}{U(s)} \sum_{u \in \mathcal{U}(s)} \sum_{j \in \mathcal{W}_u} \frac{\Delta_j(k' \tau_s^G)}{\bar{\Delta}_u(k' \tau_s^G)} (\sigma_j^F(\tau_s^L \tau_s^G k' - 1))^2,
\end{aligned} \tag{82}$$

using (a) Jensen's inequality, and (b) Lemma 1. Next, we bound $\|Y\|^2$ as follows:

$$\begin{aligned}\mathbb{E}[\|Y\|^2] &= \mathbb{E}\left[\left\|\frac{1}{U(s)} \sum_{u \in \mathcal{U}(s)} \sum_{j \in \mathcal{W}_u} \frac{\Delta_j(k' \tau_s^G)}{\Delta_u(k' \tau_s^G)} \left(\nabla F_j(\mathbf{w}_j(\tau_s^L \tau_s^G k' - 1)) - \nabla F_j(\bar{\mathbf{w}}(\tau_s^L \tau_s^G k' - 1)) \right)\right\|^2\right] \\ &\stackrel{(a)}{\leq} \mu_F^2 \mathbb{E}\left[\left\|\frac{1}{U(s)} \sum_{u \in \mathcal{U}(s)} \sum_{j \in \mathcal{W}_u} \frac{\Delta_j(k' \tau_s^G)}{\Delta_u(k' \tau_s^G)} \left(\mathbf{w}_j(\tau_s^L \tau_s^G k' - 1) - \bar{\mathbf{w}}(\tau_s^L \tau_s^G k' - 1) \right)\right\|^2\right] \\ &\stackrel{(b)}{\leq} \mu_F^2 \Upsilon(k' \tau_s^L \tau_s^G),\end{aligned}\tag{83}$$

where (a) uses μ_F -Lipschitz gradient property of F_j , and (b) follows from Proposition 1, note that the recursion step which bounds $\mathbf{w}_j(t) - \bar{\mathbf{w}}(t)$ in Proposition 1 also bounds $\mathbf{w}_j(t-1) - \bar{\mathbf{w}}(t-1)$. Using these results, we first analyze (79)(i) as follows:

$$\begin{aligned}& -\eta_2 \mathbb{E}\left[\nabla \bar{F}(\bar{\mathbf{w}}(\tau_s^L \tau_s^G k' - 1))^T \left(\frac{1}{U(s)} \sum_{u \in \mathcal{U}(s)} \sum_{j \in \mathcal{W}_u} \frac{\Delta_j(k' \tau_s^G)}{\Delta_u(k' \tau_s^G)} \nabla \tilde{F}_j(\mathbf{w}_j(\tau_s^L \tau_s^G k' - 1)) \right)\right] \\ &\stackrel{(a)}{=} -\eta_2 \mathbb{E}\left[\nabla \bar{F}(\bar{\mathbf{w}}(\tau_s^L \tau_s^G k' - 1))^T \left(X + Y + \frac{1}{U(s)} \sum_{u \in \mathcal{U}(s)} \sum_{j \in \mathcal{W}_u} \frac{\Delta_j(k' \tau_s^G)}{\Delta_u(k' \tau_s^G)} \nabla F_j(\bar{\mathbf{w}}(\tau_s^L \tau_s^G k' - 1)) \right)\right] \\ &\stackrel{(b)}{=} -\eta_2 \mathbb{E}\left[\nabla \bar{F}(\bar{\mathbf{w}}(\tau_s^L \tau_s^G k' - 1))^T \left(X + Y + \nabla \bar{F}(\bar{\mathbf{w}}(\tau_s^L \tau_s^G k' - 1)) \right)\right] \\ &\stackrel{(c)}{=} -\eta_2 \left(\mathbb{E}[\nabla \bar{F}(\bar{\mathbf{w}}(\tau_s^L \tau_s^G k' - 1))^T (X + Y)] + \mathbb{E}[\|\nabla \bar{F}(\bar{\mathbf{w}}(\tau_s^L \tau_s^G k' - 1))\|^2] \right) \\ &\stackrel{(d)}{\leq} \frac{-\eta_2}{2} \mathbb{E}[\|\nabla \bar{F}(\bar{\mathbf{w}}(\tau_s^L \tau_s^G k' - 1))\|^2] + \eta_2 \left(\mathbb{E}[\|X\|^2] + \mathbb{E}[\|Y\|^2] \right) \\ &\stackrel{(e)}{\leq} \frac{-\eta_2}{2} \mathbb{E}[\|\nabla \bar{F}(\bar{\mathbf{w}}(\tau_s^L \tau_s^G k' - 1))\|^2] + \eta_2 \left(\frac{1}{U(s)} \sum_{u \in \mathcal{U}(s)} \sum_{j \in \mathcal{W}_u} \frac{\Delta_j(k' \tau_s^G)}{\Delta_u(k' \tau_s^G)} (\sigma_j^F(\tau_s^L \tau_s^G k' - 1))^2 + \mu_F^2 \Upsilon(k', \tau_s^L, \tau_s^G) \right),\end{aligned}\tag{84}$$

where (a) comes from introducing $\nabla F_j(\mathbf{w}_j)$ and $\nabla F_j(\bar{\mathbf{w}})$ terms, (b) is the definition of $\nabla \bar{F}$, (c) follows from linearity of expectation, (d) is due to

$$\begin{aligned}& -\eta_2 \mathbb{E}[\nabla \bar{F}(\bar{\mathbf{w}}(\tau_s^L \tau_s^G k' - 1))^T (X + Y)] \leq \frac{1}{2} \eta_2 \mathbb{E}[\|\nabla \bar{F}(\bar{\mathbf{w}}(\tau_s^L \tau_s^G k' - 1))\|^2] + \frac{1}{2} \mathbb{E}[\|X + Y\|^2] \\ &\leq \frac{1}{2} \eta_2 \mathbb{E}[\|\nabla \bar{F}(\bar{\mathbf{w}}(\tau_s^L \tau_s^G k' - 1))\|^2] + \eta_2 \mathbb{E}[\|X\|^2] + \eta_2 \mathbb{E}[\|Y\|^2]\end{aligned}\tag{85}$$

(i.e., $(A + B)^2 \geq 0$ and Cauchy-Schwarz), and (e) applies the results of (82) and (83). Next, we analyze (79)(ii) as follows:

$$\begin{aligned}& \mathbb{E}\left[\left\|\frac{1}{U(s)} \sum_{u \in \mathcal{U}(s)} \sum_{j \in \mathcal{W}_u} \frac{\Delta_j(k' \tau_s^G)}{\Delta_u(k' \tau_s^G)} \nabla \tilde{F}_j(\mathbf{w}_j(\tau_s^L \tau_s^G k' - 1))\right\|^2\right] \\ &\stackrel{(a)}{\leq} \mathbb{E}\left[\left\|X + Y + \frac{1}{U(s)} \sum_{u \in \mathcal{U}(s)} \sum_{j \in \mathcal{W}_u} \frac{\Delta_j(k' \tau_s^G)}{\Delta_u(k' \tau_s^G)} \nabla F_j(\bar{\mathbf{w}}(\tau_s^L \tau_s^G k' - 1))\right\|^2\right] \\ &\stackrel{(b)}{\leq} 3\mathbb{E}[\|X\|^2] + 3\mathbb{E}[\|Y\|^2] + 3\mathbb{E}\left[\left\|\frac{1}{U(s)} \sum_{u \in \mathcal{U}(s)} \sum_{j \in \mathcal{W}_u} \frac{\Delta_j(k' \tau_s^G)}{\Delta_u(k' \tau_s^G)} \nabla F_j(\bar{\mathbf{w}}(\tau_s^L \tau_s^G k' - 1))\right\|^2\right] \\ &\stackrel{(c)}{\leq} 3 \frac{1}{U(s)} \sum_{u \in \mathcal{U}(s)} \sum_{j \in \mathcal{W}_u} \frac{\Delta_j(k' \tau_s^G)}{\Delta_u(k' \tau_s^G)} (\sigma_j^F(\tau_s^L \tau_s^G k' - 1))^2 + 3\mu_F^2 \Upsilon(k' \tau_s^L \tau_s^G) \\ &\quad + 3\mathbb{E}\left[\left\|\frac{1}{U(s)} \sum_{u \in \mathcal{U}(s)} \sum_{j \in \mathcal{W}_u} \frac{\Delta_j(k' \tau_s^G)}{\Delta_u(k' \tau_s^G)} \nabla F_j(\bar{\mathbf{w}}(\tau_s^L \tau_s^G k' - 1))\right\|^2\right] \\ &\stackrel{(d)}{\leq} 3 \frac{1}{U(s)} \sum_{u \in \mathcal{U}(s)} \sum_{j \in \mathcal{W}_u} \frac{\Delta_j(k' \tau_s^G)}{\Delta_u(k' \tau_s^G)} (\sigma_j^F(\tau_s^L \tau_s^G k' - 1))^2 + 3\mu_F^2 \Upsilon(k' \tau_s^L \tau_s^G) \\ &\quad + 3\mathbb{E}\left[\left\|\frac{1}{U(s)} \sum_{u \in \mathcal{U}(s)} \sum_{j \in \mathcal{W}_u} \frac{\Delta_j(k' \tau_s^G)}{\Delta_u(k' \tau_s^G)} \left(\nabla F_j(\bar{\mathbf{w}}(\tau_s^L \tau_s^G k' - 1)) - \nabla \bar{F}(\bar{\mathbf{w}}(\tau_s^L \tau_s^G k' - 1)) + \nabla \bar{F}(\bar{\mathbf{w}}(\tau_s^L \tau_s^G k' - 1)) \right)\right\|^2\right] \\ &\stackrel{(e)}{\leq} 3 \frac{1}{U(s)} \sum_{u \in \mathcal{U}(s)} \sum_{j \in \mathcal{W}_u} \frac{\Delta_j(k' \tau_s^G)}{\Delta_u(k' \tau_s^G)} (\sigma_j^F(\tau_s^L \tau_s^G k' - 1))^2 + 3\mu_F^2 \Upsilon(k' \tau_s^L \tau_s^G)\end{aligned}\tag{86}$$

$$\begin{aligned}
& + 6\mathbb{E}\left[\left\|\frac{1}{U(s)} \sum_{u \in \mathcal{U}(s)} \left(\sum_{j \in \mathcal{W}_u} \frac{\Delta_j(k' \tau_s^G)}{\Delta_u(k' \tau_s^G)} \nabla F_j(\bar{\mathbf{w}}(\tau_s^L \tau_s^G k' - 1)) - \nabla F_u(\bar{\mathbf{w}}(\tau_s^L \tau_s^G k' - 1)) \right)\right\|^2\right] + 6\mathbb{E}\left[\left\|\nabla \bar{F}(\bar{\mathbf{w}}(\tau_s^L \tau_s^G k' - 1))\right\|^2\right] \\
& \stackrel{(f)}{\leq} 6\mathbb{E}[\|\nabla \bar{F}(\bar{\mathbf{w}}(\tau_s^L \tau_s^G k' - 1))\|^2] + 3\frac{1}{U(s)} \sum_{u \in \mathcal{U}(s)} \sum_{j \in \mathcal{W}_u} \frac{\Delta_j(k' \tau_s^G)}{\Delta_u(k' \tau_s^G)} (\sigma_j^F(\tau_s^L \tau_s^G k' - 1))^2 + 3\mu_F^2 \Upsilon(k' \tau_s^L \tau_s^G) + 6\frac{1}{U(s)} \sum_{u \in \mathcal{U}(s)} (\gamma_F^u)^2,
\end{aligned}$$

where, we (a) substitute the result from (80), (b) apply $(\sum_i^n a_i)^2 \leq n(\sum_i a_i^2)$, (c) combine the results of (82) and (83), (d) introduce the global gradient $\nabla \bar{F}$, (e) recall that $\nabla \bar{F} = \frac{1}{U(s)} \sum_{u \in \mathcal{U}(s)} \nabla F_u$ and use $(\sum_i^n a_i)^2 \leq n(\sum_i a_i^2)$, and (f) apply Jensen's inequality and Lemma 2. Combining the results of (84) and (86) in (79) yields:

$$\begin{aligned}
& \mathbb{E}[\bar{F}(\bar{\mathbf{w}}(\tau_s^L \tau_s^G k'))] - \mathbb{E}[\bar{F}(\bar{\mathbf{w}}(\tau_s^L \tau_s^G k' - 1))] \\
& \leq -\frac{\eta_2}{2} \mathbb{E}[\|\nabla \bar{F}(\bar{\mathbf{w}}(\tau_s^L \tau_s^G k' - 1))\|^2] + \eta_2 \left(\frac{1}{U(s)} \sum_{u \in \mathcal{U}(s)} \sum_{j \in \mathcal{W}_u} \frac{\Delta_j(k' \tau_s^G)}{\Delta_u(k' \tau_s^G)} (\sigma_j^F(\tau_s^L \tau_s^G k' - 1))^2 + \mu_F^2 \Upsilon(k' \tau_s^L \tau_s^G) \right) \\
& + \eta_2^2 \frac{\mu_F}{2} \left(6\mathbb{E}[\|\nabla \bar{F}(\bar{\mathbf{w}}(\tau_s^L \tau_s^G k' - 1))\|^2] + 3\frac{1}{U(s)} \sum_{u \in \mathcal{U}(s)} \sum_{j \in \mathcal{W}_u} \frac{\Delta_j(k' \tau_s^G)}{\Delta_u(k' \tau_s^G)} (\sigma_j^F(\tau_s^L \tau_s^G k' - 1))^2 + 3\mu_F^2 \Upsilon(k' \tau_s^L \tau_s^G) + 6\frac{1}{U(s)} \sum_{u \in \mathcal{U}(s)} (\gamma_F^u)^2 \right). \tag{87}
\end{aligned}$$

With some algebra, we obtain:

$$\begin{aligned}
& \mathbb{E}[\bar{F}(\bar{\mathbf{w}}(\tau_s^L \tau_s^G k'))] - \mathbb{E}[\bar{F}(\bar{\mathbf{w}}(\tau_s^L \tau_s^G k' - 1))] \leq (6\eta_2^2 \frac{\mu_F}{2} - \frac{\eta_2}{2}) \mathbb{E}[\|\nabla \bar{F}(\bar{\mathbf{w}}(\tau_s^L \tau_s^G k' - 1))\|^2] \\
& + (3\eta_2^2 \frac{\mu_F}{2} + \eta_2) \left(\frac{1}{U(s)} \sum_{u \in \mathcal{U}(s)} \sum_{j \in \mathcal{W}_u} \frac{\Delta_j(k' \tau_s^G)}{\Delta_u(k' \tau_s^G)} (\sigma_j^F(\tau_s^L \tau_s^G k' - 1))^2 + \mu_F^2 \Upsilon(k' \tau_s^L \tau_s^G) \right) + 3\eta_2^2 \mu_F \frac{1}{U(s)} \sum_{u \in \mathcal{U}(s)} (\gamma_F^u)^2. \tag{88}
\end{aligned}$$

Since our goal from the beginning was to find an upper bound for the first-order stationary point, $\mathbb{E}[\|\nabla \bar{F}(\bar{\mathbf{w}}(t))\|^2]$, we now take the average of (88) over all time t , which yields:

$$\begin{aligned}
& \frac{1}{\tau_s^L \tau_s^G K_s^G} \sum_{k'=1}^{K_s^G} \sum_{k=(k'-1)\tau_s^G+1}^{\tau_s^G k'} \sum_{t=(k-1)\tau_s^L+1}^{\tau_s^L k} \mathbb{E}[\bar{F}(\bar{\mathbf{w}}(t))] - \mathbb{E}[\bar{F}(\bar{\mathbf{w}}(t-1))] = \frac{1}{\tau_s^L \tau_s^G K_s^G} (\mathbb{E}[\bar{F}(\bar{\mathbf{w}}(\tau_s^L \tau_s^G K_s^G))] - \mathbb{E}[\bar{F}(\bar{\mathbf{w}}(0))]) \\
& \leq \frac{1}{\tau_s^L \tau_s^G K_s^G} \sum_{k'=1}^{K_s^G} \sum_{k=(k'-1)\tau_s^G+1}^{\tau_s^G k'} \sum_{t=(k-1)\tau_s^L+1}^{\tau_s^L k} \left[(6\eta_2^2 \frac{\mu_F}{2} - \frac{\eta_2}{2}) \mathbb{E}[\|\nabla \bar{F}(\bar{\mathbf{w}}(t-1))\|^2] \right. \\
& \left. + (3\eta_2^2 \frac{\mu_F}{2} + \eta_2) \left(\frac{1}{U(s)} \sum_{u \in \mathcal{U}(s)} \sum_{j \in \mathcal{W}_u} \frac{\Delta_j(k' \tau_s^G)}{\Delta_u(k' \tau_s^G)} (\sigma_j^F(t-1))^2 + \mu_F^2 \Upsilon(k' \tau_s^L \tau_s^G) \right) + 3\eta_2^2 \mu_F \frac{1}{U(s)} \sum_{u \in \mathcal{U}(s)} (\gamma_F^u)^2 \right]. \tag{89}
\end{aligned}$$

We set $\eta_2 < \frac{1}{6\mu_F}$ and obtain:

$$\begin{aligned}
& - \frac{6\eta_2^2 \frac{\mu_F}{2} - \frac{\eta_2}{2}}{\tau_s^L \tau_s^G K_s^G} \sum_{k'=1}^{K_s^G} \sum_{k=\tau_s^G(k'-1)+1}^{\tau_s^G k'} \sum_{t=\tau_s^L(k-1)+1}^{\tau_s^L k} \mathbb{E}[\|\nabla \bar{F}(\bar{\mathbf{w}}(t-1))\|^2] \\
& \leq \frac{1}{\tau_s^L \tau_s^G K_s^G} \left(\mathbb{E}[\bar{F}(\bar{\mathbf{w}}(0))] - \mathbb{E}[\bar{F}(\bar{\mathbf{w}}(\tau_s^L \tau_s^G K_s^G))] + \sum_{k'=1}^{K_s^G} \sum_{k=\tau_s^G(k'-1)+1}^{\tau_s^G k'} \sum_{t=\tau_s^L(k-1)+1}^{\tau_s^L k} \right. \\
& \left. \left[(3\eta_2^2 \frac{\mu_F}{2} + \eta_2) \left(\frac{1}{U(s)} \sum_{u \in \mathcal{U}(s)} \sum_{j \in \mathcal{W}_u} \frac{\Delta_j(k' \tau_s^G)}{\Delta_u(k' \tau_s^G)} (\sigma_j^F(t-1))^2 + \mu_F^2 \Upsilon(k' \tau_s^L \tau_s^G) \right) + 3\eta_2^2 \mu_F \frac{1}{U(s)} \sum_{u \in \mathcal{U}(s)} (\gamma_F^u)^2 \right] \right). \tag{90}
\end{aligned}$$

Finally, noting that $\mathbb{E}[\bar{F}(\bar{\mathbf{w}}(0))] = \bar{F}(\bar{\mathbf{w}}(0))$ and that $-\mathbb{E}[\bar{F}(\bar{\mathbf{w}}(\tau_s^L \tau_s^G K_s^G))] \leq -F^*$, we have the result:

$$\begin{aligned}
& \frac{1}{\tau_s^L \tau_s^G K_s^G} \sum_{k'=1}^{K_s^G} \sum_{k=(k'-1)\tau_s^G+1}^{\tau_s^G k'} \sum_{t=(k-1)\tau_s^L+1}^{\tau_s^L k} \mathbb{E}[\|\nabla \bar{F}(\bar{\mathbf{w}}(t-1))\|^2] \leq \frac{1}{\frac{\eta_2}{2} - 6\eta_2^2 \frac{\mu_F}{2}} \frac{1}{\tau_s^L \tau_s^G K_s^G} \left[\bar{F}(\bar{\mathbf{w}}(0)) - F^* + \sum_{k'=1}^{K_s^G} \sum_{k=(k'-1)\tau_s^G+1}^{\tau_s^G k'} \right. \\
& \left. \sum_{t=(k-1)\tau_s^L+1}^{\tau_s^L k} \left[(3\eta_2^2 \frac{\mu_F}{2} + \eta_2) \left(\frac{1}{U(s)} \sum_{u \in \mathcal{U}(s)} \sum_{j \in \mathcal{W}_u} \frac{\Delta_j(k' \tau_s^G)}{\Delta_u(k' \tau_s^G)} (\sigma_j^F(t-1))^2 + \mu_F^2 \Upsilon(k' \tau_s^L \tau_s^G) \right) + 3\eta_2^2 \mu_F \frac{1}{U(s)} \sum_{u \in \mathcal{U}(s)} (\gamma_F^u)^2 \right] \right]. \tag{91}
\end{aligned}$$

■

APPENDIX C

AN OVERVIEW OF GEOMETRIC PROGRAMMING

A prerequisite to geometric programming (GP) is the notion of *monomials* and *posynomials*, which we provide below.

Definition 2. A monomial is a function $f : \mathbb{R}_{++}^n \rightarrow \mathbb{R}$: $f(\mathbf{y}) = d y_1^{a_1} y_2^{a_2} \cdots y_n^{a_n}$, with $d \geq 0$, $\mathbf{y} = [y_1, \dots, y_n]$, and $a_j \in \mathbb{R}$, $\forall j$, where \mathbb{R}_{++}^n denotes the strictly positive quadrant of n -dimensional Euclidean space. Also, a posynomial g is a sum of monomials: $g(\mathbf{y}) = \sum_{m=1}^M d_m y_1^{\alpha_m^{(1)}} \cdots y_n^{\alpha_m^{(n)}}$.

A standard GP is a non-convex problem formulated as minimizing a posynomial under posynomial inequality constraints and monomial equality constraints [62], [68]:

$$\begin{aligned} & \min_{\mathbf{y}} g_0(\mathbf{y}) \\ & \text{s.t.} \\ & g_i(\mathbf{y}) \leq 1, \quad i = 1, \dots, I, \\ & f_\ell(\mathbf{y}) = 1, \quad \ell = 1, \dots, L, \end{aligned} \tag{92}$$

where $g_i(\mathbf{y}) = \sum_{m=1}^{M_i} d_{i,m} y_1^{a_{i,m}^{(1)}} \cdots y_n^{a_{i,m}^{(n)}}$, $\forall i$, and $f_\ell(\mathbf{y}) = d_\ell y_1^{a_\ell^{(1)}} \cdots y_n^{a_\ell^{(n)}}$, $\forall \ell$. Since the log-sum-exp function $f(\mathbf{y}) = \log \sum_{j=1}^n e^{y_j}$ is convex, where log denotes the natural logarithm, with logarithmic change of variables and constants $z_i = \log(y_i)$, $b_{i,k} = \log(d_{i,k})$, $b_\ell = \log(d_\ell)$, and applying the log on the objective and constraints of (92), the GP in its standard format can be transformed to the following convex programming formulation:

$$\begin{aligned} & \min_{\mathbf{z}} \log \sum_{m=1}^{M_0} e^{(\mathbf{a}_{0,m}^\top \mathbf{z} + b_{0,m})} \\ & \text{s.t.} \log \sum_{m=1}^{M_i} e^{(\mathbf{a}_{i,m}^\top \mathbf{z} + b_{i,m})} \leq 0, \quad i = 1, \dots, I, \\ & \mathbf{a}_\ell^\top \mathbf{z} + b_\ell = 0, \quad \ell = 1, \dots, L, \end{aligned} \tag{93}$$

where $\mathbf{z} = [z_1, \dots, z_n]^\top$, $\mathbf{a}_{i,m} = [a_{i,m}^{(1)}, \dots, a_{i,m}^{(n)}]^\top$, $\forall i, m$, and $\mathbf{a}_\ell = [a_\ell^{(1)}, \dots, a_\ell^{(n)}]^\top$, $\forall \ell$.

As can be seen, in \mathcal{P} , there are multiple terms in the objective function (in the upper bound of convergence of the ML model) that are in the format of ratio between two posynomials, which are not posynomial. We thus aim to transform a ratio of two posynomials to a ratio between a posynomial (in the numerator) and a monomial (in the denominator). Given the fact that the ratio between a posynomial and a monomial is a posynomial, we then aim to transform the problem to the standard GP format. To carry out this transformation, we exploit arithmetic-geometric mean inequality which lower bounds a posynomial with a monomial.

Lemma 5 (Arithmetic-geometric mean inequality [62]). A posynomial $g(\mathbf{x}) = \sum_{k=1}^K u_k(\mathbf{x})$, where $u_k(\mathbf{x})$ is a monomial, $\forall k$, can be lower-bounded via a monomial as follows:

$$g(\mathbf{x}) \geq \hat{g}(\mathbf{x}) \triangleq \prod_{k=1}^K \left(\frac{u_k(\mathbf{x})}{a_k(\mathbf{y})} \right)^{a_k(\mathbf{y})}, \tag{94}$$

where $a_k(\mathbf{y}) = u_k(\mathbf{y})/g(\mathbf{y})$, $\forall k$, and $\mathbf{y} > 0$ is a fixed point.

APPENDIX D

PROOF OF PROPOSITION 2

Let us first rewrite problem (\mathcal{P}) in its equivalent form as follows:

$$(\mathcal{P}) : \min_{\rho, \mathbf{g}, \alpha, \mathbf{g}, \Omega} \Omega \quad (95)$$

$$\text{s.t.} \quad (96)$$

$$(25) - (46), \quad (97)$$

$$(1 - \theta)(a) + \theta(b) \leq \Omega, \quad \Omega \geq 0, \quad (98)$$

where $\Omega \in \mathbb{R}^+$ is an auxiliary variable used to move the objective function into the constraints, and (a) , and (b) are those introduced in (24). The corresponding approximated problem can also be expressed as follows:

$$(\hat{\mathcal{P}}_m) : \min_{\rho, \mathbf{g}, \alpha, \mathbf{g}, \Omega} \Omega \quad \text{s.t.} \quad (25) - (46), \quad (1 - \theta)(\widetilde{a})_m + \theta(b) \leq \Omega, \quad \Omega \geq 0, \quad (99)$$

where $\theta(\widetilde{a})$ follows from the procedure outlined to obtain $\widetilde{\mathcal{P}}_m$ in the main text, i.e., applying the posynomial condensation technique. It is easy to verify that the solution of $\widetilde{\mathcal{P}}_m$ coincides with that of $\hat{\mathcal{P}}_m$. Thus to prove the proposition, it is enough to prove that solving $\hat{\mathcal{P}}_m$ generates a sequence of improved feasible solutions for problem $\widetilde{\mathcal{P}}_m$ that converge to a point \mathbf{x}^* satisfying the Karush-Kuhn-Tucker (KKT) conditions of \mathcal{P} . Note that $\hat{\mathcal{P}}_m$ can be solved using the procedure Algorithm 1.

Following the justifications in **Observation 2** in Sec. 4.2, the constraints of $\hat{\mathcal{P}}_m$ are separable with respect to each individual UAV swam. Thus, the performance of the distributed algorithm proposed to solve $\hat{\mathcal{P}}_m$ distributedly at each UAV swarm coincides with that of the centralized one for a fixed set of estimated parameters. Under the approximations described in (48) and (51), the algorithm in fact solves an *inner approximation* of problem \mathcal{P} [64]. Hence, it is sufficient to prove the following three conditions for the sequence of generated solutions by the algorithm [64]:

- 1) *The approximations used in problem $\hat{\mathcal{P}}_m$ should tighten the constraints of problem \mathcal{P} :* Since the constraints (25)-(46) are common to both Problems (\mathcal{P}) and $\hat{\mathcal{P}}_m$, it is enough to show that $(1 - \theta)(a) + \theta(b) \leq (1 - \theta)(\widetilde{a}) + \theta(b)$ for the approximated constraint, assuming some solution $\mathbf{x}[m]$ (\mathbf{x} is the solution vector defined in Algorithm 1). Equivalently, it is sufficient to show that $(a) \leq (\widetilde{a})$ for $\mathbf{x}[m]$.

To show this, it is sufficient to show (i) $\Xi(s) \leq \widetilde{\Xi}(s)$, and (ii) $\widehat{\Xi}(k) \leq \widetilde{\Xi}(k)$, $\forall k$, where $\Xi(s), \widehat{\Xi}(k)$ are the two terms in (a) (see (24)) and $\widetilde{\Xi}(s)$ and $\widetilde{\Xi}(k)$ are their respective approximations obtained via (48) and (51). Condition (i) holds since $\overline{\Delta}_u(k) \geq \widehat{\Delta}_u(k)$, and condition (ii) also holds since $D_j(k) \geq \widehat{D}_j(k) \forall k$, as in equations (48) and (51).⁴

- 2) *Upon convergence, the value of each approximated constraint in problem $\hat{\mathcal{P}}_m$ should coincide with that of the corresponding original constraint in \mathcal{P} :* Since the constraints (25)-(46) are common in problems (\mathcal{P}) and $(\hat{\mathcal{P}})$, we need to show $(1 - \theta)(a) + \theta(b) = (1 - \theta)(\widetilde{a}) + \theta(b)$ for the approximated constraint upon convergence. Note that when the algorithm converges we have

$$\widetilde{\delta}_{j,i,n}(k) = \widetilde{\delta}_{j,i,n}(k; m), \quad \delta_{j,h,i,n}(k) = \delta_{j,h,i,n}(k; m), \quad n \in \{1, 2, 3\}, \quad (100)$$

where $\widetilde{\delta}_{j,i,n}(k; m)$ and $\delta_{j,h,i,n}(k; m)$ are the approximations used in (48) (see (49) for the definition of $\widetilde{\delta}_{j,i,n}(k)$ and $\delta_{j,h,i,n}(k)$). Also, upon convergence, we have:

$$\lambda_{i,j}(k) = \lambda_{i,j}(k; m), \quad \widetilde{\lambda}_{h,i,j}(k) = \widetilde{\lambda}_{h,i,j}(k; m), \quad (101)$$

where $\lambda_{i,j}(k; m), \widetilde{\lambda}_{h,i,j}(k; m)$ are the approximations used in (51) (see (52) for the definition of $\lambda_{i,j}(k), \widetilde{\lambda}_{h,i,j}(k)$).

Considering the terms inside (a), we need to show that upon convergence (i) $\Xi(s) = \widetilde{\Xi}(s)$, and (ii) $\widehat{\Xi}(k) = \widetilde{\Xi}(k)$. To demonstrate that (i) holds, it is sufficient to show that $\overline{\Delta}_u(k) = \widehat{\Delta}_u(k)$, and $D_j(k) = \widehat{D}_j(k)$, upon convergence. In the following, we demonstrate that $\overline{\Delta}_u(k) = \widehat{\Delta}_u(k)$ upon convergence:

$$\begin{aligned} \widehat{\Delta}_u(k) &= \prod_{(100), (101)} \left[\prod_{j \in \mathcal{W}_u} \left[\prod_{i \in \mathcal{C}(u,s)} \left(\frac{\widetilde{\delta}_{i,j,1}(k; m) [\overline{\Delta}_u(k; m)]}{\widetilde{\delta}_{i,j,1}(k; m)} \right)^{\frac{\widetilde{\delta}_{i,j,1}(k; m)}{\overline{\Delta}_u(k; m)}} \right. \right. \\ &\quad \times \left(\frac{\widetilde{\delta}_{i,j,2}(k; m) [\overline{\Delta}_u(k; m)]}{\widetilde{\delta}_{i,j,2}(k; m)} \right)^{\frac{\widetilde{\delta}_{i,j,2}(k; m)}{\overline{\Delta}_u(k; m)}} \times \left(\frac{\widetilde{\delta}_{i,j,3}(k; m) [\overline{\Delta}_u(k; m)]}{\widetilde{\delta}_{i,j,3}(k; m)} \right)^{\frac{\widetilde{\delta}_{i,j,3}(k; m)}{\overline{\Delta}_u(k; m)}} \left. \right] \\ &\quad \times \prod_{h \in \mathcal{W}_u} \prod_{i \in \mathcal{C}(u,s)} \left[\left(\frac{\delta_{j,h,i,1}(k; m) [\overline{\Delta}_u(k; m)]}{\delta_{j,h,i,1}(k; m)} \right)^{\frac{\delta_{j,h,i,1}(k; m)}{\overline{\Delta}_u(k; m)}} \right] \end{aligned}$$

4. Note that we replace $\overline{\Delta}_u(k)$ and $D_j(k)$ with their approximated versions in (48) and (51) only when they appear in the denominator of the terms in (a). Thus lower bounding these terms result in upper bounding (a) as desired.

$$\begin{aligned}
& \left(\frac{\delta_{j,h,i,2}(k;m) [\Delta_u(k;m)]}{\delta_{j,h,i,2}(k;m)} \right)^{\frac{\delta_{j,h,i,2}(k;m)}{\Delta_u(k;m)}} \times \left(\frac{\delta_{j,h,i,3}(k;m) [\Delta_u(k;m)]}{\delta_{j,h,i,3}(k;m)} \right)^{\frac{\delta_{j,h,i,3}(k;m)}{\Delta_u(k;m)}} \Bigg] \\
&= \prod_{j \in \mathcal{W}_u} \left[\prod_{i \in \mathcal{C}(u,s)} \left[\left([\Delta_u(k;m)] \right)^{\frac{\delta_{i,j,1}(k;m)}{\Delta_u(k;m)}} \right. \right. \\
&\quad \times \left([\Delta_u(k;m)] \right)^{\frac{\delta_{i,j,2}(k;m)}{\Delta_u(k;m)}} \times \left([\Delta_u(k;m)] \right)^{\frac{\delta_{i,j,3}(k;m)}{\Delta_u(k;m)}} \Bigg] \\
&\quad \times \prod_{h \in \widehat{\mathcal{W}}_u} \prod_{i \in \mathcal{C}(u,s)} \left[\left([\Delta_u(k;m)] \right)^{\frac{\delta_{j,h,i,1}(k;m)}{\Delta_u(k;m)}} \left([\Delta_u(k;m)] \right)^{\frac{\delta_{j,h,i,2}(k;m)}{\Delta_u(k;m)}} \right. \\
&\quad \times \left([\Delta_u(k;m)] \right)^{\frac{\delta_{j,h,i,3}(k;m)}{\Delta_u(k;m)}} \Bigg] \\
&= \overline{\Delta}_u(k) \left(\frac{\sum_{j \in \mathcal{W}_u} \sum_{i \in \mathcal{C}(u,s)} \frac{\delta_{i,j,1}(k;m) + \delta_{i,j,2}(k;m) + \delta_{i,j,3}(k;m)}{\Delta_u(k;m)}}{\Delta_u(k;m)} \right) \\
&\quad \times \overline{\Delta}_u(k) \left(\frac{\sum_{j \in \mathcal{W}_u} \sum_{h \in \widehat{\mathcal{W}}_u} \sum_{i \in \mathcal{C}(u,s)} \frac{\delta_{j,h,i,1}(k;m) + \delta_{j,h,i,2}(k;m) + \delta_{j,h,i,3}(k;m)}{\Delta_u(k;m)}}{\Delta_u(k;m)} \right) \\
&= \overline{\Delta}_u(k) \left(\frac{\overline{\Delta}_u(k;m)}{\Delta_u(k;m)} \right) = \overline{\Delta}_u(k) \Bigg|_{(100),(101)}.
\end{aligned} \tag{102}$$

Using a similar technique, it can be shown that $D_j(k) = \widehat{D}_j(k)$, upon convergence, and thus (i) holds. The proof for (ii) is similar, which is omitted for brevity.

- 3) The KKT conditions of \mathcal{P} should be satisfied after the series of approximations converges in problem $\widehat{\mathcal{P}}_m$: Since the constraints (25)-(46) are common in problems (\mathcal{P}) and $(\widehat{\mathcal{P}})$, for the approximated constraint we should have $\nabla(1 - \theta)((a) + \theta(b)) = \nabla((1 - \theta)(\widetilde{a}) + \theta(b))$, upon convergence (∇ denotes the gradient sign). Note that (a) involves the product between two ratios of posynomials (as can be seen from (18), one is $\frac{\Delta_j(k)}{\Delta_u(k)}$, where both the numerator and denominator are posynomial with respect to the optimization variables according to (37), and the other one is σ_j^F , which can be written as ratio of two posynomials according to (12)), where we approximate the denominator of each ratio via a monomial in (\widetilde{a}) . For compactness, let us define $(a) \triangleq \frac{A_1(\mathbf{x})A_2(\mathbf{x})}{B_1(\mathbf{x})B_2(\mathbf{x})}$, where $A_1(\mathbf{x})$ and $B_1(\mathbf{x})$ are posynomials corresponding to the numerator and denominator of $\frac{\Delta_j(k)}{\Delta_u(k)}$ (encompassing all the coefficients) and $A_2(\mathbf{x})$ and $B_2(\mathbf{x})$ are posynomials corresponding to the numerator and denominator of σ_j^F (\mathbf{x} denotes the set of optimization variables). We provide the proof for the general case. In general, the posynomials in the denominators can be described as $B_1(\mathbf{x}) = \sum_{k=1}^{K_1} u_k^{(1)}(\mathbf{x})$ and $B_2(\mathbf{x}) = \sum_{k=1}^{K_2} u_k^{(2)}(\mathbf{x})$, where $u_k^{(1)}$ -s and $u_k^{(2)}$ -s are monomial functions. Accordingly, we can write (\widetilde{a}) as $(\widetilde{a}) = \frac{A_1(\mathbf{x})A_2(\mathbf{x})}{\widetilde{B}_1(\mathbf{x})\widetilde{B}_2(\mathbf{x})}$, where $\widetilde{B}_1(\mathbf{x}) = \prod_{k=1}^{K_1} \left(\frac{u_k^{(1)}(\mathbf{x})}{a_k^{(1)}(\mathbf{y})} \right)^{a_k^{(1)}(\mathbf{y})}$ and $\widetilde{B}_2(\mathbf{x}) = \prod_{k=1}^{K_2} \left(\frac{u_k^{(2)}(\mathbf{x})}{a_k^{(2)}(\mathbf{y})} \right)^{a_k^{(2)}(\mathbf{y})}$ are the monomial approximation of $B_1(\mathbf{x})$ and $B_2(\mathbf{x})$ obtained according to (94) (equivalent to the condensations carried out in (48) and (51)). In the following, we show that the desired result holds for partial derivative with respect to an arbitrary element x_i considering $\mathbf{x} = [x_1, \dots, x_i, \dots, x_n]$ (note that upon convergence $\mathbf{x} = \mathbf{y}$ in (94), which in our problem translates to the equalities in (100),(101)):

$$\begin{aligned}
& \left. \frac{\partial \left(\frac{A_1(\mathbf{x})A_2(\mathbf{x})}{\widetilde{B}_1(\mathbf{x})\widetilde{B}_2(\mathbf{x})} \right)}{\partial x_i} \right|_{\mathbf{x}=\mathbf{y}} = \frac{\frac{\partial A_1(\mathbf{x})A_2(\mathbf{x})}{\partial x_i} \widetilde{B}_1(\mathbf{y})\widetilde{B}_2(\mathbf{y}) - \frac{\partial \widetilde{B}_1(\mathbf{x})\widetilde{B}_2(\mathbf{x})}{\partial x_i} A_1(\mathbf{y})A_2(\mathbf{y})}{\left(\widetilde{B}_1(\mathbf{y})\widetilde{B}_2(\mathbf{y}) \right)^2} \Bigg|_{\mathbf{x}=\mathbf{y}} \\
& \stackrel{(a)}{=} \frac{\frac{\partial A_1(\mathbf{x})A_2(\mathbf{x})}{\partial x_i} \Big|_{\mathbf{x}=\mathbf{y}} B_1(\mathbf{y})B_2(\mathbf{y}) - \frac{\partial \prod_{k=1}^{K_1} \left(\frac{u_k^{(1)}(\mathbf{x})}{a_k^{(1)}(\mathbf{y})} \right)^{a_k^{(1)}(\mathbf{y})}}{\partial x_i} \Big|_{\mathbf{x}=\mathbf{y}} B_2(\mathbf{y})A_1(\mathbf{y})A_2(\mathbf{y})}{(B_1(\mathbf{y})B_2(\mathbf{y}))^2} \\
& \quad + \frac{\frac{\partial \prod_{k=1}^{K_2} \left(\frac{u_k^{(2)}(\mathbf{x})}{a_k^{(2)}(\mathbf{y})} \right)^{a_k^{(2)}(\mathbf{y})}}{\partial x_i} \Big|_{\mathbf{x}=\mathbf{y}} B_1(\mathbf{y})A_1(\mathbf{y})A_2(\mathbf{y})}{(B_1(\mathbf{y})B_2(\mathbf{y}))^2}
\end{aligned}$$

$$\begin{aligned}
& \frac{\frac{\partial A_1(\mathbf{x})A_2(\mathbf{x})}{\partial x_i} \Big|_{\mathbf{x}=\mathbf{y}}}{(B_1(\mathbf{y})B_2(\mathbf{y}))^2} B_1(\mathbf{y})B_2(\mathbf{y}) \\
&= \frac{-\sum_{n=1}^{K_1} \frac{\partial u_n^{(1)}(\mathbf{x})}{\partial x_i} \Big|_{\mathbf{x}=\mathbf{y}} \left(\frac{u_n^{(1)}(\mathbf{y})}{\alpha_n^{(1)}(\mathbf{y})} \right)^{\alpha_n^{(1)}(\mathbf{y})-1} \left(\prod_{k=1, k \neq n}^{K_1} \left(\frac{u_k^{(1)}(\mathbf{y})}{\alpha_k^{(1)}(\mathbf{y})} \right)^{\alpha_k^{(1)}(\mathbf{y})} \right) B_2(\mathbf{y})A_1(\mathbf{y})A_2(\mathbf{y})}{(B_1(\mathbf{y})B_2(\mathbf{y}))^2} \\
&+ \frac{-\sum_{n=1}^{K_2} \frac{\partial u_n^{(2)}(\mathbf{x})}{\partial x_i} \Big|_{\mathbf{x}=\mathbf{y}} \left(\frac{u_n^{(2)}(\mathbf{y})}{a_n^{(2)}(\mathbf{y})} \right)^{a_n^{(2)}(\mathbf{y})-1} \left(\prod_{k=1, k \neq n}^{K_2} \left(\frac{u_k^{(2)}(\mathbf{y})}{a_k^{(2)}(\mathbf{y})} \right)^{a_k^{(2)}(\mathbf{y})} \right) B_1(\mathbf{y})A_1(\mathbf{y})A_2(\mathbf{y})}{(B_1(\mathbf{y})B_2(\mathbf{y}))^2} \\
&+ \frac{\frac{\partial A_1(\mathbf{y})A_2(\mathbf{y})}{\partial x_i} \Big|_{\mathbf{x}=\mathbf{y}}}{(B_1(\mathbf{y})B_2(\mathbf{y}))^2} B_1(\mathbf{y})B_2(\mathbf{y}) \\
&\stackrel{(b)}{=} \frac{-\sum_{n=1}^{K_1} \frac{\partial u_n^{(1)}(\mathbf{x})}{\partial x_i} \Big|_{\mathbf{x}=\mathbf{y}} B_1(\mathbf{y})^{\alpha_n^{(1)}(\mathbf{y})-1} \left(B_1(\mathbf{y})^{\sum_{k=1, k \neq n}^{K_1} \alpha_k^{(1)}(\mathbf{y})} \right) B_2(\mathbf{y})A_1(\mathbf{y})A_2(\mathbf{y})}{(B_1(\mathbf{y})B_2(\mathbf{y}))^2} \\
&+ \frac{-\sum_{n=1}^{K_2} \frac{\partial u_n^{(2)}(\mathbf{x})}{\partial x_i} \Big|_{\mathbf{x}=\mathbf{y}} B_2(\mathbf{y})^{a_n^{(2)}(\mathbf{y})-1} \left(B_2(\mathbf{y})^{\sum_{k=1, k \neq n}^{K_2} a_k^{(2)}(\mathbf{y})} \right) B_1(\mathbf{y})A_1(\mathbf{y})A_2(\mathbf{y})}{(B_1(\mathbf{y})B_2(\mathbf{y}))^2} \\
&\stackrel{(c)}{=} \frac{\frac{\partial A_1(\mathbf{y})A_2(\mathbf{y})}{\partial x_i} \Big|_{\mathbf{x}=\mathbf{y}}}{(B_1(\mathbf{y})B_2(\mathbf{y}))^2} B_1(\mathbf{y})B_2(\mathbf{y}) \\
&+ \frac{-\sum_{n=1}^K \frac{\partial u_n^{(1)}(\mathbf{x})}{\partial x_i} \Big|_{\mathbf{x}=\mathbf{y}} B_2(\mathbf{y})A_1(\mathbf{y})A_2(\mathbf{y}) - \sum_{n=1}^K \frac{\partial u_n^{(2)}(\mathbf{x})}{\partial x_i} \Big|_{\mathbf{x}=\mathbf{y}} B_1(\mathbf{y})A_1(\mathbf{y})A_2(\mathbf{y})}{(B_1(\mathbf{y})B_2(\mathbf{y}))^2} \\
&= \frac{\frac{\partial A_1(\mathbf{x})A_2(\mathbf{x})}{\partial x_i} \Big|_{\mathbf{x}=\mathbf{y}} B_1(\mathbf{y})B_2(\mathbf{y}) - \frac{\partial B_1(\mathbf{x})}{\partial x_i} \Big|_{\mathbf{x}=\mathbf{y}} A_1(\mathbf{y})A_2(\mathbf{y})B_2(\mathbf{y}) - \frac{\partial B_2(\mathbf{x})}{\partial x_i} \Big|_{\mathbf{x}=\mathbf{y}} A_1(\mathbf{y})A_2(\mathbf{y})B_1(\mathbf{y})}{(B_1(\mathbf{y})B_2(\mathbf{y}))^2} \\
&= \frac{\partial \left(\frac{A_1(\mathbf{x})A_2(\mathbf{x})}{B_1(\mathbf{x})B_2(\mathbf{x})} \right)}{\partial x_i} \Big|_{\mathbf{x}=\mathbf{y}}.
\end{aligned} \tag{103}$$

In (a), we used the fact that $B_1(\mathbf{y}) = \tilde{B}_1(\mathbf{y})$ and $B_2(\mathbf{y}) = \tilde{B}_2(\mathbf{y})$ (this is the equality of monomial approximation with the original posynomial upon convergence that we showed in bullet point 2 above). In (b), we used the fact that (see (94)) $a_k^{(1)}(\mathbf{y}) = u_k^{(1)}(\mathbf{y})/B_1(\mathbf{y})$ and $a_k^{(2)}(\mathbf{y}) = u_k^{(2)}(\mathbf{y})/B_2(\mathbf{y})$, $\forall k$. Also, in (c) we use the fact that $\sum_{k=1}^{K_1} \alpha_k^{(1)}(\mathbf{y}) = 1$ and $\sum_{k=1}^{K_2} a_k^{(2)}(\mathbf{y}) = 1$. The proof for the rest of partial derivatives, and thus the gradient, is similar.

Verification of the three aforementioned bullet points results in the conclusion of the proof.

APPENDIX E

PROOF OF LEMMA 4

Given the previous computed gradient for the local model at the device cluster, i.e., $\nabla F_c(\mathbf{w}_c(t_c^V)|\tilde{\mathcal{D}}_c(t_c^V))$, the value of the local gradient given the outdated model $\mathbf{w}_c(t_c^V)$ for the recent data distribution $\tilde{\mathcal{D}}_c(t)$ at time t can be expressed as follows:

$$\begin{aligned}
\left\| \nabla F_c(\mathbf{w}_c(t_c^V)|\tilde{\mathcal{D}}_c(t)) \right\|^2 &= \left\| \nabla F_c(\mathbf{w}_c(t_c^V)|\tilde{\mathcal{D}}_c(t)) - \nabla F_c(\mathbf{w}_c(t_c^V)|\tilde{\mathcal{D}}_c(t-1)) + \nabla F_c(\mathbf{w}_c(t_c^V)|\tilde{\mathcal{D}}_c(t-1)) \right. \\
&\quad \left. - \nabla F_c(\mathbf{w}_c(t_c^V)|\tilde{\mathcal{D}}_c(t-2)) + \nabla F_c(\mathbf{w}_c(t_c^V)|\tilde{\mathcal{D}}_c(t-2)) - \dots \right. \\
&\quad \left. - \nabla F_c(\mathbf{w}_c(t_c^V)|\tilde{\mathcal{D}}_c(t_c^V)) + \nabla F_c(\mathbf{w}_c(t_c^V)|\tilde{\mathcal{D}}_c(t_c^V)) \right\|^2 \\
&\stackrel{(a)}{\leq} \left(\left\| \nabla F_c(\mathbf{w}_c(t_c^V)|\tilde{\mathcal{D}}_c(t)) - \nabla F_c(\mathbf{w}_c(t_c^V)|\tilde{\mathcal{D}}_c(t-1)) \right\| + \left\| \nabla F_c(\mathbf{w}_c(t_c^V)|\tilde{\mathcal{D}}_c(t-1)) \right. \right. \\
&\quad \left. \left. - \nabla F_c(\mathbf{w}_c(t_c^V)|\tilde{\mathcal{D}}_c(t-2)) \right\| + \left\| \nabla F_c(\mathbf{w}_c(t_c^V)|\tilde{\mathcal{D}}_c(t-2)) - \nabla F_c(\mathbf{w}_c(t_c^V)|\tilde{\mathcal{D}}_c(t-3)) \right\| + \dots + \right. \\
&\quad \left. \left\| \nabla F_c(\mathbf{w}_c(t_c^V)|\tilde{\mathcal{D}}_c(t_c^V+1)) - \nabla F_c(\mathbf{w}_c(t_c^V)|\tilde{\mathcal{D}}_c(t_c^V)) \right\| + \left\| \nabla F_c(\mathbf{w}_c(t_c^V)|\tilde{\mathcal{D}}_c(t_c^V)) \right\| \right)^2 \\
&\stackrel{(b)}{\leq} (t - t_c^V + 1) \left\| \nabla F_c(\mathbf{w}_c(t_c^V)|\tilde{\mathcal{D}}_c(t_c^V)) \right\|^2 + (t - t_c^V + 1) \sum_{t'=t_c^V+1}^t \Lambda_c(t'), \tag{104}
\end{aligned}$$

where in (a) we used triangle inequality, and (b) is the result of Cauchy–Schwarz inequality (i.e, for any N numbers A_1, \dots, A_N , we have $\left(\sum_{i=1}^N A_i \right)^2 \leq N \sum_{i=1}^N (A_i)^2$).